TECHNICAL UNIVERSITY MUNICH

TUM SCHOOL OF NATURAL SCIENCE, T30D

Master Thesis in Nuclear, Particle and Astrophysics

Quantum Effects on the Lepton Number Violating Standard Model Effective Field Theory and Beyond

Nicholas Leister

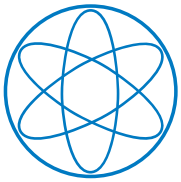

TECHNICAL UNIVERSITY MUNICH

TUM SCHOOL OF NATURAL SCIENCE, T30D

Master Thesis in Nuclear, Particle and Astrophysics

Quantum Effects on the Lepton Number Violating Standard Model Effective Field Theory and Beyond

Quanteneffekte in effektiver Feldtheorie des Standard Models mit Leptonenzahlverletzung und jenseits des Standard Models

Author:	Nicholas Leister
Supervisor:	Prof. Dr. Alejandro Ibarra
Advisor:	Prof. Dr. Alejandro Ibarra, Dr. Di Zhang
Submission Date:	16.02.2024

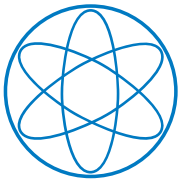

I confirm that this master thesis in nuclear, particle and astrophysics is my own work and I have documented all sources and materials used.

Munich, 16.02.2024 Nicholas Leister

Acknowledgments

First of all, I want to thank my supervisor, Prof. Alejandro Ibarra, for his support throughout my research. His vast knowledge of different aspects of particle physics has been incredibly valuable. Our discussions have really helped me to broaden my understanding.

I would like to give a special thanks to Dr. Di Zhang, with whom I had the pleasure of working with on a joint project. I learned a lot from his expertise in effective field theories and neutrino physics. I also want to say thank you to Prof. Lorenzo Tancredi for co-reviewing my thesis.

Finally, a big thanks to Mar and Andrea for peer reviewing my work, and to all members of T30d for their valuable feedback.

Abstract

Oscillation experiments have demonstrated that at least two neutrinos possess small but non-vanishing masses. The seesaw mechanisms, which include heavy particles such as Right-Handed Neutrinos (RHNs), are possible explanations for the observed neutrino masses. In the low-energy limit, the effect of heavier particles is effectively described by the dimension-five Weinberg operator. This thesis calculates the full two-loop beta functions of the Weinberg operator and examines its phenomenological implications. If one neutrino remains massless at tree level, the running effects generate a small third neutrino mass, serving as a lower limit on the lightest neutrino mass. Furthermore, the running behavior and fixed points of Majorana phases are analyzed analytically and numerically.

Similar two-loop diagrams that increase the rank of the active neutrino mass matrix also exist for the RHN mass matrix. If at least one RHN has a mass around the Planck scale, while some other RHNs remain massless at the tree level, quantum corrections radiatively generate the remaining masses at the seesaw scale. This work presents an extension of the Standard Model (SM) in the framework of left-right symmetry models, which includes both massless RHNs and massive RHNs around the Planck scale and allows for rank-increasing two-loop contributions.

Zusammenfassung

Oszillationsexperimente haben gezeigt, dass mindestens zwei Neutrinos kleine, aber nicht verschwindende Massen besitzen. Eine mögliche Erklärung für die Neutrinomassen sind die “Seesaw”-Mechanismen, welche schwere Teilchen wie rechtshändige Neutrinos (RHN) beinhaltet. Im Niederenergielimit wird die Wirkung schwerer Teilchen effektiv durch den Dimension-fünf Weinberg-Operator beschrieben. In dieser Arbeit wird die vollständige Zweischleifen-Beta-Funktion des Weinberg-Operators berechnet und ihre phänomenologischen Implikationen untersucht. Ein zunächst masseloses Neutrino erhält eine kleine, aber nicht verschwindende Masse durch diese Quantenkorrekturen, die als untere Grenze für die leichteste Neutrinomasse dient. Außerdem werden das Laufverhalten und die Fixpunkte der Majorana-Phasen sowohl analytisch als auch numerisch analysiert.

Ähnliche Zweischleifendiagramme, die den Rang der aktiven Neutrinomassenmatrix erhöhen, existieren auch für die RHN-Massenmatrix. Wenn mindestens ein RHN eine Masse um die Planck-Skala hat, während einige andere RHNs zunächst masselos bleiben, erzeugen Quantenkorrekturen die verbleibenden Massen um die “Seesaw”-Skala. In dieser Arbeit wird eine Erweiterung des Standard Models im Rahmen von Links-Rechts-Symmetrischen Vervollständigungen vorgestellt, die sowohl masselose RHNs als auch massereiche RHNs um die Planck-Skala herum einschließen und Rang erhöhende Beiträge durch Zweischleifenkorrekturen ermöglichen.

Contents

1. Introduction

Neutrinos are assumed to be massless in the Standard Model (SM) of particle physics. However, oscillation experiments have shown that solar, atmospheric, and reactor neutrinos undergo mixing, indicating the existence of at least two massive active neutrinos (see for example [1]). Unlike the quark sector, the mixing angles in the neutrino sector are relatively large, and the CP-violating phase is not suppressed. Furthermore, observations of cosmological structure formation [1] and beta decay spectra [2] have set upper bounds on the masses of neutrinos, which are many orders of magnitude smaller than all other SM masses. Despite this experimental progress, the ordering of masses as well as the nature of the neutrino - whether it is Dirac or Majorana - remains unknown. The observation of neutrinoless double beta decay would uniquely determine neutrinos to be Majorana particles. Sensitivity improvements in cosmological observation and direct measurements will eventually distinguish between different orderings.

To account for these findings, the SM must be extended to accommodate neutrino masses. Additionally, from a theoretical point of view, their smallness compared to all other SM particles should be explained in a natural way, which does not require extended fine-tuning of parameters. Neutrino mass models are often linked to other open questions in particle physics and cosmology, such as dark matter [3, 4] and baryogenesis via leptogenesis [5]. They may also be embedded into higher symmetry structures, such as grand unifying theories [6].

The seesaw type-I model extends the SM by Right-Handed Neutrinos (RHNs) [7–11], which makes it particularly simple and hence appealing. RHNs transform trivially under all gauge groups and thus allow for Majorana mass terms. The seesaw model is natural in the sense that active neutrinos become lighter while their right-handed counterparts become heavier. The type-I seesaw model and other extensions that introduce new particles at high scales can be described by effective field theories at low-energy observational scales in a model-independent manner. The introduction of Majorana neutrino masses is achieved through the unique dimension-five Weinberg operator [12], and their smallness corresponds to cut-off suppression, which marks the validity range of the effective description. Due to the large separation of scales, the running of parameters induced by quantum corrections becomes significant. Although the one-loop renormalization of the Weinberg operator is complete [13–15], the two-loop beta functions are not yet finalized. However, at this order in perturbation theory, specific diagrams exist that radiatively generate neutrino mass and increase the rank of the mass matrix [16]. One potential scenario includes two massive neutrinos and one massless neutrino at the cut-off scale. As a consequence, fewer parameters are needed, and predictivity is enhanced. Oscillation experiments do not rule out this case, making the two-loop beta function theoretically interesting.

The radiative mass corrections constitute a lower bound on neutrino masses and yield interesting phenomenological consequences that have not been considered so far. Moreover, completing the two-loop beta function improves the accuracy of numerically evaluating the running behavior of mixing parameters.

Equivalent rank-increasing diagrams for the RHN mass matrix also exist [17–19]. Assuming Majorana masses around the Planck scale translates to lepton number breaking at the aforementioned energies. The breaking of all global symmetries through gravity motivates this assumption [17]. If some RHNs remain massless at the Planck scale, two-loop quantum corrections induce lighter states around the seesaw scale. Therefore, no new scale or additional free parameters are required, and predictivity is enhanced. However, the exact form of the mass matrix at the Planck scale requires further justification. This study explores gauge extensions to the Standard Model, which are unaffected by gravity. Left-Right (LR) symmetry models naturally include Right-Handed Neutrinos and can be incorporated into larger unifying theories, making them appealing.

The thesis is structured as follows: chapter 2 provides a summary of the SM and mass generation via Spontaneous Symmetry Breaking (SSB). It also explains how particle oscillations arise in the quark and lepton sectors and clarifies the difference between Dirac and Majorana masses. The chapter reviews the three seesaw mechanisms as well as the LR extension, which provides the necessary neutrino masses. Finally, the chapter introduces the effective description of neutrino masses. Chapter 3 provides the necessary ideas and calculation techniques for renormalizing the Weinberg operator and explains the use of the Background Field Method (BFM) in this context. The rank-increasing contributions are explicitly calculated, and the results are shown for the complete two-loop beta functions. In chapter 4, the phenomenological implications of the beta functions are analyzed with regard to neutrino mixing parameters and masses. Analytical results are derived and checked by numerical evaluation. Chapter 5 deals with RHN mass models. The thesis presents general considerations before analyzing specific gauge extensions to the SM. LR symmetric models are of particular interest. Finally, chapter 6 summarizes the findings of this thesis.

2. Neutrino Masses

The Standard Model (SM) of particle physics is the most rigorously tested and precise theory of nature. It describes particles as excitations of quantum fields. All fermions – except the neutrino – obtain their mass through the Higgs mechanism, which is responsible for electroweak symmetry breaking. The Higgs mechanism is summarised below to illustrate the difference between neutrinos and other charged fermions in mass generation. Additionally, the concept of particle oscillations is introduced.

2.1. Standard Model

The SM is based on the direct product of the simple gauge groups $\mathrm{SU}(3) \times \mathrm{SU}(2)_\mathrm{L} \times \mathrm{U}(1)_Y$. The fermionic fields transform in the trivial and (anti-)fundamental representations and are denoted as $(R(\mathrm{SU}(3)), R(\mathrm{SU}(2)), Y)$, where $R(G)$ is the representation of the group and Y the hypercharge of the field under $\mathrm{U}(1)_Y$. The trivial representation is denoted by $\mathbf{1}$ and the (anti-) fundamental representation of $\mathrm{SU}(N)$ by $\mathbf{N}$ ($\overline{\mathbf{N}}$), while higher numbers correspond to higher multiplets. According to this classification, the SM fermions expanded in the $\mathrm{SU}(2)_\mathrm{L}$ indices are:

$$\begin{aligned}
&\text{left-handed fermions:} && \ell = \begin{pmatrix} \nu \\ E_\mathrm{L} \end{pmatrix} = (\mathbf{1}, \mathbf{2}, -1), \\
&\text{right-handed fermions:} && E_\mathrm{R} = (\mathbf{1}, \mathbf{1}, -2), \\
&\text{left-handed quarks:} && Q_\mathrm{L} = \begin{pmatrix} U_\mathrm{L} \\ D_\mathrm{L} \end{pmatrix} = (\mathbf{3}, \mathbf{2}, 1/3), \\
&\text{right-handed quarks:} && D_\mathrm{R} = (\mathbf{3}, \mathbf{1}, -2/3), \quad U_\mathrm{R} = (\mathbf{3}, \mathbf{1}, 4/3).
\end{aligned}$$

To deal with gauge anomalies, it is advantageous to work with fermions of the same chirality (section 5.1). Utilizing the charge conjugation operator

$$\psi^c = \begin{pmatrix} \psi^\mathrm{c}_\mathrm{L} \\ \psi^\mathrm{c}_\mathrm{R} \end{pmatrix} = C\overline{\psi}^\mathrm{T} = \mathrm{i}\gamma^0\gamma^2\overline{\psi}^\mathrm{T} = \begin{pmatrix} \mathrm{i}\sigma_2\psi^*_\mathrm{R} \\ -\mathrm{i}\sigma_2\psi^*_\mathrm{L}, \end{pmatrix} \tag{2.1}$$

which switches chirality, the re-expressed fermions are: $e^c_R = (\mathbf{1}, \mathbf{1}, -2)$, $u^\mathrm{c}_\mathrm{R} = (\overline{\mathbf{3}}, \mathbf{1}, -4/3)$, $d^\mathrm{c}_\mathrm{R} = (\overline{\mathbf{3}}, \mathbf{1}, 2/3)$. Based upon the previously introduced symmetry groups and matter fields, the most general gauge invariant chiral Lagrangian contains the following terms:

$$\mathcal{L}_\mathrm{Gauge} = \bar{\psi}(i\partial_\mu + g_A A^a_\mu T^a_R)\gamma^\mu\psi - \frac{1}{4}F^a_{\mu\nu}F^{a\mu\nu} + \mathcal{L}_\mathrm{GF} + \mathcal{L}_\mathrm{FP}, \tag{2.2}$$

where $\psi = \ell, E_R, Q_L, D_R, U_R$ represents all fermionic fields, $A^a_\mu = G^a_\mu, W^a_\mu, B_\mu$ all gauge boson fields with the respective representation T^a_R for the fermion ψ and $F^a_{\mu\nu} = \partial_\mu A^a_\nu + \partial_\nu A^a_\mu + g_A f^a_{bc} A^b_\mu A^c_\nu$. $\mathcal{L}_{\text{GF}}$ and $\mathcal{L}_{\text{FP}}$ denote the gauge fixing and ghost term, respectively, which follow from the Faddeev-Popov quantization procedure for non-abelian gauge theories. They read [20]:

$$\mathcal{L}_{\text{GF}} = -\frac{1}{2\xi}\mathcal{G}^a[A]^2, \tag{2.3}$$

$$\mathcal{L}_{\text{FP}} = \bar{\theta}^a_A \frac{\delta \mathcal{G}^a[A]}{\delta \omega^b} \theta^b_A, \tag{2.4}$$

where $\mathcal{G}^a[A]$ describes the gauge fixing condition and θ^a_A the anticommunting scalar ghost fields related to the gauge field A. While $\mathcal{G}^a[A]$ is often chosen to be the Feynman gauge ($\xi = 1$), in this work, the background field gauge is used, as it offers great advantages regarding the renormalization of gauge theories. A detailed introduction to the background field method can be found in section 3.2.

2.1.1. Higgs Mechanism

Mass terms for chiral fermions of the form $m\bar{\psi}_L\psi_R$ violate gauge invariance due to their non-trivial transformation behavior under SU(2)_L. The mechanism that gives the charged fermions their mass proceeds via the coupling to a scalar field, the so-called Higgs field $H = (1, \mathbf{2}, 1)$, which transforms as a SU(2)_L doublet. The associated potential can be parameterized as follows:

$$V(H^\dagger H) = \mu^2 (H^\dagger H) + \lambda (H^\dagger H)^2, \tag{2.5}$$

where in case of $\mu^2 < 0$, the Ground State (GS) of H (Vacuum Expectation Value (VEV)) is non-zero (fig. 2.1). The Higgs field can be developed around that GS (v) [21], which is conventionally chosen to be real-valued [22]:

$$H = \frac{1}{\sqrt{2}} \begin{pmatrix} H^+ \\ \frac{1}{\sqrt{2}}(v + h(x) + \mathrm{i}A) \end{pmatrix}, \tag{2.6}$$

in terms of the physical Higgs boson h and the three Nambu-Goldstone bosons A, $H^\pm$.

2.1.2. Spontaneous Symmetry Breaking

Since the potential is invariant under rotation in the complex H-plane, infinite VEVs exist. By using the SU(2)_L generators $T_a = \frac{\sigma_a}{2}$ (σ^i being the Pauli matrices) and the radial parameterization of the Higgs field around the GS, eq. 2.6 simplifies to [22, 23]:

$$H = e^{\mathrm{i}T^a\xi^a} \begin{pmatrix} 0 \\ \frac{1}{\sqrt{2}}(v + h(x)) \end{pmatrix} \xrightarrow{SU(2)_L \times U(1)_Y} \begin{pmatrix} 0 \\ \frac{1}{\sqrt{2}}(v + h(x)) \end{pmatrix}, \tag{2.7}$$

where the VEV v and the radial excitation $h(x)$ are real-valued [23]. The pre-factor $e^{\mathrm{i}T^a\xi^a}$, which unifies all imaginary parts, is eliminated in the unitary gauge through a

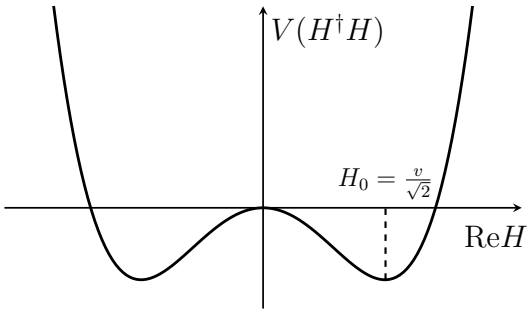

Figure 2.1.: Higgs potential with $\mu^2 < 0$ along the real part $\Re$ of H along one slice in SU(2) plane. The vacuum expectation value (H_0) is non-zero.

gauge transformation. However, this results in the system no longer being gauge invariant because a specific VEV breaks the symmetry, a phenomenon known as Spontaneous Symmetry Breaking (SSB) (see eq. 2.7). The radial excitation $h(x)$ is identified as the Higgs boson, while the massive gauge fields absorbed the radial ξ^a fields [23]. After SSB, the VEV of the Higgs doublet remains invariant under one specific transformation, which is a combination of the $\mathrm{SU(2)_L}$ generator T^3 and the hypercharge Y:

$$Q_{\mathrm{EM}} = T_{3L} + \frac{1}{2} Y_\phi, \tag{2.8}$$

which is neutral for the second component of H. This remaining U(1) symmetry relates to the well-known electromagnetism with the photon as massless gauge boson [23].

The coupling of boson and fermion fields with the Higgs field maintains the local symmetries and results in mass terms for the fermions and the electroweak bosons after SSB. In the latter case, the explicit form for the coupling and resulting W and h mass terms is given by [21]:

$$\mathcal{L}_{\mathrm{Higgs}} = (D_\mu H)^\dagger (D^\mu H) - V(H^\dagger H) \supset 2\lambda v^2 h^2 + \frac{1}{4} g^2 v^2 W_\mu^+ W_\mu^-, \tag{2.9}$$

where the charged $W_\mu^\pm = \frac{1}{\sqrt{2}}(W_\mu^1 \mp \mathrm{i} W_\mu^2)$ are superpositions of two SU(2) generators. The mixing of W_μ^3 and B_μ gives the massless photon and massive Z boson. These concepts will later be relevant for understanding the symmetry-breaking patterns of extensions to the SM.

2.1.3. Fermion Masses

Fermion masses are generated through Yukawa couplings Y_Ψ

$$\mathcal{L}_{\mathrm{Yuk}} = -\overline{Q_{\alpha \mathrm{L}}} \left(Y_{\mathrm{u}}\right)_{\alpha\beta} \widetilde{H} U_{\beta \mathrm{R}} - \overline{Q_{\alpha \mathrm{L}}} (Y_{\mathrm{d}})_{\alpha\beta} H D_{\beta \mathrm{R}} - \overline{\ell_{\alpha \mathrm{L}}} (Y_l)_{\alpha\beta} H E_{\beta \mathrm{R}} + \mathrm{h.c.}, \tag{2.10}$$

where Greek indices refer to the generation of the quarks and leptons, respectively. $\widetilde{H} = i\sigma_2 H^* = (1, \mathbf{2}, -1)$ is the conjugated Higgs field, which also transforms as a $\mathrm{SU(2)_L}$ doublet (SU(2) is pseudoreal) but with inverse hypercharge.

After SSB, the (conjugated) Higgs fields acquire its VEV in the (first) second component, which leads to mass matrices

$$M_{\mathrm{u}} = \frac{v}{\sqrt{2}} Y_{\mathrm{u}}, \quad M_{\mathrm{d}} = \frac{v}{\sqrt{2}} Y_{\mathrm{d}}, \quad M_l = \frac{v}{\sqrt{2}} Y_l. \tag{2.11}$$

The Left-Handed Neutrinos (LHNs) (also called active neutrinos) stay massless, as there are no Right-Handed Neutrinos (RHNs) $N = (1, \mathbf{1}, 0)$ within the SM, which enable a mass term of the form: $\overline{\ell_{\alpha \mathrm{L}}} (Y_\nu)_{\alpha\beta} \widetilde{H} N_{\beta \mathrm{R}}$.

2.1.4. Particle Oscillations

The mass matrices obtained in section 2.1.3 are, in general, non-diagonal with arbitrary complex entries. The flavor eigenstates present in the tree-level Lagrangian thus do not correspond to the mass eigenstates. Through field redefinitions of the type $\psi = U_\psi \psi'$ ($\psi = \ell, E_R, U_L, D_L, D_R, U_R$), the mass matrices can be diagonalized (D_ψ) via the Singular Value Decomposition (SVD) procedure:

$$\begin{aligned} U_{U_L}^\dagger M_U U_{U_R} &= D_U, \\ U_{D_L}^\dagger M_D U_{D_R} &= D_D, \\ U_\ell^\dagger M_\ell U_{E_R} &= D_\ell. \end{aligned} \tag{2.12}$$

The procedure is slightly modified for Majorana mass terms, which are introduced in eq. 2.20 in the next section. In this case, one unitary matrix is sufficient for the SVD of the symmetric Majorana mass matrix

$$U_\nu^T M_\nu U_\nu = D_\nu. \tag{2.13}$$

Subsequently, the weak current from eq. 2.2 after SSB is modified in terms of the mass eigenstates ψ'

$$\begin{aligned} \overline{U_L} \gamma^\mu D_L &= \overline{U'_L} \gamma^\mu \tilde{U}_{\mathrm{CKM}} D'_L \\ \overline{E_L} \gamma^\mu \nu_L &= \overline{E'_L} \gamma^\mu \tilde{U}_{\mathrm{PMNS}} \nu'_L, \end{aligned} \tag{2.14}$$

with

$$\tilde{U}_{\mathrm{CKM}} = U_{U_L}^\dagger \tilde{U}_{D_L}, \quad \tilde{U}_{\mathrm{PMNS}} = U_{E_L}^\dagger \tilde{U}_\nu. \tag{2.15}$$

The rotation matrices are called Cabibbo-Kobayashi-Maskawa (CKM) matrix and Pontecorvo–Maki–Nakagawa–Sakata (PMNS) matrix for quarks and leptons, respectively. Both $\tilde{U}_{\mathrm{CKM}}$ and $\tilde{U}_{\mathrm{PMNS}}$ contain unphysical Degrees-of-Freedom (DOFs), which can be removed by global phase transformation of the fermionic fields. In the case of up- and down-type quarks, three (two) individual phase transformations $P_U = \mathrm{diag}(e^{\mathrm{i}\phi_u}, e^{\mathrm{i}\phi_c}, e^{\mathrm{i}\phi_t})$ ($P_D = \mathrm{diag}(e^{\mathrm{i}\phi_d}, e^{\mathrm{i}\phi_s}, 1)$) on $U'_{\alpha L/R} \to P_U U'_{\alpha L/R}$ ($D'_{\alpha L/R} \to P_D D'_{\alpha L/R}$) can be made, without changing the diagonal mass matrix. Global phase transformations are unphysical; hence, only two independent transformations exist for $D_{\alpha L}$.

This transformation is no longer possible for Majorana neutrinos. While the equivalent phase redefinitions $P_E = \mathrm{diag}(e^{\mathrm{i}\phi_e}, e^{\mathrm{i}\phi_\mu}, e^{\mathrm{i}\phi_\tau})$ exist for $E'_{\alpha L/R} \to P_E\, E'_{\alpha L/R}$, the same does not hold for $\nu_{\alpha L}$ because it would change the mass matrix according to eq. 2.13. Only 3 DOFs can be removed compared to the five from the quark sector:

$$V_{\mathrm{CKM}} = P_U^\dagger \tilde{U}_{\mathrm{CKM}} P_D, \quad V_{\mathrm{PMNS}} = P_E^\dagger \tilde{U}_{\mathrm{PMNS}}, \tag{2.16}$$

defining the PMNS matrix. The standard parameterization for the CKM and PMNS matrix [24] will be used throughout this work:

$$V = \begin{pmatrix} c_{12}c_{13} & s_{12}c_{13} & s_{13}e^{-\mathrm{i}\delta} \\ -c_{23}s_{12} - s_{23}c_{12}s_{13}e^{\mathrm{i}\delta} & c_{23}c_{12} - s_{23}s_{12}s_{13}e^{\mathrm{i}\delta} & s_{23}c_{13} \\ s_{23}s_{12} - c_{23}c_{12}s_{13}e^{\mathrm{i}\delta} & -s_{23}c_{12} - c_{23}s_{12}s_{13}e^{\mathrm{i}\delta} & c_{23}c_{13} \end{pmatrix} \tag{2.17}$$

for the CKM matrix and

$$V \cdot \begin{pmatrix} e^{\mathrm{i}\rho} & 0 & 0 \\ 0 & e^{\mathrm{i}\sigma} & 0 \\ 0 & 0 & 1 \end{pmatrix} \tag{2.18}$$

for the PMNS matrix. The two phases eliminated in the quark sector by the down-type quarks were reintroduced. c_{ij} (s_{ij}) abbreviates $\cos\theta_{ij}$ ($\sin\theta_{ij}$), with θ_{ij} being the mixing angle between the generations i and j. δ is referred to as the Dirac phase because it emerges for both Majorana and Dirac particles, while the Majorana phases ρ and σ only appear in the Majorana case. All three provide a source for CP violation.

Particles are produced in the flavor basis but will propagate in the mass basis, giving rise to neutrino oscillation. Table 2.1 [25] summarizes the experimental data from oscillation experiments regarding the three mixing angles, the Dirac phase, and the mass differences $\Delta m^2_{ij} = m^2_i - m^2_j$ which are responsible for the oscillation length.

From the oscillation length, only the absolute value of the mass difference Δm^2_{ij} can be

	Normal Ordering [3σ]	Inverted Ordering [3σ]
$\sin^2\theta_{12}$	$0.304^{+0.039}_{-0.035}$	$0.304^{+0.039}_{-0.035}$
$\sin^2\theta_{23}$	$0.573^{+0.043}_{-0.158}$	$0.575^{+0.042}_{-0.156}$
$\sin^2\theta_{13}$	$0.2219^{+0.0191}_{-0.0187}$	$0.02238^{+0.00190}_{-0.00186}$
$\delta\,[^\circ]$	232^{+118}_{-88}	276^{+68}_{-82}
$\frac{\Delta m^2_{21}}{10^{-5}\mathrm{eV}^2}$	$7.42^{+0.62}_{-0.60}$	$7.42^{+0.62}_{-0.60}$
$\frac{\Delta m^2_{32}}{10^{-3}\mathrm{eV}^2}$	$+2.517^{+0.081}_{-0.082}$	$-2.498^{+0.084}_{-0.083}$

Table 2.1.: Neutrino Oscillation Parameters. Summarized are the global fits regarding oscillation experiments for normal and inverted ordering [25].

determined, allowing for two possible mass orderings:

$$\begin{aligned} m_3 > m_2 > m_1 \qquad & \text{NormalOrdering(NO)}, \\ m_2 > m_1 > m_3 \qquad & \text{InvertedOrdering(IO)}. \end{aligned} \tag{2.19}$$

Table 2.1 includes the experimental data for both mass orderings. Since Δm^2_{21} and Δm^2_{32} are non-zero, at least two neutrinos must be massive.

2.2. Neutrino Mass Models

Neutrino mass models describe renormalizable extensions to the SM, so-called Ultraviolet (UV) completions, as opposed to the model-independent Effective Field Theory (EFT) approach, which will be introduced in section 2.3.3. These models are categorized as Majorana or Dirac types depending on the nature of the neutrino. Dirac mass terms include distinct left- and right-handed fields $m\overline{\psi_R}\psi_L$, while Majorana mass terms only contain either one:

$$\mathcal{L}_M = \overline{N_{\alpha R}} \mathrm{i}\partial\!\!\!/ N_{\alpha R} - \frac{1}{2} M_{\alpha\beta} \overline{N^c_{\alpha R}} N_{\beta R} - \frac{1}{2} M^\dagger_{\alpha\beta} \overline{N_{\alpha R}} N^c_{\beta R}. \tag{2.20}$$

$\beta = 1, ..., n_\mathrm{R}$ denotes the generation index analogous to the SM with n_R being the number of generations, and the hermitian conjugated was explicitly written in this case. The structure $\overline{N^c_{\alpha R}} N_{\beta R}$ demands a symmetric mass matrix and implies that the Majorana particle (later the RHN) cannot carry any charges. Furthermore, it excludes certain representations of the gauge groups (such as the fundamental). Hence, only the neutrino can be of Majorana type after SSB. For Dirac neutrinos, particle and antiparticle are distinct, while a Majorana neutrino is its own antiparticle.

2.2.1. Type-I Seesaw Model

The inclusion of RHNs $N_R = (\mathbf{1}, \mathbf{1}, 0)$ is the most straightforward method to generate neutrino masses and account for their smallness. RHNs transform trivially under the SM gauge group and can, therefore, acquire a Majorana mass. The extension of the SM Lagrangian reads:

$$\mathcal{L}_\mathrm{RHN} = -\frac{1}{2} M_{\alpha\beta} \overline{N^c_{\alpha R}} N_{\beta R} - \overline{\ell_{\alpha \mathrm{L}}} Y_{\alpha\beta} \widetilde{H} N_{\beta \mathrm{R}} + \mathrm{h.c.} \tag{2.21}$$

After SSB, the Yukawa coupling provides Dirac masses as for the other SM fermions along with an additional Majorana mass term. Rewriting this in terms of a standard Majorana mass matrix for the multiplet $(\nu^c_{\alpha L}, N_{\beta R})$ gives:

$$\mathcal{L} \subset -\frac{1}{2} \begin{pmatrix} \overline{\nu_{\alpha L}}^\mathrm{T} & \overline{N^c_{\beta R}}^\mathrm{T} \end{pmatrix} \begin{pmatrix} 0 & \frac{v}{\sqrt{2}} Y_{\alpha\beta'} \\ \frac{v}{\sqrt{2}} Y^\mathrm{T}_{\beta\alpha'} & M_{\beta\beta'} \end{pmatrix} \begin{pmatrix} \nu^c_{\alpha' L} \\ N_{\beta' R} \end{pmatrix}. \tag{2.22}$$

Again, the mass matrix is non-diagonal, and flavor eigenstates need to be redefined via $(\nu^c_L, N_R) = U(\nu'^c_L, N'_R)$ and $U^T M U = D$ as in eq. 2.13. Consequently, left- and

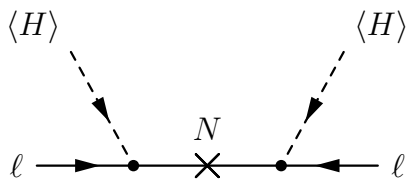

Figure 2.2.: Tree level diagrams for type-I seesaw mechanism. It describes the Majorana mass generation for left-handed neutrinos ν after SSB $\langle H \rangle$ by including a fermion singlets N (right-handed neutrinos).

right-handed neutrinos mix, but also LHNs among themselves, which gives rise to the aforementioned neutrino-oscillations. The resulting mass eigenvalues are for $M \gg vY$:

$$\begin{aligned} m_{\text{light}} &= m_{\nu'} \approx -\frac{v^2}{2} Y^T M^{-1} Y \\ m_{\text{heavy}} &= m_{N'} \approx M \end{aligned} \tag{2.23}$$

As M increases, $m_{\nu'}$ decreases, while the mixing between ν and N ($\mathcal{O}(M^{-1})$) becomes smaller, hence the name seesaw model. Fig. 2.2 shows a diagrammatic representation of the type-I seesaw model.

Nevertheless, not all active neutrinos necessarily acquire mass through this process. The number of massless Majorana neutrinos at the tree level depends on the number of generations of the RHN and reads $n_{\text{L}} - n_{\text{R}}$ ($n_{\text{L/R}}$ is the number of left-/right-handed neutrino generations) [26].

2.2.2. Type-II and III Seesaw Models

Other possibilities that accommodate left-handed Majorana neutrinos exist besides heavy fermion singlets.

In the type-II seesaw model (fig. 2.3 (a)), triplet scalars $\Delta = (\mathbf{1}, \mathbf{3}, +2)$ are added to generate the Majorana mass term [27, 28]:

$$\mathcal{L}^{\text{II}} = -\frac{1}{2} \overline{\ell^{\text{c}}_{\alpha\text{L}}} \left(Y_\nu^\Delta\right)_{\alpha\beta} \text{i}\sigma_2 \left(\vec{\sigma} \cdot \vec{\Delta}\right) \ell_{\alpha\text{L}} - \mu_\Delta H^{\text{T}} \text{i}\sigma_2 \left(\vec{\sigma} \cdot \vec{\Delta}^\dagger\right) H + \text{h.c.} \tag{2.24}$$

Here, Δ is written in the adjoint basis – which transforms in the triplet representation. The shown combination is gauge invariant, because the tensor representation of $\ell_{\alpha L}$, $\ell_{\beta L}$ $(\mathbf{1}, \mathbf{2}, -1) \times (\mathbf{1}, \mathbf{2}, -1) \subset (\mathbf{1}, \mathbf{3}, -2)$ contains a triplet representation and thus gives a singlet together with Δ. The invariance can also be seen from the explicit transformation behavior under SU(2): $\ell \to U\ell$ and $\Delta \to U\Delta U^\dagger$. The neutrino mass follows from the VEV of Δ and its relation to M_Δ through the scalar potential and ultimately yields:

$$m_\nu = \frac{v^2 \mu_\Delta Y_\nu^\Delta}{2 M_\Delta}. \tag{2.25}$$

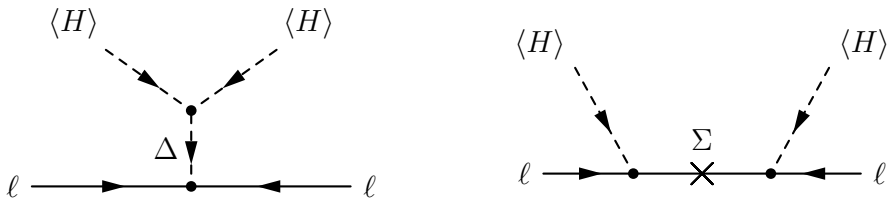

(a) Type-II (b) Type-III

Figure 2.3.: Tree level diagrams for type-II (a) and type-III (b) seesaw mechanism. They describe the Majorana mass generation for left-handed neutrinos ν after SSB $\langle H \rangle$ by including a scalar triplet Δ or a scalar fermion Σ.

An easier way to obtain the same result is via the effective description of neutrino mass and integrating-out (section 2.3.2) the heavy scalar triplet.

The type III seesaw model (fig. 2.3 (b)) combines the type I and II by introducing fermionic triplets Σ to the SM. The resulting Lagrangian reads [29]:

$$\mathcal{L}^{\text{III}} = -M_{\Sigma}^{ij}\text{Tr}\left[\overline{\Sigma_{iR}^{c}}\Sigma_{jR}\right] - \sqrt{2}Y_{\Sigma}^{i\alpha}\widetilde{H}^{\dagger}\overline{\Sigma_{iR}}\ell_{\alpha L} + \text{h.c.}, \tag{2.26}$$

where $\Sigma = \vec{\sigma}\cdot\vec{\Sigma}$ is also written in the adjoint basis and $\Sigma^{\text{c}} = C\Sigma^{*}$ according to the definition in eq. 2.1. The easiest way to obtain the mass matrix is to revert to the effective description, which gives after SSB:

$$m_{\nu} = -\frac{v^2}{2}Y_{\Sigma}^{T}M_{\Sigma}^{-1}Y_{\Sigma}. \tag{2.27}$$

Type-II and type-III predict neutrino masses inversely proportional to the mass of a heavy particle, justifying the classification of seesaw models.

2.2.3. Left Right Symmetric Models

Another possibility for accommodating Majorana neutrinos is to extend the SM gauge group and naturally include RHN in contrast to the seesaw models, which maintain the gauge structure and only extend the matter content.

The SM breaks parity by differentiating between left-and right-handed particles in terms of their $\text{SU}(2)_{\text{L}}$ representations. LR symmetric models [30–34] restore parity invariance at high energies and break it dynamically via SSB, yielding the SM as low energy limit. In analogy to the $\text{SU}(2)_{\text{L}}$ gauge group, $\text{SU}(2)_{\text{R}}$ is introduced. The full SM gauge groups consist of

$$\text{SU}(3)\times\text{SU}(2)_{L}\times\text{SU}(2)_{R}\times\text{U}(1)_{\tilde{Y}}, \tag{2.28}$$

with a modified hypercharge $\tilde{Y}$ that will break down to Y. In the context of LR models, representations are denoted with regard to $\tilde{Y}$. Following the $\text{SU}(2)_{\text{L}}$ structure, D_{R} and U_{R} are grouped into an $\text{SU}(2)_{\text{R}}$ doublet and RHNs are introduced to complete the right-handed leptonic doublet with E_{R}. The matter content with respect to eq. 2.28 reads:

left-handed fermions: $L_L = \begin{pmatrix} \nu \\ E_L \end{pmatrix} = (\mathbf{1}, \mathbf{2}, \mathbf{1}, -1),$

right-handed fermions: $L_R = \begin{pmatrix} N_R \\ E_R \end{pmatrix} = (\mathbf{1}, \mathbf{1}, \mathbf{2}, -1),$

left-handed quarks: $Q_L = \begin{pmatrix} U_L \\ D_L \end{pmatrix} = (\mathbf{3}, \mathbf{2}, \mathbf{1}, 1/3),$

right-handed quarks: $Q_R = \begin{pmatrix} U_R \\ D_R \end{pmatrix} = (\mathbf{3}, \mathbf{1}, \mathbf{2}, 1/3).$

Gauge anomaly cancelation (section 5.1) is ensured and explicitly checked in section 5.4. The matter content suggests that $\tilde{Y}$ can be identified with $B-L$ (baryon number – lepton number). While being an anomaly-free global symmetry in the SM, $B-L$ is promoted to a gauge symmetry in LR models. To be consistent with current observations, it is necessary that

$$\mathrm{SU}(2)_R \times \mathrm{U}(1)_{\tilde{Y}} \to \mathrm{U}(1)_Y \tag{2.29}$$

via SSB. Therefore, the breaking patterns should satisfy the relation:

$$Y = \tilde{Y} + 2T_{3R}, \tag{2.30}$$

or reformulated using eq. 2.8 in terms of Q_{EM}

$$Q_{\mathrm{EM}} = \frac{1}{2}\tilde{Y} + T_{3R} + T_{3L}. \tag{2.31}$$

In the following, only a brief summary of the standard symmetry-breaking mechanism is provided since section 5.4 will introduce a modified approach that maintains one or two RHNs massless at the tree level. The scalar sector includes three scalar fields, two of which ($\Delta_L = (\mathbf{1}, \mathbf{3}, \mathbf{1}, 1)$, $\Delta_R = (\mathbf{1}, \mathbf{1}, \mathbf{3}, 1)$) transform in the triplet representation and one as bidoublet ($\Phi = (\mathbf{1}, \mathbf{2}, \overline{\mathbf{2}}, 0)$):

$$\begin{aligned}
\Delta_{\mathrm{L}} = \frac{\vec{\sigma}}{2} \cdot \vec{\Delta}_{\mathrm{L}} &= \begin{pmatrix} \delta_{\mathrm{L}}^{+}/\sqrt{2} & \delta_{\mathrm{L}}^{++} \\ \delta_{\mathrm{L}}^{0} & -\delta_{\mathrm{L}}^{+}/\sqrt{2} \end{pmatrix}, \qquad \Delta_{\mathrm{L}} \to U_{\mathrm{L}} \Delta_{\mathrm{L}} U_{\mathrm{L}}^{\dagger}, \\
\Delta_{\mathrm{R}} = \frac{\vec{\sigma}}{2} \cdot \vec{\Delta}_{\mathrm{R}} &= \begin{pmatrix} \delta_{\mathrm{R}}^{+}/\sqrt{2} & \delta_{\mathrm{R}}^{++} \\ \delta_{\mathrm{R}}^{0} & -\delta_{\mathrm{R}}^{+}/\sqrt{2} \end{pmatrix}, \qquad \Delta_{\mathrm{R}} \to U_{\mathrm{R}} \Delta_{\mathrm{R}} U_{R}^{\dagger}, \\
\Phi = \phi_{\mathrm{L}} \times \phi_{\mathrm{R}}^{\dagger} &= \begin{pmatrix} \Phi_1^0 & \Phi_1^+ \\ \Phi_2^- & \Phi_2^0 \end{pmatrix}, \qquad \Phi \to U_{\mathrm{L}} \Phi U_{\mathrm{R}}^{\dagger}.
\end{aligned} \tag{2.32}$$

The charges indicated in eq. 2.32 follow eq. 2.31 with $T_{3\mathrm{L/R}}$ expressed in the according representation: $T_{3\mathrm{L/R}}(\Delta) = \left[T_{3\mathrm{L/R}}^{\mathrm{fun}}, \Delta\right]$, $T_{3\mathrm{L/R}}(\Phi_{ij}) = T_{3\mathrm{L}}\phi_{i\mathrm{L}} - T_{3\mathrm{R}}\phi_{j\mathrm{R}}^{\dagger}$. $\delta_{L/R}^0$ and Φ will aquire VEVs as they remain invariant under $\mathrm{U}(1)_{\mathrm{EM}}$. Assuming $v_{\Delta\mathrm{R}} \gg v_{\Phi 1,2}$ and thus only taking into account the effect of Δ_{R}, the symmetry will be broken according to eq 2.29. Φ takes the role of H and gives the fermions their masses:

$$\mathcal{L}^{\mathrm{Yuk}} = -\overline{Q_{\alpha\mathrm{L}}} \left(h_{\alpha\beta}\Phi + \tilde{h}_{\alpha\beta}\tilde{\Phi}\right) Q_{\beta\mathrm{R}} - \overline{L_{\alpha\mathrm{L}}} \left(g_{\alpha\beta}\Phi + \tilde{g}_{\alpha\beta}\tilde{\Phi}\right) L_{\beta\mathrm{R}} + \mathrm{h.c.} \tag{2.33}$$

with $\tilde{\Phi} = \mathrm{i}\sigma_2\Phi(-\mathrm{i})\sigma_2$ being the charge conjugated bidoublet (same transformation properties) and analog for the lepton doublets $L_{\mathrm{L/R}}$. However, for the latter, the scalar triplet induces additional Majorana mass terms (compared to eq. 2.24 from seesaw type-II):

$$\mathcal{L}_{\mathrm{M}} = -\frac{1}{2} h^{\Delta}_{\alpha\beta} \overline{L^c_{\alpha \mathrm{L/R}}} i\sigma_2 \Delta_{\mathrm{L/R}} L_{\beta \mathrm{L/R}}, \tag{2.34}$$

which leads to a modified seesaw mechanism for $v_{\Delta R} \gg v_{\Delta L}$. More detailed discussions on the scalar and Yukawa sector follow in section 5.4.

2.3. Effective Description

The new particles introduced in the neutrino mass models are typically very heavy to explain the tinny active neutrino masses via the seesaw mechanism. Therefore, they cannot be directly observed in present-day experiments. Effective Field Theorys (EFTs) [35, 36] describe the low energy limit in terms of low energy observables. The influence of high-energy components is incorporated through a systematic expansion series based on the cut-off scale Λ, which represents the typical energy or mass scale of the high-energy contribution (referred to as the UV completion) to the theory. The EFT is derived by systematically eliminating high-energy DOFs.

From a Lagrangian point of view, the expansion in Λ will take place in terms of operators made up of fields with a lower mass scale:

$$\mathcal{L}_{\mathrm{EFT}} = \mathcal{L}_{\mathcal{D}\leq 4} + \frac{c^{(5)}}{\Lambda}\mathcal{O}^{(5)} + \frac{c^{(6)}}{\Lambda^2}\mathcal{O}^{(6)} + \frac{c^{(7)}}{\Lambda^3}\mathcal{O}^{(7)} + ... \tag{2.35}$$

until the desired precision $\mathcal{O}(\Lambda_{\mathrm{Obs}}/\Lambda)^n$. $\mathcal{O}^{(n)}$ describe higher dimensional operators built from low mass fields that are contained in the low energy Lagrangian $\mathcal{L}_{\mathcal{D}\leq 4}$ ($\dim(\mathcal{O}) < 4$). $c^{(n)}$ denote the dimensionless Wilson coefficients belonging to the corresponding operator $\mathcal{O}^{(n)}$. In case of $\mathcal{L}_{\mathcal{D}\leq 4} = \mathcal{L}_{\mathrm{SM}}$ the EFT is called Standard Model Effective Field Theory (SMEFT) and higher dimensional operators are build from the SM fields $\ell, E_R, Q_L, U_R, D_R, H$.

2.3.1. Effective Action

The mapping between the operators appearing in the expansion and the UV completion, as well as their corresponding Wilson coefficients, is determined by the matching procedure. It ensures that UV theory and EFT produce the same results in the low energy limit or $\Lambda \to \infty$ respectively.

The functional approach compares the effective potentials Γ from the UV completion and the EFT. They must be equal to produce matching amplitudes. To calculate the effective potential, one starts with the generating functional Z, which is defined as

$$Z[\phi] = \int \mathcal{D}[\phi] e^{\mathrm{i}\int d^4x(\mathcal{L}[\phi] + J_\phi \phi)} \tag{2.36}$$

via the path integral. The effective action is defined as the Legendre transform of the generating functional:

$$\Gamma[\phi_{\text{cl}}] = -\underbrace{\text{i}\log Z\left[J_\phi\right]}_{\equiv W[J_\phi]} - \int d^4x J_\phi \phi_{\text{cl}}. \tag{2.37}$$

The classical field $\phi_{\text{cl}} = \langle\Omega|\phi|\Omega\rangle_{J_\phi}$ corresponds to the vacuum expectation value and satisfies

$$\phi_{\text{cl}} = \frac{\delta W[J_\phi]}{\delta J_\phi} \tag{2.38}$$

in agreement with the Legendre transformation. The effective action is the generating functional for all One-Particle-Irreducible (1PI) correlation functions [37] and therefore contains all quantum corrections. Hence, Γ describes a theory completely, demanding that Γ_{EFT} and Γ_{UV} must agree to provide matching results.

2.3.2. Functional Matching

The definition of the effective potential of eq. 2.37 is extended with a heavy field Φ

$$\Gamma_{\text{UV}}[\phi_{\text{cl}}, \Phi_{\text{cl}}] = -\text{i}\log Z\left[J_\phi, J_\Phi = 0\right] - \int d^4x J_\phi \phi_{\text{cl}}. \tag{2.39}$$

The heavy particle current is set to zero $J_\Phi = 0$ such that Φ cannot be produced on-shell but only runs inside loops [38]. The EFT is obtained by integrating out this heavy DOF. The matching condition based on the effective potentials becomes

$$\Gamma_{\text{EFT}}[\phi_{\text{cl}}] = \Gamma_{\text{UV}}[\phi_{\text{cl}}, \Phi_{\text{cl}}]. \tag{2.40}$$

At tree level Φ_{cl} solves the classical Equations-of-Motion (EOM)

$$\frac{\delta \mathcal{S}_{\text{UV}}[\phi, \Phi_{\text{cl}}[\phi_{\text{cl}}]]}{\delta \Phi} = 0. \tag{2.41}$$

As a result, the effective Lagrangian $\mathcal{L}_{\text{EFT}}$ at tree level is obtained by solving the EOM for Φ

$$\frac{\delta \mathcal{S}_{\text{UV}}[\phi, \Phi_{\text{cl}}[\phi_{\text{cl}}]]}{\delta \Phi} = F[\phi] + \left(\partial^2 - M^2\right)\Phi = 0 \tag{2.42}$$

and expanding the denominator unit to the desired order

$$\Phi_{\text{cl}} = \frac{1}{M^2} F[\phi] + \frac{\partial^2}{M^4} F[\phi] + \ \ldots \tag{2.43}$$

to get local operators $\mathcal{O}^{(n)}$. As can be seen from eq. 2.43, Λ corresponds to the mass scale of the heavy particle. Matching can be performed to higher loop orders by expanding Φ around the classical solution and performing the path-integral. However, this technique is not used in this thesis.

2.3.3. Weinberg Operator and Neutrino Masses

The unique dimension-five SMEFT operator is called Weinberg operator and reads:

$$\mathcal{L}^{(5)} = \frac{1}{2} C_5^{\alpha\beta} \overline{\ell_{\alpha L}} \widetilde{H} \widetilde{H}^T \ell^c_{\beta L} + \text{h.c.} \tag{2.44}$$

For convenience, the cut-off scale was included in the coefficient C_5, because $\mathcal{O}^{(5)}$ arises from multiple models with different cut-off scales. The Feynman diagrams (figs. 2.2, 2.3) responsible for the neutrino mass generation in the seesaw models 2.2.2 contain the exact structure of the Weinberg operator as external states correspond to the ones of $\mathcal{O}^{(5)}$. After SSB, the Weinberg operator induces a Majorana mass term for the neutrinos

$$\frac{1}{2} C_5^{\alpha\beta} \overline{\ell_{\alpha \mathrm{L}}} \widetilde{H} \widetilde{H}^{\mathrm{T}} \ell^{\mathrm{c}}_{\beta \mathrm{L}} \xrightarrow{\text{SSB}} \frac{1}{2} M^{\dagger}_{\alpha\beta} \overline{\nu_{\alpha \mathrm{L}}} \nu^{\mathrm{c}}_{\beta \mathrm{L}} \tag{2.45}$$

with the convention introduced in eq. 2.21 for Majorana masses and the identification

$$M^{\dagger}_{\alpha\beta} = \frac{1}{2} v^2 C_5^{\alpha\beta}. \tag{2.46}$$

The diagrammatic representation of the neutrino mass generation via the Weinberg operator is shown in fig. 2.4. Naturally, the Wilson coefficient for the Weinberg operator will be small, because it includes the cut-off scale suppression. Generally, the EFT approach enables an analysis of neutrino parameters for a broad class of neutrino mass models – that generate the Weinberg operator when integrating out heavy DOFs – without ever going into details of a specific model. This extensive applicability is the advantage of using the effective description.

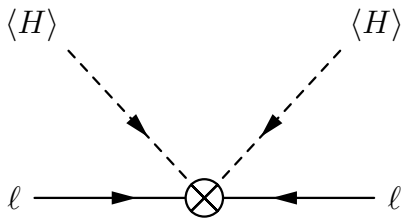

Figure 2.4.: Tree level diagrams for type-I seesaw mechanism. It describes the Majorana mass generation for left-handed neutrinos ν after SSB $\langle H \rangle$ by the effective description using the Weinberg operator.

3. Two-Loop RGEs for Weinberg Operator

3.1. Renormalization Group

3.1.1. Renormalization of Quantum Fields

When performing loop corrections to physical processes, UV divergences appear. These stem from the integration to infinite momenta or zero distances. The effect of unknown physics at very high energies can be fully absorbed into the theory's parameters. Quantum field theories are most likely only an effective description of nature. The renormalization of parameters then corresponds to integrating out all momentum shells above a cut-off energy scale from the Wilsonian renormalization group's point of view.

To make predictions, the theory must be regularized, and the quantities appearing in the Lagrangian renormalized to cancel these divergences. Observables should not depend on the regularization method, as this would allow testing of arbitrarily small scales at finite energies. This thesis will use dimensional regularization:

$$\int \mathrm{d}^4x \to \int \mathrm{d}^dx, \tag{3.1}$$

which continues the theory to $d = 4 - 2\varepsilon$ dimensions. As a result, the mass dimensions of the fields are altered to $[\psi] = \frac{d-1}{2}$, $[\phi, A] = \frac{d-2}{2}$. To maintain dimensionless κ_i, they are rescaled by the renormalization scale μ

$$\kappa_i \to \mu^{\rho_i \varepsilon} \kappa_i. \tag{3.2}$$

ρ_i denotes the tree level anomalous dimension of κ_i and is determined by the dimension of the corresponding operator $\mathcal{O}_i$ belonging to κ_i: $\rho_i = d - [\mathcal{O}_i]$.

Bare quantities m_B, κ_B, ψ_B (masses, coupling, fields) appearing in the Lagrangian are renormalized in terms of renormalized quantities m_r, κ_r, ψ_r and renormalization constants

$$\psi_B = Z_\phi^{\frac{1}{2}} \psi_r, \qquad \kappa_{i,B} = \mu^{\rho_i \varepsilon} Z_i \kappa_{i,r}, \qquad m_B = Z_m m_r. \tag{3.3}$$

The renormalization constants are conventionally expressed as

$$Z = 1 + \delta Z \tag{3.4}$$

with the Counterterms (CTs) δZ. Hence, the Lagrangian can be split into a renormalized contribution $\mathcal{L}_r$ containing only renormalized quantities and a counterterm Lagrangian

$\mathcal{L}_{\rm CT}$ containing all counterterms δZ. $\mathcal{L}_{\rm CT}$ is treated as a perturbation and included in all loop calculations. The CTs are chosen to cancel all arising divergences. In renormalized Pertubation Theory (PT), divergences are canceled order by order (in powers of couplings)

$$\delta Z = \delta Z^{(1)} + \delta Z^{(2)} + ... \ . \tag{3.5}$$

This implies that tree-level CTs diagrams cancel one-loop divergences in first order PT. At second order, tree-level CT cancel two-loop divergences and one-loop CT diagrams and so on.

Renormalization schemes vary regarding the finite part in the CTs. Here, the Modified-Minimal-Substration ($\overline{\rm MS}$) scheme [39] will be used, subtracting the mandatory divergent part and universal constants that always arise in dimensional regularization. A convenient way to remove these constants is by rescaling

$$\mu \to \tilde{\mu} = \mu \sqrt{\frac{e^{\gamma_E}}{4\pi}}, \tag{3.6}$$

with γ_E being the Euler-Mascheroni constant.

Furthermore, calculations are performed in the unbroken phase of the SM – before SSB. Keeping all gauge symmetries intact greatly simplifies the calculations. SSB does not change the renormalizability of theory, and CTs that renormalize the theory before SSB will renormalize it after SSB as well [20, 37, 40]. Afterwards, the Renormalization Group Equations (RGEs) can be translated into observables following SSB, depending on whether low or higher energy behavior is of interest.

3.1.2. Renormalization of EFTs

The renormalization of EFTs goes along the same line even though these are non-renormalizable theories by power counting. To render the theory finite to all orders in PT, infinitely many CTs are necessary. However, only a finite number is needed at a given order in $1/\Lambda$. Here, only $1/\Lambda$ contributions – thus single insertions of the Weinberg operator – are considered. Higher dimensional operators and multiple insertions are assumed to be strongly cut-off suppressed.

In contrast to eq. 3.3, a slightly different convention for the Wilson coefficient CT is used ($\delta Z_5 C_5 \equiv \delta C_5$):

$$C_5^{\alpha\beta} = \tilde{\mu}^{2\varepsilon} \left(C_{5,r}^{\alpha\beta} + \delta C_5^{\alpha\beta} \right). \tag{3.7}$$

3.1.3. Renormalization Group Equations

Renormalization Group Equations (RGEs) relate renormalized quantities between different energy scales. In Wilson renormalization, integrating out momentum shells corresponds to a continuous change in the renormalized quantities. Differential equations describe this transformation behavior and are called RGEs. Evolving a quantity from one scale Λ to another $\Lambda_{\rm obs}$ improves PT as it resumes potentially large logarithms $\log \Lambda/\Lambda_{\rm obs}$.

In practice, the RGEs are obtained by starting from the bare quantities, which are independent on the renormalization scale:

$$\frac{\mathrm{d}\kappa_{i,B}}{\mathrm{d}\mu} = 0. \tag{3.8}$$

Rewriting $\kappa_{i,r}$ in terms of $\kappa_{i,B}$ to abitrary loop order

$$\kappa_{i,B}\tilde{\mu}^{-\rho_i\varepsilon} = \kappa_{i,r} + \sum_{n=1}^{\infty} \frac{a_i^{(n)}(\kappa_l)}{\varepsilon^n}, \tag{3.9}$$

where the CTs for κ_i may also depend on other couplings ($a^{(n)}(\kappa_l)$). Hence, the RGE for $\kappa_{i,r}$ can be derived from:

$$\begin{aligned} \mu\frac{d\kappa_{i,r}}{d\mu} &= \mu\frac{d}{d\mu}\left(\kappa_{i,B}\tilde{\mu}^{-\rho_i\varepsilon} - \sum_{n=1}^{\infty}\frac{a_i^{(n)}(\kappa_l)}{\varepsilon^n}\right) \\ &= -\rho_i\kappa_{i,r}\varepsilon - \rho_i a_i^{(1)} \\ &\quad -\sum_{n=1}^{\infty}\left(\rho_i\frac{a_i^{(n+1)}(\kappa_{r,l})}{\varepsilon^n} + \frac{\partial a_i^{(n)}(\kappa_{r,l})}{\partial\kappa_l}\mu\frac{d\kappa_{r,l}}{d\mu}\frac{1}{\varepsilon^n}\right) \end{aligned} \tag{3.10}$$

Recasting the equation in this form motivates the definition of the beta function β_i for the coupling $\kappa_{i,r}$

$$\mu\frac{d\kappa_{i,r}}{d\mu} = \beta_i - \rho_i\kappa_i\varepsilon. \tag{3.11}$$

The beta function cannot contain poles in ε as it describes the evolution of κ_i. Thus, all poles have to cancel. Reusing the definition of the beta function in eq. 3.10 for $\mu\frac{d\kappa_{l,r}}{d\mu}$ gives:

$$\begin{aligned} \mu\frac{d\kappa_{i,r}}{d\mu} &= -\rho_i\kappa_i\varepsilon - \underbrace{\left(\rho_i a_i^{(1)} - \frac{\partial a_i^{(1)}}{\partial\kappa_l}\kappa_l\rho_l\right)}_{\equiv\beta_i} \\ &\quad \underbrace{-\left(\sum_{n=1}^{\infty}\rho_i\frac{a_i^{(n+1)}}{\varepsilon^n} + \frac{\partial a_i^{(n)}}{\partial\kappa_l}\beta_l\frac{1}{\varepsilon^n} - \rho_l\kappa_{l,r}\frac{\partial a_i^{(n+1)}}{\partial\kappa_l}\frac{1}{\varepsilon^n}\right)}_{\text{need to cancel}}. \end{aligned} \tag{3.12}$$

A summation over all other couplings κ_l is implied. One can read off the beta function – now with an explicit sum for clarity – which only depends on the coefficient of the single pole, as well as recurrence relations between the coefficients of higher order poles:

$$\beta_i = \rho_i a_i^{(1)} - \sum_l \frac{\partial a_i^{(1)}}{\partial\kappa_l}\kappa_l\rho_l \tag{3.13}$$

$$a_i^{(n+1)} = -\frac{1}{\rho_i}\sum_l\left(\frac{\partial a_i^{(n)}}{\partial\kappa_l}\beta_l - \rho_l\kappa_{r,l}\frac{\partial a_i^{(n+1)}}{\partial\kappa_l}\right) \tag{3.14}$$

3.2. Background Field Method

Gauge fixing terms explicitly break the gauge symmetry and result in gauge-dependent quantities, such as off-shell Green functions and counterterms. Consequently, the latter obey the more complicated Slavnov-Taylor identities instead of the simpler Ward identities for gauge-invariant quantities [41]. However, using the Background Field Method (BFM) [42–44] preserves explicit gauge invariance for Green functions, greatly simplifying the renormalization of the gauge sector.

In the BFM, one splits the gauge field $A \to A + \hat{A}$, into a background field A and a quantum field $\hat{A}$. $\hat{A}$ denotes the integration variable in the path integral and runs inside loops, while A only emerges in external states and tree-level propagators. The background-field-gauge will break gauge invariance for the quantum fields but not the background fields.

Therefore, the effective action of the background field (after setting the quantum fields to zero) is of interest as it retains gauge invariance. The equivalence between the background effective action and the effective action from the conventional approach (section 2.3.1) will be demonstrated below, justifying the method.

According to eq. 2.36, the generating functional of a gauge theory expressed with background and quantum fields is

$$\tilde{Z}[J, A] = \int \mathcal{D}\hat{A} \det\left[\frac{\delta \mathcal{G}^a}{\delta \omega^b}\right] \exp \mathrm{i} \int \left[\mathcal{L}(A + \hat{A}) - \frac{1}{2\xi}(\mathcal{G}^a)^2 + J^a_\mu \hat{A}^a_\mu\right], \tag{3.15}$$

where $\mathcal{G}^a$ denotes the gauge-fixing condition and $\frac{1}{2\xi}(\mathcal{G}^a)^2$ the gauge-fixing term. The effective action follows from eq. 2.37

$$\tilde{\Gamma}[\tilde{A}_{\mathrm{cl}}, A] = -\tilde{W}[J, A] - \int \mathrm{d}^4x J^a_\mu Q^{a\mu} \tag{3.16}$$

using $\tilde{W} = -\mathrm{i} \log \tilde{Z}$ and alongside with $\tilde{A}^a_{\mathrm{cl},\mu} = \delta \tilde{W}[J, A]/\delta J^a_\mu$ from eq. 2.38. By choosing the background field gauge for the gauge-fixing condition

$$\mathcal{G}^a = \partial_\mu A^{a\mu} + g f^{abc} \hat{A}^b_\mu A^{b\mu}, \tag{3.17}$$

$\tilde{W}$ remains invariant under the infinitesimal transformations

$$\delta \hat{A}^a_\mu = -f^{aba} \omega^b \hat{A}^c_\mu + \frac{1}{g} \partial_\mu \omega^a, \tag{3.18}$$

$$\delta J^a_\mu = -f^{abc} \omega^b J^c_\mu, \tag{3.19}$$

which translates to the gauge invariance of $\tilde{\Gamma}[\tilde{A}_{\mathrm{cl}}, A]$ via $\delta \tilde{A}^a_{\mathrm{cl},\mu} = -f^{abc} \omega^b \tilde{A}^c_{\mathrm{cl},\mu}$. $\tilde{\Gamma}[0, A]$ is invariant under the infinitesimal transformation of the background field (eq. 3.18), which expresses an ordinary gauge transformation of the background field. Setting $\tilde{A}_{\mathrm{cl}}$ to zero means quantum fields cannot appear as external legs, but only run inside loops.

The effective action contains quantum corrections to propagators and vertices to all orders in PT and should thus agree for the BFM and the conventional approach to give consistent results. Their relation follows from the definition in eq. 3.15

$$Z[\tilde{J}, A] = Z[J] e^{-i \int \mathrm{d}^4 x J^a_\mu A^{a\mu}} \tag{3.20}$$

as well as

$$\tilde{W}[J, A] = W[J] - \int \mathrm{d}^4 x J^a_\mu A^{a\mu} \ , \qquad \tilde{A}^a_{\mathrm{cl},\mu} = A^a_{\mathrm{cl},\mu} - A^a_\mu. \tag{3.21}$$

Applying the definition from eq. 3.16 finally yields

$$\begin{aligned} \tilde{\Gamma}[\tilde{A}_{\mathrm{cl}}, A] &= \Gamma[A_{\mathrm{cl}}]\big|_{A_{\mathrm{cl}}=\tilde{A}_{\mathrm{cl}}+A} \\ \tilde{\Gamma}[0, A] &= \Gamma[A_{\mathrm{cl}}]\big|_{A_{\mathrm{cl}}=A} \end{aligned} \tag{3.22}$$

and hence justifies the BFM approach. Fermions and the Higgs bosons do not appear in the gauge fixing condition and consequently do not affect explicit gauge invariance. Therefore, they do not need to be split into quantum and background fields.

Since the gauge quantum fields run only inside loops, counterterms stemming from the vertices will always cancel those stemming from the propagators and thus do not need renormalization. Furthermore, the remaining gauge invariance of the background field demands the background field strength

$$F^a_{\mu\nu} = Z_A^{1/2} \left[\partial_\mu A^a_\nu - \partial_\nu A^a_\mu + g Z_g Z_A^{1/2} f^{abc} A^b_\mu A^b_\nu \right] \tag{3.23}$$

to be gauge invariant under $g_0 = Z_g g$, $A_0 = Z_A^{1/2} A_r$ and $\xi_0 = Z_\xi \xi$, requiring

$$Z_g = Z_A^{-1/2}. \tag{3.24}$$

The gauge field wave function renormalization determines the gauge coupling renormalization, which does not need to be calculated separately. However, the counterterms for the gauge fixing parameter are still required. The BFM is then applied to all gauge fields of the SM, namely $A = B, W, G$. For calculation convenience, the Feynman gauge $\xi = 1$ is chosen for all gauge fields:

$$\mathcal{L}_{\mathrm{GF}} = -\frac{1}{2\xi} \left(\partial_\mu \hat{A}^\mu \right)^2. \tag{3.25}$$

Finally, the interaction of ghost and quantum field follows from eq. 2.4 and the gauge fixing condition of eq. 3.17:

$$\mathcal{L}_{\mathrm{FP}} = -\overline{\theta^a} D_\mu \hat{D}^\mu \theta^a. \tag{3.26}$$

D_μ ($\hat{D}_\mu$) stands for the covariant derivative using only background fields (using $A + \hat{A}$ in the covariant derivative).

3.3. Renormalization of the Weinberg Operator

3.3.1. Complete Renormalized Lagrangian for BFM

This section summarizes the full Lagrangian in the unbroken phase using the BFM. The SM contribution is

$$\begin{aligned}\mathcal{L}_{\text{SM}} =& -\frac{1}{4}G^A_{\mu\nu}G^{A\mu\nu} - \frac{1}{4}W^I_{\mu\nu}W^{I\mu\nu} - \frac{1}{4}B_{\mu\nu}B^{\mu\nu} \\ &+ \left(D_\mu H\right)^\dagger \left(D^\mu H\right) - M^2 H^\dagger H - \lambda\left(H^\dagger H\right)^2 + \sum_\psi \overline{\psi}\mathrm{i}\not{D}\psi \\ &- \left[\overline{Q_{\alpha\text{L}}}\left(Y_\text{u}\right)_{\alpha\beta}\widetilde{H}U_{\beta\text{R}} + \overline{Q_{\alpha\text{L}}}(Y_\text{d})_{\alpha\beta}HD_{\beta\text{R}} + \overline{\ell_{\alpha\text{L}}}(Y_l)_{\alpha\beta}HE_{\beta\text{R}} + \text{h.c.}\right] \\ &+ \mathcal{L}_{\text{GF}} + \mathcal{L}_{\text{FP}}\end{aligned} \tag{3.27}$$

which is supplemented by the unique dimension-five Weinberg operator

$$\mathcal{L} = \mathcal{L}_{\text{SM}} + \left(\frac{1}{2}C_5^{\alpha\beta}\overline{\ell_{\alpha\text{L}}}\widetilde{H}\widetilde{H}^T\ell^c_{\beta\text{L}} + \text{h.c.}\right). \tag{3.28}$$

A, I are the adjoint indices of the $\text{SU}(3), \text{SU}(2)_\text{L}$ group and the gauge bosons in D_μ, $G^A_{\mu\nu}$, $W^I_{\mu\nu}$, $B_{\mu\nu}$ are understood to written as $G + \hat{G}$, $W + \hat{W}$, $B + \hat{B}$ according to the BFM. $\psi = Q_\text{L}, U_\text{R}, D_\text{R}, \ell_\text{L}, E_\text{R}$ denotes all SM fermions. The gauge fixing and ghost terms are

$$\mathcal{L}_{\text{GF}} = -\frac{1}{2\xi_{\hat{B}}}\left(\partial^\mu \hat{B}_\mu\right)^2 - \frac{1}{2\xi_{\hat{W}}}\left(D^\mu \hat{W}^I_\mu\right)^2 - \frac{1}{2\xi_{\hat{G}}}\left(D^\mu \hat{G}^A_\mu\right)^2 \tag{3.29}$$

$$\mathcal{L}_{\text{FP}} = -\overline{\theta}_{\hat{B}}\partial_\mu\partial^\mu\theta_{\hat{B}} - \overline{\theta}^I_{\hat{W}}D_\mu\hat{D}^\mu\theta^I_{\hat{W}} - \overline{\theta}^A_{\hat{G}}D_\mu\hat{D}^\mu\theta^A_{\hat{G}} \tag{3.30}$$

where $D_\mu$is expressed in quantum and background field, while $\hat{D}_\mu$ is the background only covariant derivative. The conventions for the renormalization constants of the fields are:

$$\begin{aligned}&\xi_V = Z_{\xi_V}\xi_{V,r}, \\ &\varphi = Z_\varphi^{1/2}\varphi_r\,, \quad \psi_\alpha = \left(Z_\psi^{1/2}\right)_{\alpha\beta}\psi_{\beta,r}, \qquad M_H = Z_{M_H}M_{H,r} \\ &\kappa = \mu^{\rho_\kappa\varepsilon}Z_\kappa\kappa_r, \quad \left(Y_i\right)_{\alpha\beta} = \mu^\varepsilon\left(Y_{i,r}\right)_{\alpha\gamma}\left(Z_{Y_i}\right)_{\gamma\beta}, \\ &C_5^{\alpha\beta} = \mu^{2\varepsilon}\left(C_{5,r}^{\alpha\beta} + \delta C_5^{\alpha\beta}\right),\end{aligned} \tag{3.31}$$

with $V \in \{\hat{B}, \hat{W}, \hat{G}\}$, $\varphi \in \{H, B, W, G\}$, $\psi \in \{Q_\text{L}, U_\text{R}, D_\text{R}, \ell_\text{L}, E_\text{R}\}$, $\kappa \in \{g_1, g_2, g_3, m^2, \lambda\}$, $i \in \{\text{u}, \text{d}, l\}$. Here, the generational index structure of the fermionic fields is considered. Yukawa couplings do not preserve flavor symmetries and will lead to mixing among the generations, hence demanding non-diagonal generation renormalization constants. The gauge coupling renormalization follows from

$$Z_{g_1} = Z_B^{-1/2}, \quad Z_{g_2} = Z_W^{-1/2}, \quad Z_{g_3} = Z_G^{-1/2}. \tag{3.32}$$

3.3.2. Rank increasing diagrams

A UV model that does not generate masses for all LHNs provides a mass matrix rank of less than 3. One such possibility was introduced in section 2.2.1 by including only one (or two) RHN, which in turn leaves two (one) LHNs massless at the tree-level [26]. When matching the UV theory to the effective description at the cut-off scale, the rank of the mass matrix is transferred to the rank of the Weinberg operator Wilson coefficient due to eq.2.46 relating C_5 and M_ν. However, quantum corrections can cause the massless neutrino to become massive, because it is not protected by global symmetries. Such a symmetry would emerge if all neutrinos were massless ($\ell \to U\ell$) or if some massless neutrinos were accompanied by vanishing Yukawa couplings. For at least one massive neutrino and a lepton Yukawa matrix of full rank, the massless neutrino will become massive at the two-loop level. This effect has been studied in [16, 45] for the Weinberg operator and in a similar fashion for RHNs in [17–19].

In this section, the rank-increasing diagrams are revisited before considering the complete renormalization afterwards. These diagrams must contribute to the beta function in the form

$$\beta \subset \alpha \left(Y_l Y_l^\dagger\right)^T C_5 Y_l Y_l^\dagger \tag{3.33}$$

as was shown for RHNs [18] before and based on rewriting the beta functions for the mass eigenvalues. The procedure is repeated for the LHNs in section 4.1 when investigating

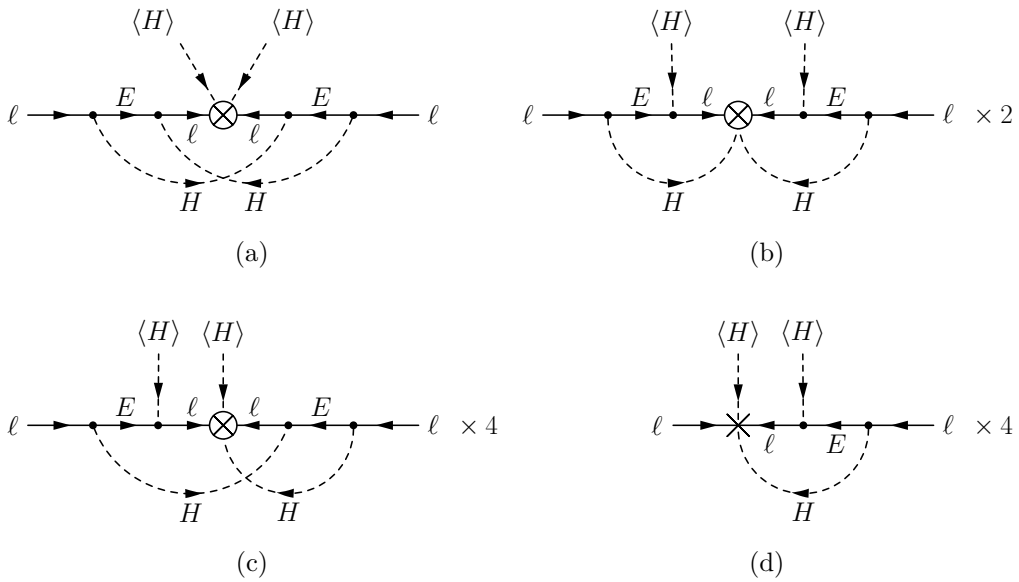

Figure 3.1.: Rank increasing two loop diagrams. Shown are the two-loop corrections of the Weinberg operator along with the number of equivalent diagrams (crossing of external legs), which increase the rank of the neutrino mass matrix after SSB. Diagram (d) contains the one-loop vertex CT of the Weinberg operator, while (a), (b) and (c) display pure two-loop corrections.

the running of neutrino parameters. The only diagrams that contribute to the term in eq. 3.33 are displayed in fig. 3.1, while only diagram (a) was showcased in [16]. The results obtained here are cross-checked with [16] to see if the additional diagrams ((b),(c) and (d)) provide additional contributions or were considered but not shown. Diagram (d) is a one-loop diagram but includes the one-loop CT of the Weinberg operator, making it the same order in PT.

Only UV divergences need to be considered for renormalization purposes. Since the Higgs mass serves as an Infrared (IR) regulator, preventing spurious IR divergences (divergences that appear for external momenta approaching zero), all external momenta can safely be set to zero. This will not change the form of the CTs as they – like all other operators in the Lagrangian – must obey locality to conserve causality. Terms like $\frac{1}{\varepsilon}\log P^2/\mu^2$ arise in loop calculations but necessarily cancel to maintain locality, justifying the approach. In $\overline{\text{MS}}$:

$$
\begin{aligned}
\mathcal{M}_a &= \mathrm{i}\left(\epsilon^{ac}\epsilon^{bd}+\epsilon^{ad}\epsilon^{bc}\right)\left(Y_l Y_l^\dagger\right)_{\rho\beta}\left(C_5^\dagger\right)^{\rho\lambda}\left(Y_l Y_l^\dagger\right)_{\lambda\alpha} \\
&\quad\times \overline{u}(0)P_{\mathrm{L}}\int\frac{\mathrm{d}^d k}{(2\pi)^d}\int\frac{\mathrm{d}^d l}{(2\pi)^d}\frac{\not{l}\not{k}}{k^2 l^2\left(l-k\right)^2\left(k^2-M^2\right)\left(l^2-M^2\right)}u(0) \\
&= \mathrm{i}\left(\epsilon^{ac}\epsilon^{bd}+\epsilon^{ad}\epsilon^{bc}\right)\left(Y_l Y_l^\dagger\right)_{\rho\beta}\left(C_5^\dagger\right)^{\rho\lambda}\left(Y_l Y_l^\dagger\right)_{\lambda\alpha}\overline{u}(0)P_{\mathrm{L}}u(0) \\
&\quad\times\frac{1}{(4\pi)^d}\left[\frac{1}{2\left(d-3\right)M^4}\left(A^{(d)}_{\{1,M\}}\right)^2-\frac{1}{M^2}K^{(d)}_{\{1,M\},\{1,0\},\{1,0\}}\right] \\
&\supset \mathrm{i}\left(\epsilon^{ac}\epsilon^{bd}+\epsilon^{ad}\epsilon^{bc}\right)\left(Y_l Y_l^\dagger\right)_{\rho\beta}\left(C_5^\dagger\right)^{\rho\lambda}\left(Y_l Y_l^\dagger\right)_{\lambda\alpha}\overline{u}(0)P_{\mathrm{L}}u(0) \\
&\quad\times\left[-\frac{1}{(16\pi^2)^2}\frac{1}{2\varepsilon}\right],
\end{aligned}
\tag{3.34}
$$

$$
\begin{aligned}
\mathcal{M}_b &= -2\mathrm{i}\left(\epsilon^{ac}\epsilon^{bd}+\epsilon^{ad}\epsilon^{bc}\right)\left(Y_l Y_l^\dagger\right)_{\rho\beta}\left(C_5^\dagger\right)^{\rho\lambda}\left(Y_l Y_l^\dagger\right)_{\lambda\alpha}\overline{u}(0)P_{\mathrm{L}}u(0) \\
&\quad\times\int\frac{\mathrm{d}^d k}{(2\pi)^d}\int\frac{\mathrm{d}^d l}{(2\pi)^d}\frac{1}{k^2 l^2\left(k^2-M^2\right)\left(l^2-M^2\right)} \\
&= -2\mathrm{i}\left(\epsilon^{ac}\epsilon^{bd}+\epsilon^{ad}\epsilon^{bc}\right)\left(Y_l Y_l^\dagger\right)_{\rho\beta}\left(C_5^\dagger\right)^{\rho\lambda}\left(Y_l Y_l^\dagger\right)_{\lambda\alpha} \\
&\quad\times\overline{u}(0)P_{\mathrm{L}}u(0)\frac{1}{(4\pi)^d}\frac{1}{M^4}\left(A^{(d)}_{\{1,M\}}\right)^2 \\
&\supset \mathrm{i}\left(\epsilon^{ac}\epsilon^{bd}+\epsilon^{ad}\epsilon^{bc}\right)\left(Y_l Y_l^\dagger\right)_{\rho\beta}\left(C_5^\dagger\right)^{\rho\lambda}\left(Y_l Y_l^\dagger\right)_{\lambda\alpha}\overline{u}(0)P_{\mathrm{L}}u(0) \\
&\quad\times\left[\frac{1}{(16\pi^2)^2}\frac{2}{\varepsilon^2}\left(1+2\varepsilon-2\varepsilon\Delta\right)\right],
\end{aligned}
\tag{3.35}
$$

$$
\begin{aligned}
\mathcal{M}_c &= \mathrm{i}\left(\epsilon^{ac}\epsilon^{bd}+\epsilon^{ad}\epsilon^{bc}\right)\left(Y_l Y_l^\dagger\right)_{\rho\beta}\left(C_5^\dagger\right)^{\rho\lambda}\left(Y_l Y_l^\dagger\right)_{\lambda\alpha} \\
&\quad\times \overline{u}(0)P_{\mathrm{L}}\int\frac{\mathrm{d}^d k}{(2\pi)^d}\int\frac{\mathrm{d}^d l}{(2\pi)^d}\frac{\not{l}\left(\not{l}-\not{k}\right)-\left(\not{l}-\not{k}\right)\not{k}}{k^2 l^2\left(l-k\right)^2\left(k^2-M^2\right)\left(l^2-M^2\right)}u(0) \\
&= \mathrm{i}\left(\epsilon^{ac}\epsilon^{bd}+\epsilon^{ad}\epsilon^{bc}\right)\left(Y_l Y_l^\dagger\right)_{\rho\beta}\left(C_5^\dagger\right)^{\rho\lambda}\left(Y_l Y_l^\dagger\right)_{\lambda\alpha} \\
&\quad\times \overline{u}(0)P_{\mathrm{L}}u(0)\frac{1}{(4\pi)^d}\frac{1}{M^4}\left(A^{(d)}_{\{1,M\}}\right)^2 \\
&\supset \mathrm{i}\left(\epsilon^{ac}\epsilon^{bd}+\epsilon^{ad}\epsilon^{bc}\right)\left(Y_l Y_l^\dagger\right)_{\rho\beta}\left(C_5^\dagger\right)^{\rho\lambda}\left(Y_l Y_l^\dagger\right)_{\lambda\alpha}\overline{u}(0)P_{\mathrm{L}}u(0) \\
&\quad\times\left[-\frac{1}{\left(16\pi^2\right)^2}\frac{1}{\varepsilon^2}\left(1+2\varepsilon-2\varepsilon\Delta\right)\right],
\end{aligned}
\tag{3.36}
$$

$$
\begin{aligned}
\mathcal{M}_d &= \left(\epsilon^{ac}\epsilon^{bd}+\epsilon^{ad}\epsilon^{bc}\right)\left[\left(\delta V_5^{(1)\dagger}Y_l Y_l^\dagger\right)_{\alpha\beta}+\left(\delta V_5^{(1)\dagger}Y_l Y_l^\dagger\right)_{\beta\alpha}\right] \\
&\quad\times \overline{u}(0)P_{\mathrm{L}}u(0)\int\frac{\mathrm{d}^d k}{(2\pi)^d}\frac{1}{k^2\left(k^2-M^2\right)} \\
&= \left(\epsilon^{ac}\epsilon^{bd}+\epsilon^{ad}\epsilon^{bc}\right)\left[\left(\delta V_5^{(1)\dagger}Y_l Y_l^\dagger\right)_{\alpha\beta}+\left(\delta V_5^{(1)\dagger}Y_l Y_l^\dagger\right)_{\beta\alpha}\right] \\
&\quad\times \overline{u}(0)P_{\mathrm{L}}u(0)\frac{1}{(4\pi)^{d/2}}\frac{1}{M^2}A^{(d)}_{\{1,M\}} \\
&\supset \mathrm{i}\left(\epsilon^{ac}\epsilon^{bd}+\epsilon^{ad}\epsilon^{bc}\right)\left(Y_l Y_l^\dagger\right)_{\rho\beta}\left(C_5^\dagger\right)^{\rho\lambda}\left(Y_l Y_l^\dagger\right)_{\lambda\alpha}\overline{u}(0)P_{\mathrm{L}}u(0) \\
&\quad\times\left[-\frac{1}{\left(16\pi^2\right)^2}\frac{2}{\varepsilon^2}\left(1+\varepsilon-\varepsilon\Delta\right)\right],
\end{aligned}
\tag{3.37}
$$

where $\Delta = \log M^2/\mu^2$. The calculation of diagram (d) included the one-loop CT of the Weinberg operator $\delta C_5^{(1)}$ (for more details see eq. 3.72)

$$
\delta V_5^{(1)} \subset -\frac{1}{16\pi^2}\frac{3}{4\varepsilon}\left[\left(Y_l Y_l^\dagger\right)C_5 + C_5\left(Y_l Y_l^\dagger\right)^T\right]. \tag{3.38}
$$

Terms not contributing to the rank-increasing structure (eq. 3.33) were dropped. The calculation of the full one-loop renormalization constant can be found in section 3.3.4. For the calculation of the two-loop integrals, the tensor reduction function of FeynCalc [46–48] was used to simplify to scalar integrals. Afterwards, these were expressed in TARCER [49] notation and reduced to master integrals with the Integration-by-Parts (IBP) technique. The evaluation of all emerging massive one- and two-loop master integrals can be found in appendix A.1. The IBP relation used for $\mathcal{M}_a$ is

$$
\int \mathrm{d}\Pi_{k,l}\frac{1}{(l^2-M^2)(k^2-M^2)(k-l)^2} = \frac{d-2}{2(d-3)M^2}\left(\int \mathrm{d}\Pi_k\frac{1}{(k^2-M^2)}\right)^2, \tag{3.39}
$$

where the invariant phase-space volume element was abbreviated with $\mathrm{d}\Pi$. Denoting $P_1 = k^2-M^2$, $P_2 = l^2-M^2$ and $P_3 = (k-l)^2$ the result follows from:

$$\mathcal{J} = \frac{\partial}{\partial k_\mu}\left(\alpha k_\mu + \beta l_\mu\right)\frac{1}{P_1 P_2 P_3}. \tag{3.40}$$

α, β are parameters and α can be set to 1 as this amounts to a global rescaling. Using $\partial/\partial k_\mu k_\mu = d$, $2k_\mu l^\mu = (k-l)^2 - k^2 - l^2$ and canceling symmetric term in l, k reads

$$\mathcal{J} = \frac{d}{P_1 P_2 P_3} + 2(1+\beta)\frac{m^2}{P_1^2 P_2 P_3} + \beta\frac{1}{P_1^2 P_2} - \beta\frac{\cancel{1}}{\cancel{P_1^2 P_3}}. \tag{3.41}$$

The last term is scaleless and quadratically divergent. Therefore, no quantity of dimension can accompany the UV poles, which consequently vanishes. Upon choosing $\beta = -1$ the second term vanishes and one remains with $1/P_1^2 P_2$ which follows from

$$\frac{\partial}{\partial k_\mu}\frac{k^\mu}{P_1^n} = \frac{d-2n}{P_1^n} - \frac{2nM^2}{P_1^{n+1}}. \tag{3.42}$$

The phase space integrations are reinserted, and surface terms, which vanish in Euclidian space after Wick rotating, are dropped. Hence $\mathcal{J} \to 0$ and $\frac{1}{P_1^2 P_2} \to \frac{d-2}{M^2}\frac{1}{P_1 P_2}$ (eq. 3.42) yields

$$\int \mathrm{d}\Pi_{k,l}\frac{d-3}{P_1 P_2 P_3} = \frac{d-2}{2M^2}\int \mathrm{d}\Pi_{k,l}\frac{1}{P_1 P_2}, \tag{3.43}$$

which is equivalent to eq. 3.39. The vertex renormalization then follows from the two-loop CT

$$\frac{1}{2}\delta V_5^{(2)\alpha\beta}\overline{\ell_{\alpha\mathrm{L}}}\widetilde{H}\widetilde{H}^{\mathrm{T}}\ell^{\mathrm{c}}_{\beta\mathrm{L}} + \mathrm{h.c.} \tag{3.44}$$

expressed in terms of vertex and wavefunction renormalization constants

$$\delta V_5^{(2)} = \delta C_5^{(2)} + \frac{1}{2}\delta Z_\ell^{(1)}\delta C_5^{(1)} + \frac{1}{2}\delta C_5^{(1)}\delta Z_\ell^{(1)\mathrm{T}} + \frac{1}{2}Z_\ell^{(1)}C_5\delta Z_\ell^{(1)\mathrm{T}} + ... \tag{3.45}$$

with all non-rank increasing contributions dropped. The pure two-loop contribution obtained from eq. 3.34-3.37 is

$$\begin{aligned} V_5^{(2)} &\subset V_{5,a}^{(2)} + V_{5,b}^{(2)} + V_{5,c}^{(2)} + V_{5,d}^{(2)} \\ &= \frac{1}{(16\pi^2)^2}\left(\frac{1}{\varepsilon^2} + \frac{1}{2\varepsilon}\right)\left(Y_l Y_l^\dagger\right) C_5 \left(Y_l Y_l^\dagger\right)^{\mathrm{T}}, \end{aligned} \tag{3.46}$$

with

$$\begin{aligned} \delta V_{5,a}^{(2)} &= \frac{1}{(16\pi^2)^2}\frac{1}{2\varepsilon}\left(Y_l Y_l^\dagger\right) C_5 \left(Y_l Y_l^\dagger\right)^{\mathrm{T}}, \\ \delta V_{5,b}^{(2)} &= -\frac{1}{(16\pi^2)^2}\frac{2}{\varepsilon^2}\left(1 + 2\varepsilon - 2\varepsilon\Delta\right)\left(Y_l Y_l^\dagger\right) C_5 \left(Y_l Y_l^\dagger\right)^{\mathrm{T}}, \\ \delta V_{5,c}^{(2)} &= \frac{1}{(16\pi^2)^2}\frac{1}{\varepsilon^2}\left(1 + 2\varepsilon - 2\varepsilon\Delta\right)\left(Y_l Y_l^\dagger\right) C_5 \left(Y_l Y_l^\dagger\right)^{\mathrm{T}}, \\ \delta V_{5,d}^{(2)} &= \frac{1}{(16\pi^2)^2}\frac{2}{\varepsilon^2}\left(1 + \varepsilon - \varepsilon\Delta\right)\left(Y_l Y_l^\dagger\right) C_5 \left(Y_l Y_l^\dagger\right)^{\mathrm{T}}. \end{aligned} \tag{3.47}$$

It is worth noting that all 'non-local' terms Δ cancel completely when summed (as expected). Furthermore, all $1/\varepsilon$ poles in $\delta V^{(2)}_{5,b,c,d}$ cancel completely, while diagram (a) determines the single pole of $\delta V^{(2)}$. This might be the reason why diagrams (b) – (d) were not shown in [16]. Again referring to section 3.3.4 for the one-loop CTs the rank-increasing part to the Weinberg Operator renormalization constant (eq. 3.45) reads

$$\delta C_5^{(2)} = \frac{1}{(16\pi^2+)^2}\left(\frac{9}{16\varepsilon^2}\frac{1}{2\varepsilon}\right)\left(Y_l Y_l^\dagger\right) C_5 \left(Y_l Y_l^\dagger\right)^{\mathrm{T}}. \tag{3.48}$$

Finally, the beta function follows from eq. 3.13

$$\mu\frac{\mathrm{d}C_5}{\mathrm{d}\mu} \subset \frac{2}{(16\pi^2)^2}\left(Y_l Y_l^\dagger\right) C_5 \left(Y_l Y_l^\dagger\right)^{\mathrm{T}} \tag{3.49}$$

in agreement with [16]. Furthermore, recurrence relations between the second-order pole $1/\varepsilon^2$ and the one-loop CTs exist (eq. 3.14). These relations do not prove the beta function – as they solely depend on the $1/\varepsilon$ pole (eq. 3.13) – but prove a consistency check on the calculation itself. In the notation of eq. 3.14, the coefficients in the ε expansion (one-loop CT eq. 3.38) are

$$\begin{aligned} a^{(1)} &= -\frac{1}{16\pi^2}\frac{3}{4}\left[\left(Y_l Y_l^\dagger\right) C_5 + C_5 \left(Y_l Y_l^\dagger\right)^{\mathrm{T}}\right] + \dots \ , \\ a^{(2)} &= \frac{1}{(16\pi^2)^2}\frac{9}{16}\left(Y_l Y_l^\dagger\right) C_5 \left(Y_l Y_l^\dagger\right)^{\mathrm{T}} + \dots \ . \end{aligned} \tag{3.50}$$

Plugging them into the right-hand side of eq. 3.14 and using the one-loop beta functions (section 3.3.4 or appendix A.2) confirms

$$\begin{aligned} a^{(2)} &= -\frac{1}{2}\sum_j \left(\beta_j \frac{\partial a^{(1)}}{\partial \kappa_j} - \rho_{\kappa_j}\kappa_j \frac{\partial a^{(2)}}{\partial \kappa_j}\right) \\ &= -\frac{1}{2}\frac{1}{(16\pi^2)^2}\left(2\cdot\left(\frac{3}{4}\cdot\frac{6}{4}\right) - 6\cdot\frac{9}{16}\right)\left(Y_l Y_l^\dagger\right) C_5 \left(Y_l Y_l^\dagger\right)^{\mathrm{T}} + \dots , \\ &= \frac{1}{(16\pi^2)^2}\frac{9}{16}\left(Y_l Y_l^\dagger\right) C_5 \left(Y_l Y_l^\dagger\right)^{\mathrm{T}} + \dots \ . \end{aligned} \tag{3.51}$$

3.3.3. Renormalization of SM parameters in BFM

The two-loop renormalization of the SM is repeated in the BFM to set up the Weinberg operator calculations and ensure consistency of all CTs. This section presents an overview of the approach:

- All Feynman diagrams and the respective amplitudes are generated with FeynArts [50, 51]. The model file is based on the Lagrangian presented in eqs. 3.27 and 3.28 and was created in FeynRules [52, 53]. Subsequently, the SU(N) and generation algebra is simplified, and all integrals tensor-reduced to scalar ones with the help of FeynCalc [46–48]. TARCER [49] then converts all two-loop integrals to standard

Tarcer notation and reduces them to a set of master integrals using IBP techniques. A concrete example for the sequence of calculational steps was presented in section 3.3.2.

- On the one hand, one-loop CTs of all SM parameters are needed as they contribute to second-order quantum corrections in the form of insertions in one-loop diagrams. On the other hand, only a small selection of two-loop CTs contribute to the renormalization of the Weinberg operator in the second order of PT. Apart from the obvious two-loop Weinberg operator CT, only the two-loop wave-function renormalization of the external legs ℓ and H contribute, as can be seen from eqs. 3.44 and 3.45.
- Multiple insertions of the Weinberg operator are not considered as they are cut-off-suppressed. Single insertions cannot appear in the SM renormalization as they would violate lepton number conservation, which is absent in any interactions. Thus, SM renormalization stays unaffected by the Weinberg operator.
- Spurious IR divergences in renormalization (not to be confused with those related to soft and collinear parton emission) should be avoided as they exhibit the same structure as UV divergences in dimensional regularization in the form of $1/\varepsilon^n$ poles. They appear whenever an integral is scaleless and IR, and UV divergences cancel exactly. This makes reconstructing the UV divergences much harder. A scheme that introduces the fewest scales (which corresponds to IR regulators in the form of external momenta or particle masses) is preferable to simplify one-loop and (especially) two-loop integrals. As discussed earlier, the scheme can differ for different CTs as all non-local terms must be canceled.
- When dealing with wave-function renormalization, working in a scheme with zero external momenta is impossible because the two-point CT vertex depends on the momentum. They can, however, simultaneously regulate all IR divergences and allow for the Higgs mass to be zero. It is important to note that, apart from the mass counterterm itself, no coupling can depend on M due to power counting. With the help of TARCER, which specializes in massless two-loop integrals, all scalar integrals were reduced to master integrals and subsequently evaluated. This approach was used for both one- and two-loop wave function renormalizations.
- A similar approach can be used for the SM one-loop 3- and 4-point vertices CTs. Only choosing two external states with momenta leads to spurious IR divergences, as some subdivergent structures remain scaleless. This situation is discussed in more detail in section 3.3.4, dealing with the renormalization of the Weinberg operator. For the SM one-loop CTs, it is enough to work with a general external momentum configuration and utilize the divergent part of the Passarino-Veltman functions [54, 55].

In the following, the results of the renormalization of all SM parameters in the unbroken phase using BFM are summarized. All one- and two-loop CTs can be found in closed form in appendix A.2.

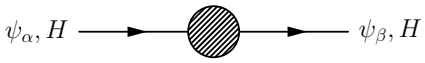

Figure 3.2.: Wave function renormalization. This diagram shows a representative contribution of quantum corrections to any propagator to arbitrary order in PT. Here $\psi = Q_\mathrm{L}, U_\mathrm{R}, D_\mathrm{R}, \ell_\mathrm{L}, E_\mathrm{R}$ and α, β denote generation.

One-loop CTs

First, one-loop CTs are calculated as they contribute to the second-order corrections. Fermion and Higgs wave function renormalization constants are calculated order by order according to the 1PI corrections in fig. 3.2. Only schematic representations of the quantum corrections will be given, as the number of two-loop diagrams ranges in the hundreds. To account for mixing between generations, the two-point function for ψ_i to ψ_j and the renormalization constant $\delta Z_{\alpha\beta}$ according to eq. 3.31 are investigated. The CTs amplitudes read (a, b denote $\mathrm{SU}(2)_\mathrm{L}$ indices):

$$\psi: \ \mathrm{i}\delta^{ab}\not{p}\left(\delta Z_\psi^{(1)}\right)_{\alpha\beta} P_{L/R} \qquad H: \ \mathrm{i}\delta^{ab}\left(\delta Z_H^{(1)} p^2 + \left(\delta Z_H^{(1)} + \delta Z_{M_H}^{(1)}\right) M_H^2\right). \tag{3.52}$$

This means the Higgs wave function has to be determined from the p^2 part before subtracting it from the p independent part to acquire the mass renormalization constant. Here and in all following loop calculations, only quantum gauge fields can appear inside loops, although they behave exactly like gauge fields in conventional gauges. Their propagators have the same form as the common gauge field, and the Feynman gauge was chosen for convenience. As a result, fermion and Higgs counterterms read:

$$\begin{aligned}
\delta Z_\ell^{(1)} &= -\frac{1}{16\pi^2\varepsilon\cdot 4}\left(g_1^2 + 3g_2^2 + 2Y_l Y_l^\dagger\right), \\
\delta Z_e^{(1)} &= -\frac{1}{16\pi^2\varepsilon}\left(g_1^2 + Y_l^\dagger Y_l\right), \\
\delta Z_q^{(1)} &= -\frac{1}{16\pi^2\varepsilon\cdot 36}\left(g_1^2 + 27g_2^2 + 48g_3^2 + 18Y_\mathrm{d}Y_\mathrm{d}^\dagger + 18Y_\mathrm{u}Y_\mathrm{u}^\dagger\right), \\
\delta Z_u^{(1)} &= -\frac{1}{16\pi^2\varepsilon\cdot 9}\left(4g_1^2 + 12g_3^2 + 9Y_\mathrm{u}^\dagger Y_\mathrm{u}\right), \\
\delta Z_d^{(1)} &= -\frac{1}{16\pi^2\varepsilon\cdot 9}\left(g_1^2 + 12g_3^2 + 9Y_\mathrm{d}^\dagger Y_\mathrm{d}\right), \\
\delta Z_H^{(1)} &= \frac{1}{16\pi^2\varepsilon\cdot 2}\left(g_1^2 + 3g_2^2 - 2T\right), \\
\delta Z_{M_H}^{(1)} &= \frac{1}{16\pi^2\varepsilon}\left(6\lambda + T\right),
\end{aligned} \tag{3.53}$$

with $T = \mathrm{Tr}\left[Y_l Y_l^\dagger + 3Y_\mathrm{u}Y_\mathrm{u}^\dagger + 3Y_\mathrm{d}Y_\mathrm{d}^\dagger\right]$. Continuing with the renormalization of the Yukawa and quartic Higgs coupling, the corresponding schematic diagram is shown in fig. 3.3, where only 1PI contributions are considered. Following the convention to define vertex

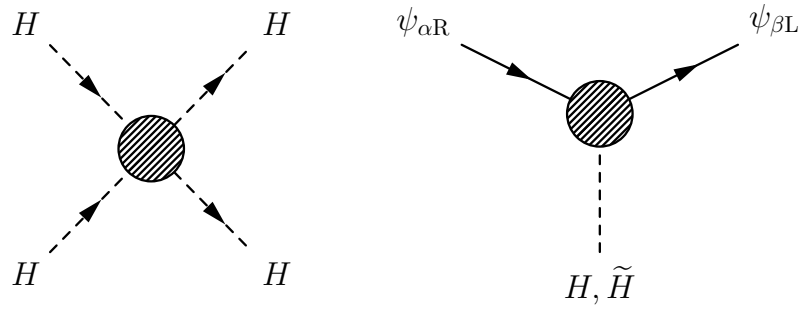

(a) Quartic H Interaction (b) Yukawa Interaction

Figure 3.3.: Vertex renormalization. The diagrams show a representative contribution of quantum corrections to the quartic Higgs coupling (left) and the Yukawa coupling (right) to any order in PT. Here $\psi_L = Q, \ell$ and $\psi_R = D, R, E$. $\widetilde{H}$ belongs to the up Yukawa vertex, while H belongs to the down and lepton Yukawa vertex.

CTs in eq. 3.3 external wave-function renormalization must be included. Those can be found in 3.53 and affect the vertex CTs according to the structure of the vertex (eq. 3.27) as follows

$$\begin{aligned} \delta V_\lambda^{(1)} &= \left(\delta Z_\lambda^{(1)} + 2\delta Z_H^{(1)}\right)\lambda \\ \delta V_Y^{(1)} &= \delta Z_Y^{(1)} Y + \frac{1}{2}\delta Z_{\psi_L}^{(1)} Y + \frac{1}{2} Y \delta Z_{\psi_R}^{(1)} + \frac{1}{2}\delta Z_H^{(1)} Y, \end{aligned} \tag{3.54}$$

with $Y = Y_{\mathrm{u,d},l}$ and $\psi_L = Q, \ell$ and $\psi_R = D, R, E$. The coupling renormalization constant can be extracted from δV, which cancels all 1PI vertex corrections. Using the wave function renormalization constants and solving for δZ_Y and δZ_λ gives:

$$\begin{aligned} \delta Z_\lambda^{(1)} &= \frac{1}{16\pi^2\varepsilon \cdot 16\lambda}\left[32\lambda T + 3(g1^2 + g2^2)^2 + 6g_2^4 - 24\lambda(g_1^2 + 3g_2^2) + 192\lambda^2 - 16T'\right], \\ \delta Z_{Y_\mathrm{u}}^{(1)} &= \frac{1}{16\pi^2\varepsilon \cdot 24} Y_\mathrm{u}^{-1}\left[Y_\mathrm{u}\left(12T - 17g_1^2 - 27g_2^2 - 96g_3^2\right) + 18 Y_\mathrm{u} Y_\mathrm{u}^\dagger Y_\mathrm{u} - 18 Y_\mathrm{d} Y_\mathrm{d}^\dagger Y_\mathrm{u}\right], \\ \delta Z_{Y_\mathrm{d}}^{(1)} &= \frac{1}{16\pi^2\varepsilon \cdot 24} Y_\mathrm{d}^{-1}\left[Y_\mathrm{d}\left(12T - 5g_1^2 - 27g_2^2 - 96g_3^2\right) - 18 Y_\mathrm{u} Y_\mathrm{u}^\dagger Y_\mathrm{d} + 18 Y_\mathrm{d} Y_\mathrm{d}^\dagger Y_\mathrm{d}\right], \\ \delta Z_{Y_l}^{(1)} &= \frac{1}{16\pi^2\varepsilon \cdot 8} Y_l^{-1}\left(Y_l\left[4T - 15g_1^2 - 9g_2^2\right) + 6 Y_l Y_l^\dagger Y_l\right], \end{aligned} \tag{3.55}$$

with $T' = \mathrm{Tr}\left[\left(Y_l Y_l^\dagger\right)^2 + 3\left(Y_\mathrm{u} Y_\mathrm{u}^\dagger\right)^2 + 3\left(Y_\mathrm{d} Y_\mathrm{d}^\dagger\right)^2\right]$. By using the BFM, the renormalization of the gauge sector is simplified. For the gauge couplings, it is sufficient to renormalize the background field two-point function shown in fig. 3.4. Inside the 1PI corrections, the background fields cannot appear but only their quantum field analogon

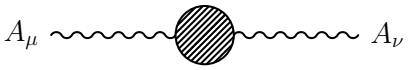

Figure 3.4.: Background field wave function renormalization. This shows a representative contribution of quantum corrections to any background field propagator $A = B, W, G$ to arbitrary order in PT.

$\hat{B}, \hat{W}, \hat{G}$. The mixed interaction vertices follow from the Lagrangian in eq. 3.27 by substituting $A \to A + \hat{A}$ and expanding the expression. The background field wave-function renormalization constants are

$$\begin{aligned} \delta Z_G^{(1)} &= \frac{7g_3^2}{16\pi^2\varepsilon}, \\ \delta Z_W^{(1)} &= \frac{19g_2^2}{16\pi^2\varepsilon \cdot 6}, \\ \delta Z_B^{(1)} &= -\frac{41g_1^2}{16\pi^2\varepsilon \cdot 6}, \end{aligned} \tag{3.56}$$

and the coupling renormalization constant follows from 3.32. Now, only the gauge fixing parameters are missing. These are intrinsically related to the quantum gauge fields; hence, two-point functions like the one in 3.4 need to be considered but for $A = \hat{B}, \hat{W}, \hat{G}$. This also corresponds to renormalizing the quantum fields. However, the wave function renormalization will not appear in any one-loop + CT diagram, as the propagator renormalization will always cancel with the adjacent vertices. The quantum gauge field 2-point in Feynman gauge CT respects the form:

$$\begin{aligned} \mathcal{L}_{\text{ren}}^{\text{BFM}} &\subset -\frac{1}{2(1+\delta\xi)}(1+\delta Z_A)\left(\partial_\mu A^\mu\right)^2 - \frac{1}{2}(1+\delta Z_A)F_{\mu\nu}F^{\mu\nu} \\ &\xrightarrow{\text{CT}} \mathrm{i}\left[p^\mu p^\nu(\delta Z_A - \delta Z_A + \delta\xi) - \delta Z_A p^2 g^{\mu\nu}\right] \\ &\longrightarrow \mathrm{i}\left[p^\mu p^\nu \delta\xi - \delta Z_A p^2 g^{\mu\nu}\right] \end{aligned} \tag{3.57}$$

Thus, the gauge fixing parameter can be directly determined from the $p^\mu p^\nu$ part of the 2-point quantum field renormalization. The result reads:

$$\begin{aligned} \delta Z_{\xi_{\hat{G}}}^{(1)} &= \frac{g_3^2}{16\pi^2\varepsilon}, \\ \delta Z_{\xi_{\hat{W}}}^{(1)} &= -\frac{5g_2^2}{16\pi^2\varepsilon \cdot 6}, \\ \delta Z_{\xi_{\hat{B}}}^{(1)} &= -\frac{41g_1^2}{16\pi^2\varepsilon \cdot 6}, \end{aligned} \tag{3.58}$$

and concludes the one-loop renormalization of all SM parameters.

Two Loop CTs

Only the two-loop renormalization constants of the lepton and Higgs wavefunction contribute to the renormalization of the Weinberg operator. Beginning with the charged leptons, the pure two-loop corrections $\delta Z_l^{(2)}$ to the propagator (according to fig.3.2) read:

$$\begin{aligned}\delta Z_\ell^{(2,2)} = &\frac{1}{(16\pi^2)^2\,\varepsilon^2\cdot 32}\left[-g_1^4-6g_1^2g_2^2-57g_2^4-2\left(17g_1^2+15g_2^2\right)Y_lY_l^\dagger\right.\\ &\left.+8TY_lY_l^\dagger+8Y_lY_l^\dagger Y_lY_l^\dagger\right]\\ &+\frac{1}{(16\pi^2)^2\,\varepsilon\cdot 32}\left\{\frac{1}{2}\left[\left(4\Delta'+81\right)g_1^4+6\left(4\Delta'-1\right)g_1^2g_2^2+3\left(76\Delta'-153\right)g_2^4\right]\right.\\ &+\left[\left(68\Delta'-139\right)g_1^2+3\left(20\Delta'-47\right)g_2^2\right]Y_lY_l^\dagger-4\left(4\Delta'-11\right)TY_lY_l^\dagger\\ &\left.+4\left(9-4\Delta'\right)Y_lY_l^\dagger Y_lY_l^\dagger\right\}.\end{aligned} \tag{3.59}$$

The non-local terms $\Delta' = \log p^2/\mu^2$ in $\overline{\text{MS}}$ cancel once one-loop topologies with one CT insertion are included in the propagator correction. Their contribution is

$$\begin{aligned}\delta Z_\ell^{(2,1)} = &\frac{1}{16\pi^2\varepsilon\cdot 4}\left\{g_1^2\left(\delta Z_B-\delta Z_{\alpha_B}\right)+3g_2^2\left(\delta Z_W-\delta Z_{\alpha_W}\right)-\left(g_1^2+3g_2^2\right)\delta Z_\ell\right.\\ &\left.-\left(\delta Z_\ell Y_lY_l^\dagger+Y_lY_l^\dagger\delta Z_\ell+2Y_l\delta Z_{Y_l}Y_l^\dagger+2Y_l\delta Z_{Y_l}^\dagger Y_l^\dagger\right)\right\}\\ &+\frac{1}{16\pi^2\cdot 4}\left\{(1-\Delta)\left[g_1^2\left(\delta Z_B-\delta Z_{\alpha_B}\right)+3g_2^2\left(\delta Z_W-\delta Z_{\alpha_W}\right)\right.\right.\\ &\left.-\left(g_1^2+3g_2^2\right)\delta Z_\ell\right]-(2-\Delta)\left(\delta Z_\ell Y_lY_l^\dagger+Y_lY_l^\dagger\delta Z_\ell\right.\\ &\left.\left.+\;2Y_l\delta Z_{Y_l}Y_l^\dagger+2Y_l\delta Z_{Y_l}^\dagger Y_l^\dagger\right)\right\}.\end{aligned} \tag{3.60}$$

Adding the two together gives the two-loop lepton wave function renormalization constant:

$$\begin{aligned}\delta Z_\ell^{(2)} = &\frac{1}{(16\pi^2)^2\,\varepsilon^2\cdot 32}\left[g_1^4+6g_1^2g_2^2+57g_2^4+2\left(17g_1^2+15g_2^2\right)Y_lY_l^\dagger\right.\\ &\left.-8TY_lY_l^\dagger-8Y_lY_l^\dagger Y_lY_l^\dagger\right]\\ &+\frac{1}{(16\pi^2)^2\,\varepsilon\cdot 64}\left[85g_1^4+18g_1^2g_2^2-231g_2^4-2\left(7g_1^2+33g_2^2\right)Y_lY_l^\dagger\right.\\ &\left.+24TY_lY_l^\dagger+8Y_lY_l^\dagger Y_lY_l^\dagger\right],\end{aligned} \tag{3.61}$$

where all non-local terms containing Δ' vanishe as expected. The same procedure applies to the Higgs wave function renormalization, where the pure two-loop, one-loop + CT and total corrections read:

$$\begin{aligned}\delta Z_H^{(2,2)} = &\frac{1}{\left(16\pi^2\right)^2\varepsilon^2}\left\{-\frac{43}{16}g_1^4-\frac{3}{4}g_1^2g_2^2+\frac{15}{16}g_2^4+\frac{1}{8}g_1^2\mathrm{Tr}\left(7Y_\mathrm{d}Y_\mathrm{d}^\dagger-5Y_\mathrm{u}Y_\mathrm{u}^\dagger-11Y_lY_l^\dagger\right)\right.\\&+\frac{3}{8}g_2^2T-12g_3^2\mathrm{Tr}\left(Y_\mathrm{d}Y_\mathrm{d}^\dagger+Y_\mathrm{u}Y_\mathrm{u}^\dagger\right)+\frac{3}{4}\mathrm{Tr}\left(Y_lY_l^\dagger Y_lY_l^\dagger+3Y_\mathrm{u}Y_\mathrm{u}^\dagger Y_\mathrm{u}Y_\mathrm{u}^\dagger\right.\\&\left.\left.+\;3Y_\mathrm{d}Y_\mathrm{d}^\dagger Y_\mathrm{d}Y_\mathrm{d}^\dagger-6Y_\mathrm{u}Y_\mathrm{u}^\dagger Y_\mathrm{d}Y_\mathrm{d}^\dagger\right)\right\}\\&+\frac{1}{\left(16\pi^2\right)^2\varepsilon}\left\{\left(\frac{43}{8}\Delta-\frac{613}{64}\right)g_1^4+\left(\frac{3}{2}\Delta-\frac{105}{32}\right)g_1^2g_2^2-\left(\frac{15}{8}\Delta-\frac{483}{64}\right)g_2^4-3\lambda^2\right.\\&+\frac{1}{48}g_1^2\mathrm{Tr}\left[\left(143-84\Delta\right)Y_\mathrm{d}Y_\mathrm{d}^\dagger+5\left(12\Delta-41\right)Y_\mathrm{u}Y_\mathrm{u}^\dagger+3\left(44\Delta-113\right)Y_lY_l^\dagger\right]\\&-\frac{3}{16}\left(4\Delta-3\right)g_2^2T+2\left(12\Delta-29\right)g_3^2\mathrm{Tr}\left(Y_\mathrm{d}Y_\mathrm{d}^\dagger+Y_\mathrm{u}Y_\mathrm{u}^\dagger\right)+\frac{3}{8}\mathrm{Tr}\left[\left(11-4\Delta\right)\right.\\&\left.\left.\times\;\left(Y_lY_l^\dagger Y_lY_l^\dagger+3Y_\mathrm{u}Y_\mathrm{u}^\dagger Y_\mathrm{u}Y_\mathrm{u}^\dagger+3Y_\mathrm{d}Y_\mathrm{d}^\dagger Y_\mathrm{d}Y_\mathrm{d}^\dagger\right)-2\left(25-12\Delta\right)Y_\mathrm{u}Y_\mathrm{u}^\dagger Y_\mathrm{d}Y_\mathrm{d}^\dagger\right]\right\},\end{aligned}\tag{3.62}$$

$$\begin{aligned}\delta Z_H^{(2,1)} = &\frac{1}{16\pi^2\varepsilon}\left\{-\frac{1}{4}g_1^2\left(2\delta Z_B+\delta Z_{\alpha_B}-2\delta Z_H\right)-\frac{3}{4}g_2^2\left(2\delta Z_W+\delta Z_{\alpha_W}-2\delta Z_H\right)-T\delta Z_H\right.\\&\left.-\;\mathrm{Tr}\left[Y_l\left(\delta Z_{Y_l}+\delta Z_{Y_l}^\dagger\right)Y_l^\dagger+3Y_\mathrm{u}\left(\delta Z_{Y_\mathrm{u}}+\delta Z_{Y_\mathrm{u}}^\dagger\right)Y_\mathrm{u}^\dagger+3Y_\mathrm{d}\left(\delta Z_{Y_\mathrm{d}}+\delta Z_{Y_\mathrm{d}}^\dagger\right)Y_\mathrm{d}^\dagger\right]\right\}\\&+\frac{1}{16\pi^2}\left\{\frac{1}{4}g_1^2\left[2\left(\Delta-2\right)\delta Z_B+\Delta\delta Z_{\alpha_B}-2\left(\Delta-2\right)\delta Z_H\right]+\frac{3}{4}g_2^2\left[2\left(\Delta-2\right)\delta Z_W\right.\right.\\&+\;\Delta\delta Z_{\alpha_W}-2\left(\Delta-2\right)\delta Z_H\left.\right]+\left(\Delta-2\right)T\delta Z_H+\left(\Delta-2\right)\mathrm{Tr}\left[Y_l\left(\delta Z_{Y_l}+\delta Z_{Y_l}^\dagger\right)Y_l^\dagger\right.\\&\left.\left.+\;3Y_\mathrm{u}\left(\delta Z_{Y_\mathrm{u}}+\delta Z_{Y_\mathrm{u}}^\dagger\right)Y_\mathrm{u}^\dagger+3Y_\mathrm{d}\left(\delta Z_{Y_\mathrm{d}}+\delta Z_{Y_\mathrm{d}}^\dagger\right)Y_\mathrm{d}^\dagger\right]\right\},\end{aligned}\tag{3.63}$$

$$\begin{aligned}\delta Z_H^{(2)} = &\frac{1}{\left(16\pi^2\right)^2\varepsilon^2}\left\{\frac{43}{16}g_1^4+\frac{3}{4}g_1^2g_2^2-\frac{15}{16}g_2^4+\frac{1}{8}g_1^2\mathrm{Tr}\left(11Y_lY_l^\dagger+5Y_\mathrm{u}Y_\mathrm{u}^\dagger-7Y_\mathrm{d}Y_\mathrm{d}^\dagger\right)\right.\\&-\frac{3}{8}g_2^2T+12g_3^2\mathrm{Tr}\left(Y_\mathrm{d}Y_\mathrm{d}^\dagger+Y_\mathrm{u}Y_\mathrm{u}^\dagger\right)-\frac{3}{4}\mathrm{Tr}\left(Y_lY_l^\dagger Y_lY_l^\dagger+3Y_\mathrm{u}Y_\mathrm{u}^\dagger Y_\mathrm{u}Y_\mathrm{u}^\dagger\right.\\&\left.\left.+\;3Y_\mathrm{d}Y_\mathrm{d}^\dagger Y_\mathrm{d}Y_\mathrm{d}^\dagger-6Y_\mathrm{u}Y_\mathrm{u}^\dagger Y_\mathrm{d}Y_\mathrm{d}^\dagger\right)\right\}\\&+\frac{1}{\left(16\pi^2\right)^2\varepsilon}\left\{-\frac{431}{192}g_1^4-\frac{9}{32}g_1^2g_2^2+\frac{163}{64}g_2^4-3\lambda^2\right.\\&-\frac{15}{16}g_2^2T+\frac{3}{8}\mathrm{Tr}\left(3Y_lY_l^\dagger Y_lY_l^\dagger+9Y_\mathrm{u}Y_\mathrm{u}^\dagger Y_\mathrm{u}Y_\mathrm{u}^\dagger+9Y_\mathrm{d}Y_\mathrm{d}^\dagger Y_\mathrm{d}Y_\mathrm{d}^\dagger-2Y_\mathrm{u}Y_\mathrm{u}^\dagger Y_\mathrm{d}Y_\mathrm{d}^\dagger\right)\\&\left.-\frac{5}{48}g_1^2\mathrm{Tr}\left(15Y_lY_l^\dagger+17Y_\mathrm{u}Y_\mathrm{u}^\dagger+5Y_\mathrm{d}Y_\mathrm{d}^\dagger\right)-10g_3^2\mathrm{Tr}\left(Y_\mathrm{d}Y_\mathrm{d}^\dagger+Y_\mathrm{u}Y_\mathrm{u}^\dagger\right)\right\}.\end{aligned}\tag{3.64}$$

All non-local terms canceled as expected.

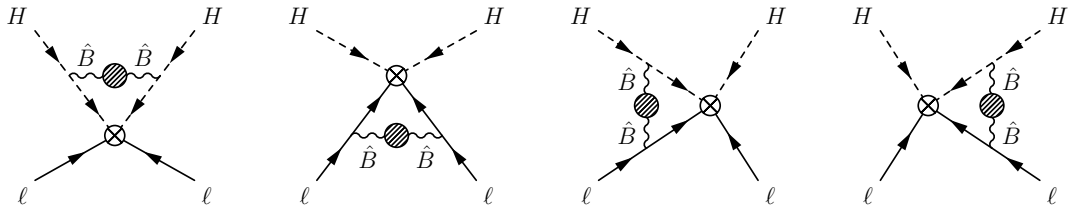

Figure 3.5.: Scaleless substructure. The diagrams show representative two-loop corrections to the Weinberg of the form $g_1^2 \times \text{Coupling}^2$. There is no configuration with just two external momenta that eliminates all spurious IR divergences, as there is always a scaleless correction involving only the two external legs with zero momenta.

3.3.4. Renormalization of Weinberg Operator

In the previous section, the renormalization of the standard model parameters in the BFM was performed. The general approach needs some modifications to avoid spurious IR divergences to calculate the two-loop Weinberg operator corrections. At the one-loop level, having non-zero external momenta will prevent these, and the integral can be evaluated using the Passarino-Veltman function, as in the SM renormalization. Therefore, the approach introduced earlier remains valid for the one-loop CT $\delta C_5^{(1)}$. However, the two-loop corrections present a challenge when considering all external momenta. The loop-integral becomes significantly more complex, and many topologies exist. Hence, an alternative scheme is required. The CTs are independent of the scheme results as all non-local terms cancel if performed properly.

Using two external momenta to reduce the topologies to wave function renormalization type diagrams, which can be evaluated by TARCER, is not a viable option due to emerging IR divergences. For one collection of couplings, the same configuration of external momenta must be chosen to cancel all $\log\left(\frac{p^2}{\mu^2}\right)$ type terms. Still, a configuration that prevents all IR divergences does not always exist. A simple two-loop example is shown in fig. 3.5 to illustrate the problem.

Therefore, an alternative scheme (similarly in [56, 57]) is chosen, which sets all external momenta to zero, but introduces IR regulators in the form of artificial mass terms. This scheme reintroduces the Higgs mass in calculations, which was set to zero for calculational convenience. Additionally, mass terms are added for the quantum and ghost fields. These do not break gauge symmetry as the background effective action (eq. 3.22) only depends on the background fields, which maintain gauge invariance. The mass terms that render the diagrams IR finite are:

$$\mathcal{L}_{\text{IR}} = -M^2 H^\dagger H - \frac{1}{2} M^2 \hat{B}_\mu \hat{B}^\mu - \frac{1}{2} M^2 \hat{W}^I_\mu \hat{W}^{I\mu} - M^2 \overline{\theta}_{\hat{B}} \theta_{\hat{B}} - M^2 \overline{\theta}^I_{\hat{W}} \theta^I_{\hat{W}} \tag{3.65}$$

To simplify the master integrals, all IR regulators have been chosen the same (M). SU(3) quantum field and ghost masses have been omitted as they will not participate in the second-order corrections. M constitutes a new parameter in the Lagrangian that needs

to be renormalized. Yet, individual CTs for the different particles are necessary as every mass term gets different corrections. Another perspective is to assign distinct masses for the different particles, renormalize each of them, and then equate the renormalized masses. That explains the varying CTs

$$-\frac{1}{2}\delta Z_{M_{\hat{B}}} M^2 \hat{B}_\mu \hat{B}^\mu - \frac{1}{2}\delta Z_{M_{\hat{W}}} M^2 \hat{W}^I_\mu \hat{W}^{I\mu}. \tag{3.66}$$

Ghost fields do not appear in one-loop Weinberg operator corrections. Therefore, ghost mass terms CTs were ignored, as they would only enter at the three-loop level, while the Higgs mass renormalization constant was already calculated eq. 3.53. The IR mass regulators render all two-loop diagrams finite by introducing a scale to all integrals. Consequently, all external momenta can be set to zero, giving only vacuum diagrams. After IBP reduction, only two master integrals (in TARCER notation)

$$K^{(d)}_{\{1,M\},\{1,0\},\{1,0\}} \quad \text{and} \quad K^{(d)}_{\{1,M\},\{1,M\},\{1,M\}} \tag{3.67}$$

emerge, with one or three massive propagators, respectively. Their UV divergent parts were calculated in the appendix A.1 for cross-checking purposes, as the first one is available in the TARCER package, while the second was calculated in [56]. Furthermore, it is worth noting that introducing these mass terms does not affect the CTs. Higher-dimension operators or multiple Weinberg operator insertions together with this mass scale could give contributions of the form $\frac{M}{\Lambda^2}C_6$, $\frac{M}{\Lambda^2}C_5^2$ to the dimension-five operator. However, their contribution is cut-off suppressed by at least two orders of Λ. Here, only the first order in $1/\Lambda$ is considered.

IR-Regulator Renormalization

The mass term renormalization for the gauge quantum fields follows from the propagator corrections (fig. 3.4 with $A = \hat{B}, \hat{W}$) similar to the gauge fixing parameter in eq. 3.57. Modifying this equation by including a mass term gives

$$\begin{aligned}\mathcal{L}_{\text{BFM,ren}} \subset & -\frac{1}{2(1+\delta\xi)}(1+\delta Z_{\hat{A}})\left(\partial_\mu \hat{A}^\mu\right)^2 - \frac{1}{2}(1+\delta Z_{\hat{A}})\hat{F}^{\mu\nu} \\ & -\frac{1}{2}\left(1+\delta Z_M\right)\left(1+\delta Z_{\hat{A}}\right)M^2 \hat{A}_\mu \hat{A}^\mu \\ & \longrightarrow \mathrm{i}\left[p^\mu p^\nu \delta\xi - \delta Z_{\hat{A}} p^2 g^{\mu\nu} - \left(\delta Z_M + \delta Z_{\hat{A}}\right) M^2\right]\end{aligned} \tag{3.68}$$

The gauge quantum field was explicitly renormalized here to uniquely separate the mass and wave function renormalization contribution terms. First, δZ_A is chosen such that it cancels the UV divergent part $\propto p^2$. Second, this contribution is subtracted from the $\propto M^2$ term to yield δZ_M. This procedure also gives the wave function renormalization of the background fields, which, however, always cancels with the factors from the two adjacent vertices. The one-loop mass CTs for $\hat{B}$ and $\hat{W}$ read:

$$\begin{aligned}\delta Z^{(1)}_{M_{\hat{B}}} &= \frac{1}{16\pi^2\varepsilon}\frac{41}{6}g_1^2, \\ \delta Z^{(1)}_{M_{\hat{W}}} &= -\frac{1}{16\pi^2\varepsilon}\frac{7}{6}g_2^2.\end{aligned} \tag{3.69}$$

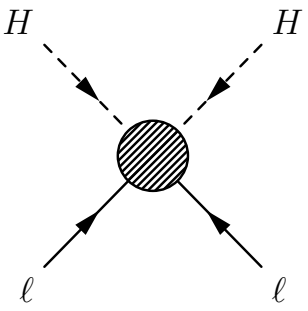

Figure 3.6.: Weinberg Operator Renormalization. The diagram shows a representative contribution of quantum corrections to the Weinberg operator coupling to any order in PT.

One-loop Contribution

The one-loop 1PI corrections to the Weinberg operator vertex depicted in fig. 3.6 are calculated using the Passarino-Veltman integrals and are independent of the scheme, as the momentum configuration and mass terms only affect finite parts. Those, however, are not included in $\overline{\text{MS}}$.

The method to include charge conjugated spinors and lepton number violating interaction is presented in [58]. It amounts to choosing a fermion flow in a given diagram. Whenever the introduced fermion flow goes against the fermion number flow direction, the momentum sign of the propagator is exchanged, and the vertex κ is replaced by the charge conjugated vertex ($\kappa \to C\kappa C^{-1}$ with C from eq. 2.1). FeynCalc can handle fermion number violating processes based on the approach in [58]. The vertex correction

$$\delta V_5^{(1)} = \frac{1}{16\pi^2\varepsilon}\left[-Y_l Y_l^\dagger C_5 - C_5\left(Y_l Y_l^\dagger\right)^{\mathrm{T}} + C_5\left(g_1^1 - 3g_2^2 + 8\lambda\right)\right] \tag{3.70}$$

together with the contribution from the lepton and Higgs wavefunction renormalizations

$$\delta V_5^{(1)} = \delta C_5^{(1)} + \frac{1}{2}\delta Z_\ell^{(1)} C_5 + \frac{1}{2} C_5 \delta Z_\ell^{(1)\mathrm{T}} + \delta Z_H^{(1)}, \tag{3.71}$$

which follows from the vertex CT given in eq. 3.44, ultimately yields the one-loop Weinberg operator correction by using the one-loop CTs from eq. 3.53:

$$\delta C_5^{(1)} = \frac{1}{16\pi^2\varepsilon\cdot 4}\left[2\left(4\lambda - 3g_2^2 + 2T\right)C_5 - 3Y_l Y_l^\dagger C_5 - 3C_5\left(Y_l^\dagger Y_l\right)^{\mathrm{T}}\right]. \tag{3.72}$$

Two-Loop Contribution

The two-loop 1PI corrections in fig. 3.6 are not explicitly displayed due to the large number of diagrams involved. There are 931 pure two-loop diagrams and 116 additional one-loop diagrams with one CT insertion. The most significant diagrams, which contribute to increasing the rank, are shown in fig. 3.1. The method for addressing lepton number

violating processes introduced previously remains. The outcome for the pure two-loop diagrams, based on the approach with IR regulator masses and on external momenta described at the beginning of this section, is as follows:

$$\begin{aligned}
\delta V_5^{(2,2)} = &\frac{1}{(16\pi^2)^2}\frac{1}{\varepsilon^2}\left\{-\frac{89}{32}g_1^4 C_5 - \frac{85}{32}g_2^4 C_5 - \frac{3}{16}g_1^2 g_1^2 C_5 + \lambda\left(-14\lambda + g_1^2 + 6g_2^2\right) C_5\right.\\
&+ \left(2\lambda + \frac{1}{2}T - \frac{13}{8}g_1^2 - \frac{15}{8}g_2^2\right)\left[Y_l Y_l^\dagger C_5 + C_5\left(Y_l Y_l^\dagger\right)^{\mathrm{T}}\right] + \left(T' - 2\lambda T\right) C_5\\
&\left.+ \frac{1}{4}\left[Y_l Y_l^\dagger Y_l Y_l^\dagger C_5 + C_5\left(Y_l Y_l^\dagger Y_l Y_l^\dagger\right)^{\mathrm{T}}\right] - \left(Y_l Y_l^\dagger\right) C_5\left(Y_l Y_l^\dagger\right)^{\mathrm{T}}\right\}\\
&+ \frac{1}{(16\pi^2)^2}\frac{1}{\varepsilon}\left\{\frac{89\Delta - 26}{16}g_1^4 C_5 + \frac{255\Delta - 38}{48}g_2^4 C_5 + \frac{3\Delta - 40}{8}g_1^2 g_1^2 C_5\right.\\
&+ \frac{1}{4}\lambda\left[8\left(14\Delta + 1\right)\lambda - \left(8\Delta + 15\right)g_1^2 - \left(48\Delta + 23\right)g_2^2\right] C_5\\
&+ \left(4\lambda\Delta - \frac{1}{3}g_1^2 - \frac{5}{6}g_2^2\right) T C_5 + \left[-4\left(\Delta + 1\right)\lambda + \frac{1}{2}\left(1 - 2\Delta\right)T\right.\\
&\left.+ \frac{26\Delta - 33}{8}g_1^2 + \frac{30\Delta - 21}{8}g_2^2\right] \times \left[Y_l Y_l^\dagger C_5 + C_5\left(Y_l Y_l^\dagger\right)^{\mathrm{T}}\right]\\
&+ \left(1 - 2\Delta\right) T' C_5 + \frac{1}{4}\left(7 - 2\Delta\right)\left[Y_l Y_l^\dagger Y_l Y_l^\dagger C_5 + C_5\left(Y_l Y_l^\dagger Y_l Y_l^\dagger\right)^{\mathrm{T}}\right]\\
&\left.- \frac{1}{2}\left(3 - 4\Delta\right)\left(Y_l Y_l^\dagger\right) C_5\left(Y_l Y_l^\dagger\right)^{\mathrm{T}}\right\},
\end{aligned} \tag{3.73}$$

with the 'non-local' terms defined by $\Delta = \log M^2/\mu^2$, the same as in section 3.3.2 for the rank increasing contributions. M is the only dimensionful scale and hence the only quantity that can appear in the log alongside μ.

The one-loop CTs are split into two parts: One containing only Weinberg operator vertex CTs based on the decomposition in eq. 3.71 $\delta V_5^{(2,1.1)}$ and the other one containg all SM and mass type CTs $\delta V_5^{(2,1.2)}$. They read:

$$\begin{aligned}
\delta V_5^{(2,1.2)} = &\frac{1}{16\pi^2\varepsilon}\left\{\left(\lambda + \frac{1}{8}g_1^2 - \frac{3}{8}g_2^2\right)\left(2\delta Z_H^{(1)} C_5 + \delta Z_\ell^{(1)} C_5 + C_5 \delta Z_\ell^{(1)\mathrm{T}} + 2\delta Z_5^{(1)}\right)\right.\\
&- \frac{1}{2}\left[2\delta Z_H^{(1)} Y_l Y_l^\dagger C_5 + 2\delta Z_H^{(1)} C_5\left(Y_l Y_l^\dagger\right)^{\mathrm{T}} + Y_l Y_l^\dagger C_5 \delta Z_\ell^{(1)\mathrm{T}} + \delta Z_\ell^{(1)} C_5\left(Y_l Y_l^\dagger\right)^{\mathrm{T}}\right.\\
&\left.\left.+\ Y_l Y_l^\dagger \delta Z_\ell^{(1)} C_5 + C_5\left(Y_l Y_l^\dagger \delta Z_\ell^{(1)}\right)^{\mathrm{T}} + 2 Y_l Y_l^\dagger \delta Z_5^{(1)} + 2\delta Z_5^{(1)}\left(Y_l Y_l^\dagger\right)^{\mathrm{T}}\right]\right\}\\
&+ \frac{1}{16\pi^2}\left\{-\left[\lambda\Delta + \frac{1}{16}\left(2\Delta - 3\right)g_1^2 - \frac{3}{16}\left(2\Delta + 1\right)g_2^2\right]\left(2\delta Z_H^{(1)} C_5 + \delta Z_\ell^{(1)} C_5\right.\right.\\
&\left.+ C_5 \delta Z_\ell^{(1)\mathrm{T}} + 2\delta Z_5^{(1)}\right) - \frac{1}{2}\left(1 - \Delta\right)\left[2\delta Z_H^{(1)} Y_l Y_l^\dagger C_5 + 2\delta Z_H^{(1)} C_5\left(Y_l Y_l^\dagger\right)^{\mathrm{T}}\right.\\
&+ Y_l Y_l^\dagger C_5 \delta Z_\ell^{(1)\mathrm{T}} + \delta Z_\ell^{(1)} C_5\left(Y_l Y_l^\dagger\right)^{\mathrm{T}} + Y_l Y_l^\dagger \delta Z_\ell^{(1)} C_5 + C_5\left(Y_l Y_l^\dagger \delta Z_\ell^{(1)}\right)^{\mathrm{T}}\\
&\left.\left.+\ 2 Y_l Y_l^\dagger \delta Z_5^{(1)} + 2\delta Z_5^{(1)}\left(Y_l Y_l^\dagger\right)^{\mathrm{T}}\right]\right\}
\end{aligned} \tag{3.74}$$

$$
\begin{aligned}
\delta V_5^{(2,1.1)} = \frac{1}{16\pi^2\varepsilon}\Bigg\{ & -\frac{1}{4}\left[g_1^2\left(\delta Z_B^{(1)} + 2\delta Z_{\xi_{\hat{B}}}^{(1)}\right) - 3g_2^2\left(\delta Z_W^{(1)} - 2\delta Z_{\xi_{\hat{W}}}^{(1)}\right) - 8\lambda\delta Z_\lambda^{(1)}\right] C_5 \\
& - \frac{1}{2}\Big[\delta Z_\ell^{(1)} Y_l Y_l^\dagger C_5 + C_5\left(\delta Z_\ell^{(1)} Y_l Y_l^\dagger\right)^{\mathrm{T}} - Y_l Y_l^\dagger \delta Z_\ell^{(1)} C_5 - C_5\left(Y_l Y_l^\dagger \delta Z_\ell^{(1)}\right)^{\mathrm{T}} \\
& + 2Y_l \delta Z_{Y_l}^{(1)\dagger} Y_l^\dagger C_5 + 2C_5\left(Y_l \delta Z_{Y_l}^{(1)\dagger} Y_l^\dagger\right)^{\mathrm{T}} + 2Y_l \delta Z_{Y_l}^{(1)} Y_l^\dagger C_5 \\
& + 2C_5\left(Y_l \delta Z_{Y_l}^{(1)} Y_l^\dagger\right)^{\mathrm{T}}\Big]\Bigg\} \\
& + \frac{1}{16\pi^2}\Bigg\{\frac{1}{24}g_1^2\left[8\delta Z_{M_H}^{(1)} - 14\delta Z_{M_{\hat{B}}}^{(1)} + (6\Delta - 9)\,\delta Z_B^{(1)} + (12\Delta + 7)\,\delta Z_{\xi_{\hat{B}}}^{(1)}\right] C_5 \\
& - \frac{1}{24}g_2^2\left[-20\delta Z_{M_H}^{(1)} + 2\delta Z_{M_{\hat{W}}}^{(1)} + 9\,(2\Delta + 1)\,\delta Z_W^{(1)} - (36\Delta + 19)\,\delta Z_{\xi_{\hat{W}}}^{(1)}\right] C_5 \\
& - 2\lambda\left(\delta Z_{M_H}^{(1)} + \Delta\delta Z_\lambda^{(1)}\right) C_5 + \delta Z_{M_H}^{(1)}\left[Y_l Y_l^\dagger C_5 + \left(Y_l Y_l^\dagger C_5\right)^{\mathrm{T}}\right] - \frac{1}{2}(1 - \Delta) \\
& \times \Big[\delta Z_\ell^{(1)} Y_l Y_l^\dagger C_5 + C_5\left(\delta Z_\ell^{(1)} Y_l Y_l^\dagger\right)^{\mathrm{T}} - Y_l Y_l^\dagger \delta Z_\ell^{(1)} C_5 - C_5\left(Y_l Y_l^\dagger \delta Z_\ell^{(1)}\right)^{\mathrm{T}} \\
& + 2Y_l \delta Z_{Y_l}^{(1)\dagger} Y_l^\dagger C_5 + 2C_5\left(Y_l \delta Z_{Y_l}^{(1)\dagger} Y_l^\dagger\right)^{\mathrm{T}} + 2Y_l \delta Z_{Y_l}^{(1)} Y_l^\dagger C_5 \\
& + 2C_5\left(Y_l \delta Z_{Y_l}^{(1)} Y_l^\dagger\right)^{\mathrm{T}}\Big]\Bigg\}. \qquad (3.75)
\end{aligned}
$$

Adding these three contributions and inserting all one-loop CTs determined in this section and section 3.3.3 gives the overall two-loop Weinberg operator vertex CT:

$$
\begin{aligned}
\delta V_5^{(2)} = \frac{1}{(16\pi^2)^2\varepsilon^2}\Bigg\{ & \left[\frac{89}{32}g_1^4 + \frac{3}{16}g_1^2 g_2^2 + \frac{85}{32}g_2^4 - \lambda\left(g_1^2 + 6g_2^2 - 14\lambda - 2T\right) - T'\right] C_5 \\
& + \left(\frac{13}{8}g_1^2 + \frac{15}{8}g_2^2 - 2\lambda - \frac{1}{2}T\right)\left[Y_l Y_l^\dagger C_5 + C_5\left(Y_l Y_l^\dagger\right)^{\mathrm{T}}\right] - \frac{1}{4}Y_l Y_l^\dagger Y_l Y_l^\dagger C_5 \\
& - \frac{1}{4}C_5\left[Y_l Y_l^\dagger Y_l Y_l^\dagger\right]^{\mathrm{T}} + Y_l Y_l^\dagger C_5\left(Y_l Y_l^\dagger\right)^{\mathrm{T}}\Bigg\} \\
& - \frac{1}{(16\pi^2)^2\varepsilon}\Bigg\{\left[\frac{475}{96}g_1^4 + \frac{83}{16}g_1^2 g_2^2 + \frac{271}{96}g_2^4 + \lambda\left(g_1^2 + 10\lambda + 2T\right) - T'\right] C_5 \\
& + \left(g_1^2 - \frac{1}{2}T\right)\left[Y_l Y_l^\dagger C_5 + C_5\left(Y_l Y_l^\dagger\right)^{\mathrm{T}}\right] - \frac{5}{4}Y_l Y_l^\dagger Y_l Y_l^\dagger C_5 - \frac{5}{4}C_5\left[Y_l Y_l^\dagger Y_l Y_l^\dagger\right]^{\mathrm{T}} \\
& - \frac{1}{2}Y_l Y_l^\dagger C_5\left(Y_l Y_l^\dagger\right)^{\mathrm{T}}\Bigg\}, \qquad (3.76)
\end{aligned}
$$

which is free of $\log M^2/\mu^2$. The disappearance of all non-local terms is a crucial check on the accuracy of the calculation. Based on the structure of the Weinberg operator CT in eq. 3.71 the contribution of the external legs – expanded to second order – can be removed

and the vertex renormalization constant extracted:

$$\begin{aligned}\delta C_5^{(2)} &= \delta V_5^{(2)} - \frac{1}{2}\delta Z_\ell^{(1)}\delta C_5^{(1)} - \frac{1}{2}\delta C_5^{(1)}\left(\delta Z_\ell^{(1)}\right)^{\mathrm{T}} + \frac{1}{8}\delta Z_\ell^{(1)}\delta Z_\ell^{(1)} C_5 \\ &+ \frac{1}{8} C_5 \left(\delta Z_\ell^{(1)}\delta Z_\ell^{(1)}\right)^{\mathrm{T}} - \frac{1}{2}\delta Z_H^{(1)}\left[2\delta C_5^{(1)} + \delta Z_\ell^{(1)} C_5 + C_5\left(\delta Z_\ell^{(1)}\right)^{\mathrm{T}}\right] \\ &- \frac{1}{4}\delta Z_\ell^{(1)} C_5 \left(\delta Z_\ell^{(1)}\right)^{\mathrm{T}} - \frac{1}{2}\delta Z_\ell^{(2)} C_5 - \frac{1}{2} C_5 \left(\delta Z_\ell^{(2)}\right)^{\mathrm{T}} - \delta Z_H^{(2)} C_5.\end{aligned} \tag{3.77}$$

This is the complete result that was already used in parts eq. 3.45 to obtain the rank-increasing contribution. With it, the complete two-loop Weinberg operator vertex CT follows:

$$\begin{aligned}\delta C_5^{(2)} &= \frac{1}{\left(16\pi^2\right)^2 \varepsilon^2}\left\{\left[\frac{3}{16}g_1^4 + \frac{3}{8}g_1^2 g_2^2 + \frac{65}{16}g_2^4 - \lambda\left(\frac{3}{2}g_1^2 + \frac{15}{2}g_2^2 - 14\lambda - 4T\right)\right.\right. \\ &- \frac{1}{8}g_1^2 \mathrm{Tr}\left(15 Y_l Y_l^\dagger + 17 Y_{\mathrm{u}} Y_{\mathrm{u}}^\dagger + 5 Y_{\mathrm{d}} Y_{\mathrm{d}}^\dagger\right) - \frac{21}{8}g_2^2 T - 12 g_3^2 \mathrm{Tr}\left(Y_{\mathrm{u}} Y_{\mathrm{u}}^\dagger + Y_{\mathrm{d}} Y_{\mathrm{d}}^\dagger\right) \\ &\left.\left. + T^2 - \frac{1}{4}T' - \frac{9}{2}\mathrm{Tr}\left(Y_{\mathrm{u}} Y_{\mathrm{u}}^\dagger Y_{\mathrm{d}} Y_{\mathrm{d}}^\dagger\right)\right] C_5 + \left(\frac{45}{32}g_1^2 + \frac{63}{32}g_2^2 - \frac{3}{2}\lambda - \frac{9}{8}T\right)\right. \\ &\times \left[Y_l Y_l^\dagger C_5 + C_5\left(Y_l Y_l^\dagger\right)^{\mathrm{T}}\right] - \frac{9}{32}\left[Y_l Y_l^\dagger Y_l Y_l^\dagger C_5 + C_5\left(Y_l Y_l^\dagger Y_l Y_l^\dagger\right)^{\mathrm{T}}\right] \\ &\left. + \frac{9}{16} Y_l Y_l^\dagger C_5 \left(Y_l Y_l^\dagger\right)^{\mathrm{T}}\right\} \\ &+ \frac{1}{\left(16\pi^2\right)^2 \varepsilon}\left\{-\left[\frac{129}{32}g_1^4 + \frac{83}{16}g_1^2 g_2^2 + \frac{169}{96}g_2^4 + \lambda\left(g_1^2 + 7\lambda + 2T\right) - \frac{15}{16}g_2^2 T\right.\right. \\ &- \frac{5}{48}g_1^2 \mathrm{Tr}\left(15 Y_l Y_l^\dagger + 17 Y_{\mathrm{u}} Y_{\mathrm{u}}^\dagger + 5 Y_{\mathrm{d}} Y_{\mathrm{d}}^\dagger\right) - 10 g_3^2 \mathrm{Tr}\left(Y_{\mathrm{u}} Y_{\mathrm{u}}^\dagger + Y_{\mathrm{d}} Y_{\mathrm{d}}^\dagger\right) \\ &\left.\left. + \frac{1}{8}T' - \frac{3}{4}\mathrm{Tr}\left(Y_{\mathrm{u}} Y_{\mathrm{u}}^\dagger Y_{\mathrm{d}} Y_{\mathrm{d}}^\dagger\right)\right] C_5 - \left(\frac{57}{64}g_1^2 - \frac{33}{64}g_2^2 - \frac{5}{16}T\right)\right. \\ &\times \left[Y_l Y_l^\dagger C_5 + C_5\left(Y_l Y_l^\dagger\right)^{\mathrm{T}}\right] + \frac{19}{16}\left[Y_l Y_l^\dagger Y_l Y_l^\dagger C_5 + C_5\left(Y_l Y_l^\dagger Y_l Y_l^\dagger\right)^{\mathrm{T}}\right] \\ &\left. + \frac{1}{2} Y_l Y_l^\dagger C_5 \left(Y_l Y_l^\dagger\right)^{\mathrm{T}}\right\}.\end{aligned} \tag{3.78}$$

The recursion relations in eq. 3.14 provide another cross-check for the result. They relate the two-loop expansion coefficient $a^{(2)}$ of the second-order pole ε in eq. 3.78 to the one-loop expansion factor of the $1/\varepsilon$ from eq. 3.72 and all the one-loop beta functions. The latter can be obtained straightforwardly from the one-loop CTs determined in section 3.3.3 and the one-loop Weinberg operator vertex counterterm (again eq. 3.72). It has been verified that the recursion relation is fulfilled. Although stated above, it is important to remember that the relation does NOT prove the following result for the beta function, as it only concerns $a^{(2)}$ and not $a^{(1)}$, which solely fixes the beta function. However, canceling all non-local terms together with the fulfilled relations between $a^{(1)}$ and $a^{(2)}$ strongly indicates the correctness of all presented results as the first $1/\varepsilon$ and the second order poles $1/\varepsilon^2$ were calculated simultaneously. Finally, according to eq. 3.13, the desired two-loop

Weinberg operator beta function follows from the first-order pole:

$$\mu\frac{\mathrm{d}C_5^{(1)}}{\mathrm{d}\mu} = \frac{1}{16\pi^2}\left[\left(4\lambda - 3g_2^2 + 2T\right)C_5 - \frac{3}{2}Y_lY_l^\dagger C_5 - \frac{3}{2}C_5\left(Y_lY_l^\dagger\right)^{\mathrm{T}}\right], \tag{3.79}$$

$$\begin{aligned}\mu\frac{\mathrm{d}C_5^{(2)}}{\mathrm{d}\mu} = \frac{1}{\left(16\pi^2\right)^2}\Bigg\{&-\left[\frac{129}{8}g_1^4 + \frac{83}{4}g_1^2g_2^2 + \frac{169}{24}g_2^4 + 4\lambda\left(g_1^2 + 7\lambda + 2T\right) - \frac{15}{4}g_2^2T\right.\\ &- \frac{5}{12}g_1^2\mathrm{Tr}\left(15Y_lY_l^\dagger + 17Y_{\mathrm{u}}Y_{\mathrm{u}}^\dagger + 5Y_{\mathrm{d}}Y_{\mathrm{d}}^\dagger\right) - 40g_3^2\mathrm{Tr}\left(Y_{\mathrm{u}}Y_{\mathrm{u}}^\dagger + Y_{\mathrm{d}}Y_{\mathrm{d}}^\dagger\right)\\ &\left.+ \frac{1}{2}T' - 3\mathrm{Tr}\left(Y_{\mathrm{u}}Y_{\mathrm{u}}^\dagger Y_{\mathrm{d}}Y_{\mathrm{d}}^\dagger\right)\right]C_5 - \left(\frac{57}{16}g_1^2 - \frac{33}{16}g_2^2 - \frac{5}{4}T\right)\\ &\times\left[Y_lY_l^\dagger C_5 + C_5\left(Y_lY_l^\dagger\right)^{\mathrm{T}}\right] + \frac{19}{4}\left[Y_lY_l^\dagger Y_lY_l^\dagger C_5 + C_5\left(Y_lY_l^\dagger Y_lY_l^\dagger\right)^{\mathrm{T}}\right]\\ &+ 2Y_lY_l^\dagger C_5\left(Y_lY_l^\dagger\right)^{\mathrm{T}}\Bigg\}.\end{aligned} \tag{3.80}$$

This final form once again reproduces the rank-increasing contribution $2Y_lY_l^\dagger C_5\left(Y_lY_l^\dagger\right)^{\mathrm{T}}$ that was explicitly calculated in section 3.3.2 and found by [16, 45]. Here, however, the two-loop renormalization of the Weinberg operator was completed. It will improve the accuracy of numerics regarding neutrino oscillation parameters, which will be performed in the next chapter.

4. Analysis of Neutrino Parameters

4.1. Two-Loop RGEs for neutrino parameters

In the previous chapter, the two-loop RGE for the Weinberg operator was calculated (eq. 3.79 and 3.80). After SSB, these describe the running of the neutrino mass matrix according to eq. 2.46 by replacing $C_5 \to M_\nu$, while the additional factors $\frac{1}{2}v^2$ cancel. Following [18] on the notation for the two-loop mass matrix RGE, one gets:

$$\begin{aligned} \frac{\mathrm{d}M_\nu^\dagger}{\mathrm{d}t} &= \alpha M_\nu^\dagger + Q M_\nu^\dagger + M_\nu^\dagger Q^{\mathrm{T}} + 2P M_\nu^\dagger P^{\mathrm{T}}, \\ \frac{\mathrm{d}M_\nu}{\mathrm{d}t} &= \alpha M_\nu + M_\nu Q^\dagger + Q^* M_\nu + 2P^* M_\nu P^\dagger, \end{aligned} \tag{4.1}$$

with $t = \log\mu$. Comparing with the two-loop RGE provides the factors α, Q and P:

$$\begin{aligned} \alpha =& \frac{1}{16\pi^2}\left(4\lambda - 3g_2^2 + 2T\right) \\ &- \frac{1}{(16\pi^2)^2}\left[\frac{129}{8}g_1^4 + \frac{83}{4}g_1^2 g_2^2 + \frac{169}{24}g_2^4 + 4\lambda\left(g_1^2 + 7\lambda + 2T\right) - \frac{15}{4}g_2^2 T + \frac{1}{2}T'\right. \\ &- \frac{5}{12}g_1^2 \mathrm{Tr}\left(15 Y_l Y_l^\dagger + 17 Y_{\mathrm{u}} Y_{\mathrm{u}}^\dagger + 5 Y_{\mathrm{d}} Y_{\mathrm{d}}^\dagger\right) - 40 g_3^2 \mathrm{Tr}\left(Y_{\mathrm{u}} Y_{\mathrm{u}}^\dagger + Y_{\mathrm{d}} Y_{\mathrm{d}}^\dagger\right), \\ &\left. -3\mathrm{Tr}\left(Y_{\mathrm{u}} Y_{\mathrm{u}}^\dagger Y_{\mathrm{d}} Y_{\mathrm{d}}^\dagger\right)\right], \\ P =& \frac{1}{16\pi^2} Y_l Y_l^\dagger, \\ Q =& -\left[\frac{3}{2} + \frac{1}{16\pi^2}\left(\frac{57}{16}g_1^2 - \frac{33}{16}g_2^2 - \frac{5}{4}T\right)\right] P + \frac{19}{4}P^2. \end{aligned} \tag{4.2}$$

The equation is recast in this form to emphasize the rank-increasing contribution of $2PM_\nu P^{\mathrm{T}}$, which was explicitly calculated in section 3.3.2. The other terms related to α and Q only provide corrections to the already non-zero masses. This can be seen by rewriting eq. 4.1 in terms of diagonal mass matrices and eigenvalues, respectively. With the freedom to redefine lepton fields (compare section 2.1.4), one can choose to work in either the flavor eigenbasis and keep the lepton Yukawa matrices diagonal, or in the mass eigenbasis and non-diagonal Yukawa matrices. If the flavor basis is used, the lepton Yukawa matrix will remain diagonal during the RGE evolution, while the mass eigenvalues must be extracted at different energies. Further details on the extraction of the neutrino mass eigenvalues and mixing parameters, as well as the equivalent for the quark sector,

are presented in the following section, which focuses on the numerical evaluation of the RGE evolution.

As a side remark, depending on the convention, C_5 can be identified with $M^\dagger$ or M (if the Weinberg operator or its hermitian conjugated is used for the definition of C_5). However, with $P = P^\dagger$ being diagonal in the flavor basis, the RGE remains the same. The presented results were obtained independent of the choice of convention. With this, the definition of the Weinberg operator (eq. 2.45) and the SVD decomposition (eq. 2.13), the relation between the non-diagonal mass matrix, its eigenvalues and the PMNS matrix is:

$$U_{\mathrm{PMNS}}^{\mathrm{T}} M_\nu U_{\mathrm{PMNS}} = D_\nu, \tag{4.3}$$

with $D_\nu = \mathrm{diag}(m_1, m_2, m_3)$ and all non-physical phases eliminated. Using for simplicity $U \equiv U_{\mathrm{PMNS}}$ gives

$$U^{\mathrm{T}} \frac{\mathrm{d}M_\nu}{\mathrm{d}t} U = U^{\mathrm{T}} \frac{\mathrm{d}U^*}{\mathrm{d}t} D_\nu + D_\nu \frac{\mathrm{d}U^\dagger}{\mathrm{d}t} U + \frac{\mathrm{d}D_\nu}{\mathrm{d}t}. \tag{4.4}$$

Defining $T \equiv U^\dagger \frac{\mathrm{d}U}{\mathrm{d}t}$ allows for replacing $\frac{\mathrm{d}U^\dagger}{\mathrm{d}t} U = -T$ and $U^{\mathrm{T}} \frac{\mathrm{d}U^*}{\mathrm{d}t} = T^\dagger$. The anti-hermitian property is a result of $\frac{\mathrm{d}}{\mathrm{d}t}(U^\dagger U) = 0$. Inserting the mass matrix RGE into the left-hand side gives the analogue equation in terms of mass eigenvalues and matrices:

$$\frac{\mathrm{d}D_\nu}{\mathrm{d}t} = D_\nu T - T^* D_\nu + \alpha D_\nu + \hat{Q}^* D_\nu + D_\nu \hat{Q}^\dagger + 2\hat{P}^* D_\nu \hat{P}^\dagger, \tag{4.5}$$

with $\hat{Q} = U^\dagger Q U$ and $\hat{P} = U^\dagger P U$. This differential equation encapsulates the running behavior of the mass eigenvalues in the form of $\frac{\mathrm{d}D_\nu}{\mathrm{d}t}$ and the running behavior of the mixing parameters in the form of T. On the one hand, the mass eigenvalues m_i and diagonal entries of the hermitian matrices $\hat{Q}_{ii}$ and $\hat{P}_{ii}$ are real-valued; on the other hand, the diagonal entries of the anti-hermitian matrix T_{ii} are purely imaginary. Hence, taking real and imaginary parts of the diagonal entries gives

$$\frac{\mathrm{d}m_i}{\mathrm{d}t} = \left(\alpha + 2\hat{Q}_{ii}\right) m_i + 2 \sum_k m_k \mathrm{Re}\left(\hat{P}_{ik}^2\right), \tag{4.6}$$

$$m_i T_{ii} = \sum_k m_k \mathrm{Im}\left(\hat{P}_{ik}^2\right). \tag{4.7}$$

Repeating analogously for the off-diagonal elements provides

$$\left(m_j - m_i\right) \mathrm{Re}\left(T_{ij}\right) = \left(m_j + m_i\right) \mathrm{Re}\left(\hat{Q}_{ij}\right) + \sum_k m_k \mathrm{Re}\left(\hat{P}_{ik}\hat{P}_{jk}\right), \tag{4.8}$$

$$\left(m_j + m_i\right) \mathrm{Im}\left(T_{ij}\right) = \left(m_j - m_i\right) \mathrm{Im}\left(\hat{Q}_{ij}\right) + \sum_k m_k \mathrm{Im}\left(\hat{P}_{ik}\hat{P}_{jk}\right). \tag{4.9}$$

The acquired RGEs follow the structure obtained in [18] for RHN. The only differences compared to [18] are changing minus signs in front of all imaginary parts according to $\hat{P}_{ik} \leftrightarrow \hat{P}_{ki} = \hat{P}_{ij}^*$, a relative factor of 2 related to the rank-increasing term (in right-handed case trace over internal $\mathrm{SU(2)_L}$ indices) and of course a different definition of P, Q itself. Therefore, the discussion on the physical implications of these RGEs follows the one

from [18] closely, with the difference that the lepton Yukawa matrices are much smaller compared to the hypothetical RHN Yukawa couplings Y introduced in eq. 2.21. These are unconstrained apart from perturbative bounds and can be of $\mathcal{O}(1)$. In contrast, the biggest eigenvalue of $Y_l = \mathrm{diag}\left(y_e, y_\mu, y_\tau\right)$ is $y_\tau \simeq 10^{-2}$ at 200 GeV [59, 60] and yields $\hat{Q}, \hat{P} \simeq 6 \times 10^{-7}$. Two neutrino mass differences are measured: $\Delta m^2_{21} \simeq 7.42 \times 10^{-5}\,\mathrm{eV}^2$ and $\Delta m^2_{32} \simeq 2.517 \times 10^{-3}\,\mathrm{eV}^2$ (table 2.1), which opens the opportunity for one massless or very light neutrino respectively. The implications of the RGEs for all massive neutrinos and as well as for two massive and massless neutrinos are discussed.

4.1.1. All massive neutrinos

If all neutrinos are massive and their masses roughly the same order of magnitude, which means around $10^{-2}\,\mathrm{eV}$, $\hat{P}^2$ can be safely neglected, and the running of the mass eigenvalues is described by

$$\frac{m_i\left(\Lambda_{\mathrm{EW}}\right)}{m_i\left(\Lambda\right)} \simeq \exp\left[-\int_{\Lambda_{\mathrm{EW}}}^{\Lambda} \mathrm{d}t \left(\alpha + 2\hat{Q}_{ii}\right)\right] \sim \exp\left[-\left(\alpha + 2\hat{Q}_{ii}\right)\log\left(\frac{\Lambda}{\Lambda_{\mathrm{EW}}}\right)\right] . \quad (4.10)$$

The cut-off scale Λ typically lies around $10^{-14}\,\mathrm{GeV}$ as it corresponds to the seesaw scale. RHN masses roughly need to be at this energy range to describe the LHN masses via the seesaw mechanism. But other UV completions with varying cut-off scales are possible as well. The biggest two-loop contribution stems from $\alpha \subset \frac{169}{24\cdot(16\pi^2)^2} g_2^4 \simeq 5 \cdot 10^{-5}$ with $g_2 \simeq 0.65$ at 200 GeV [59, 60]. All other initial conditions at the electroweak scale can be found in table 4.1, which was used for the numerical evaluation of the RGEs. Compared to the biggest one-loop correction $\alpha \subset \frac{3}{(16\pi^2)} g_2^2 \sim 8 \cdot 10^{-3}$, this amounts to relative correction of around 6%. α affects all masses identically as it is a global factor not depending on the generation, while $\hat{Q}_{ii}$ could lift degeneracies in mass. However, with $\hat{Q}$ being of the order 10^{-7}, it cannot account for the measured mass differences. Furthermore, the measured mass gaps prevent any infrared quasi-fixed points discussed in [18]. Combining eqs. 4.8 and 4.9 gives (for $i \neq j$)

$$T_{ij} = \frac{m_j + m_i}{m_j - m_i}\mathrm{Re}\left(\hat{Q}_{ij}\right) + \mathrm{i}\frac{m_j - m_i}{m_j + m_i}\mathrm{Im}\left(\hat{Q}_{ij}\right) . \quad (4.11)$$

If $\hat{Q} \gg \Delta m$, T_{ij} would change rapidly until it hits a quasi-fixed point because the evolution has to stabilize at some point. As a result, T_{ii} becomes very small, demanding $\mathrm{Re}\left(\hat{Q}_{ij}\right) \simeq 0$. However, the one-loop (and two-loop, respectively) corrections are too small compared to the measured mass differences.

4.1.2. One massless neutrino

In the all-massive case, the two-loop contributions only contributed subdominantly without altering qualitatively the one-loop corrections. To account for the two non-zero squared mass differences from oscillation experiments, two neutrinos must be massive. However,

the third could be massless at tree level. For the different orderings, the following situation arises at 200 GeV:

$$\begin{aligned} &m_1 = 0 \quad m_2 = 0.00861\,\text{eV} \quad m_3 = 0.05007\,\text{eV} \qquad \text{(NO)},\\ &m_3 = 0 \quad m_1 = 0.04911\,\text{eV} \quad m_1 = 0.04986\,\text{eV} \qquad \text{(IO)}, \end{aligned} \tag{4.12}$$

by reconstructing the masses bottom-up from the massless one and using Δm^2_{ij}. Situations like this could arise, for instance, in a seesaw type-I scenario with two RHNs [26] (section 2.2.1). For one massless neutrino, the two-loop corrections significantly alter the mass matrix by increasing the rank. Section 3.3.2 discussed that no symmetry protects the particle from becoming massive.

Especially eq. 4.6 gives insights into the mass generation of massless neutrino $m_i = 0$ at the cut-off scale. While corrections proportional to α and $\hat{Q}_{ii}$ vanish as they do not couple to the heavier eigenstates (only to m_i itself), $\hat{P}$ induces corrections proportional to all masses and especially the heavier massive neutrinos. Consequently, it does not vanish for a massless neutrino. By approximately considering the τ Yukawa eigenvalue only, the mass induced by quantum corrections determined by eq. 4.6 for NO and IO respectively read:

$$\begin{aligned} m_1\left(\Lambda_{\text{EW}}\right) &\sim \frac{2y_\tau^4}{\left(16\pi^2\right)^2}\ln\left(\frac{\Lambda}{\Lambda_{\text{EW}}}\right)\cdot\sum_{i=2,3} m_i \text{Re}\left(U^*_{\tau 1}U_{\tau i}\right)^2,\\ m_3\left(\Lambda_{\text{EW}}\right) &\sim \frac{2y_\tau^4}{\left(16\pi^2\right)^2}\ln\left(\frac{\Lambda}{\Lambda_{\text{EW}}}\right)\cdot\sum_{i=1,2} m_i\, \text{Re}\left(U^*_{\tau 3}U_{\tau i}\right)^2. \end{aligned} \tag{4.13}$$

Numerically, this generated mass is around 10^{-13} eV for $\Lambda = 10^{14}$ GeV due to the tiny lepton Yukawa coupling and the two-loop suppression factor $1/\left(16\pi^2\right)^2$. Furthermore, the size of m_3 for IO is typically larger than m_1 for NO as it receives correction proportional to m_1 and m_2, which are almost equally large for IO.

A tiny or vanishing mass implies the left-hand side of eq. 4.7 is close or equal to zero. Consequently, a non-zero combination of right-handed sides necessitates a significantly high T_{ii} and a rapid variation of U with respect to μ. However, this rapid change in U cannot persist across all scales (similar to the all-massive case discussion) but come to a stop at some energy. Since the left-hand side is approximately zero, the right-hand side must also be approximately zero. This leads to a non-trivial relationship between mixing parameters expressed as:

$$0 = \sum_k m_k \text{Im}\left(\hat{P}^2_{ik}\right). \tag{4.14}$$

From this point on, T_{ii} will stay small, and the beta function for the mixing parameters runs into the infrared quasi-fix point, and from there on, the relation between parameters described in eq. 4.14 stays unchanged. Again neglecting all contributions from y_e, y_μ and only considering y_τ gives the fixed-point relation in case of NO and IO respectively:

$$\begin{aligned} 0 &= m_2 \text{Im}\left(U^*_{\tau 1}U_{\tau 2}\right)^2 + m_3 \text{Im}\left(U^*_{\tau 1}U_{\tau 3}\right)^2,\\ 0 &= m_1 \text{Im}\left(U^*_{\tau 3}U_{\tau 1}\right)^2 + m_2 \text{Im}\left(U^*_{\tau 3}U_{\tau 2}\right)^2. \end{aligned} \tag{4.15}$$

Inserting the parameterization from eqs. 2.17 and 2.18 for U gives a relation between the CP-violating phases for NO. However, the parameterization for IO needs to be adjusted. Instead of removing the Majorana phase for the third generation, the one connected to the first generation is eliminated. This can be seen as globally redefining all phases by $e^{-\mathrm{i}\rho}$ and yielding the Majorana phase matrix

$$\begin{pmatrix} 1 & 0 & 0 \\ 0 & e^{\mathrm{i}(\sigma-\rho)} & 0 \\ 0 & 0 & e^{-\mathrm{i}\rho} \end{pmatrix}, \tag{4.16}$$

in contrast to eq. 2.18. The reason to change the parameterization is to connect one phase with the third massless neutrino. As long as there is no mass term, ν_3 can be redefined with a phase that removes $e^{-\mathrm{i}\rho}$ and leaves only one physical Majorana phase. This additional unphysical DOF is harder to identify with the original parameterization. However, when the quantum corrections generate m_3, the phase can no longer be removed and $\rho, \sigma - \rho$ become physical. So ρ jumps to the physical phase in the truly massless limit. Numerical results for this behavior are presented in the next section.

Using this parametrization of the Majorana masses for IO and the one from eq. 2.18 for NO together with the parameterization for the CKM-like part V of the PMNS matrix (eq. 2.17) in the fix point relations (eq. 4.15) gives for NO and IO respectively:

$$\tan 2\rho = -\frac{m_2 \cos 2\sigma \mathrm{Im}\left(V_{\tau 1}^* V_{\tau 2}\right)^2 + m_2 \sin 2\sigma \mathrm{Re}\left(V_{\tau 1}^* V_{\tau 2}\right)^2 + m_3 \mathrm{Im}\left(V_{\tau 1}^* V_{\tau 3}\right)^2}{m_2 \sin 2\sigma \mathrm{Im}\left(V_{\tau 1}^* V_{\tau 2}\right)^2 - m_2 \cos 2\sigma \mathrm{Re}\left(V_{\tau 1}^* V_{\tau 2}\right)^2 - m_3 \mathrm{Re}\left(V_{\tau 1}^* V_{\tau 3}\right)^2}, \tag{4.17}$$

$$\tan 2\rho = -\frac{m_1 \mathrm{Im}\left(V_{\tau 3}^* V_{\tau 1}\right)^2 + m_2 \cos 2\left(\sigma-\rho\right) \mathrm{Im}\left(V_{\tau 3}^* V_{\tau 2}\right)^2 + m_2 \sin 2\left(\sigma-\rho\right) \mathrm{Re}\left(V_{\tau 3}^* V_{\tau 2}\right)^2}{m_1 \mathrm{Re}\left(V_{\tau 3}^* V_{\tau 1}\right)^2 - m_2 \sin 2\left(\sigma-\rho\right) \mathrm{Im}\left(V_{\tau 3}^* V_{\tau 2}\right)^2 + m_2 \cos 2\left(\sigma-\rho\right) \mathrm{Re}\left(V_{\tau 3}^* V_{\tau 2}\right)^2}.$$

To that matter, it is important to note, that $\sigma - \rho$ and ρ should be treated as independent variables. Furthermore, V includes with δ another CP-violating phase, similar to the quark sector. In the leptonic case, however, its impact is more noticeable as the mixing between generations is enhanced compared to the CKM matrix.

4.2. Numerical Calculations

In the previous section, analytic results on the running of neutrino oscillation parameters, based on the two-loop RGEs, were derived. Of particular interest is the scenario where a single particle, initially massless at the cut-off scale, acquires mass through the phenomenon of running effects. Furthermore, the Majorana-phase RGE connected to the light neutrino runs into a fixpoint, resulting in unique relations between the mixing parameters. In this section, these findings are confirmed by numerically evaluating the RGEs and running them from the cut-off scale to the electroweak scale. For that the Weinberg-operator RGEs are supplemented by the two-loop SM RGEs(for explicit form see appendix A.3), which were extracted from SARAH [61, 62] and RGBeta [63]. Those are based on the two-loop beta function results for general renormalizable quantum field theories [64–66].

m_{u} [MeV]	1.2504	m_e [MeV]	0.5239	δ^{q} [°]	65.55
m_{d} [MeV]	2.7176	m_μ [GeV]	0.1104	g_1	0.3589
m_{s} [MeV]	54.120	m_τ [GeV]	1.8748	g_2	0.6468
m_{c} [GeV]	0.6299	$\sin\theta^q_{12}$	0.2250	g_3	1.1525
m_{b} [GeV]	2.8731	$\sin\theta^q_{23}$	0.04182	λ	0.1235
m_{t} [GeV]	173.08	$\sin\theta^q_{13}$	0.00369	$\langle H\rangle$ [GeV]	246

Table 4.1.: Initial conditions at 200 GeV. Shown are experimental measurements regarding quark and lepton masses as well as gauge couplings and Higgs self-coupling and CKM mixing parameters (mixing angles θ^{q}_{ij} and CP phase δ^{q}) at this energy scale [67]. These input values are completed with the PMNS mixing parameters from table 2.1 and the neutrino masses from eq. 4.10 for NO and IO. For completeness, the table also includes the Higgs VEV.

4.2.1. Initial Conditions

Initial conditions should be set at the cut-off scale $\Lambda = 10^{14}$ GeV, while masses and all other parameters are evolved down to the electroweak scale. However, experiments cannot probe such high energies. Therefore, the experimental data at 200 GeV – summarized in table 4.1 [67] – are used to evolve the parameters up to the cut-off scale. These will then be modified to account for one massless neutrino, but still agree with the low energy measurements when run down again.

The input values at 200 GeV are listed in table 4.1, which includes quark and lepton masses as well as gauge couplings, Higgs self-coupling and CKM mixing parameters (mixing angles θ^{q}_{ij} and CP phase δ^{q}) at this energy scale [67]. The corresponding Yukawa coupling eigenvalues follow from eq. 2.11 via $y = \sqrt{2}m/v$. The PMNS mixing parameters from table 2.1 and the neutrino masses from eq. 4.10 for NO and IO complete the input values. Since the Yukawa matrices are kept diagonal, the off-diagonal neutrino and down-quark mass matrices are

$$\begin{aligned} M_\nu &= U^*_{\mathrm{PMNS}}\mathrm{diag}\left(y_e, y_\mu, y_\tau\right) U^\dagger_{\mathrm{PMNS}}, \\ M_{\mathrm{D}} &= U_{\mathrm{CKM}}\mathrm{diag}\left(y_{\mathrm{d}}, y_{\mathrm{s}}, y_{\mathrm{b}}\right) U^\dagger_{\mathrm{CKM}}, \end{aligned} \tag{4.18}$$

with U_{PMNS} and U_{CKM} evaluated at 200 GeV. When running the parameters up to Λ, neutrino masses, and mixing parameters are extracted by decomposing $M_\nu[\Lambda]$ according to eq. 4.3:

$$M_\lambda[\Lambda] = U^*[\Lambda] D_\nu[\Lambda] U^\dagger[\Lambda]. \tag{4.19}$$

To avoid the inclusion of unphysical phases in the PMNS matrix (eq. 2.16) and hence keep the standard parameterization, the Dirac phase is extracted via (similar to [40]):

$$\delta = -\mathrm{Arg}\left(U^*_{11}U^*_{33}U_{13}U_{31} + \cos^2\theta_{12}\cos^2\theta_{13}\sin^2\theta_{12}\cos^2\theta_{23}\right), \tag{4.20}$$

which is invariant under phase redefinitions of the charged leptons. With δ, the unphysical phases can be reconstructed and the Majorana phases determined.

As expected from the rank-increasing contributions, a tiny third neutrino mass is generated (this happens no matter if increasing or decreasing the energy scale). However, the evolution of the gauge couplings, λ, quark masses, charged lepton mass, and two heavy neutrino masses and mixing angles and Dirac phases barely depend on the exact value of the tiny third neutrino mass and Majorana phases. Hence, the generated neutrino mass can be reset to zero to make it massless at the cut-off scale, while keeping all other parameters unchanged. This defines the high-energy initial conditions, that provide the correct experimental data at Λ_{EW} and include a massless neutrino. All Majorana phases are kept arbitrary.

4.2.2. Fix Point of Majorana phases

As previously discussed, the Majorana phase associated with the initially massless neutrino runs into a fixed point, as described by eq. 4.17. This behavior has been numerically verified by evaluating the Majorana phase across all energy scales between Λ and Λ_{EW}. Fig. 4.1 illustrates the result for both NO and IO. As initial conditions $(\rho, \sigma) = (5/6\pi, \pi/6)$ for NO and $(\rho, \sigma - \rho) = (5/12\pi, -1/3\pi)$ for IO were chosen. σ $(\sigma - \rho)$ determines the position of the fixpoint, while ρ sets the starting point. Limitations in numerical precision, and the theoretical divergence of neutrino mass at the cut-off scale, preclude setting the lightest neutrino mass to precisely zero. Consequently, various non-zero initial masses are explored, focusing on values smaller than or comparable to those generated by quantum corrections. This approach allows for quantitative evaluation of the effects predicted for the massless case. Notably, decreasing the initial mass accelerates the Majorana phase evolution, consistent with the theoretical analysis detailed in section 4.1.2. Furthermore, a non-zero initial mass modifies eq. 4.7 by requiring a smaller T_{ii} value (resulting in slower evolution of the mixing parameter) to accommodate the non-zero right-hand side at the cut-off scale.

4.2.3. Parameter Scan

Figure 4.1 only showed the fixpoint of ρ for one specific set of initial conditions to illustrate the running behavior. However, there are no experimental constraints on the Majorana phases, and barely any on the Dirac phase (see table 2.1). Hence, the RGEs for the lightest neutrino mass as well as ρ are evaluated numerically for the full spectrum of initial conditions regarding $\delta[\Lambda]$ and $\sigma[\Lambda]$ ($(\sigma - \rho)[\Lambda]$) for NO (IO). $\delta[\Lambda] \in [0, 2\pi]$, while $\sigma[\Lambda] \in [0, \pi]$. The reason is, that the interval $[\pi, 2\pi]$ amounts to a relative factor of -1, under which the Majorana mass term is invariant, see eq. 2.20. The physical parameter range of σ is therefore restricted. Fig. 4.2 displays the lightest neutrino mass evaluated at the electroweak scale in dependence on the initial conditions. It can be observed, that the generated mass falls within the anticipated range of $10^{-13}\,\mathrm{eV} - 10^{-14}\,\mathrm{eV}$: notably, as discussed in section 4.1.2, the average generated mass exhibits a higher value for IO than

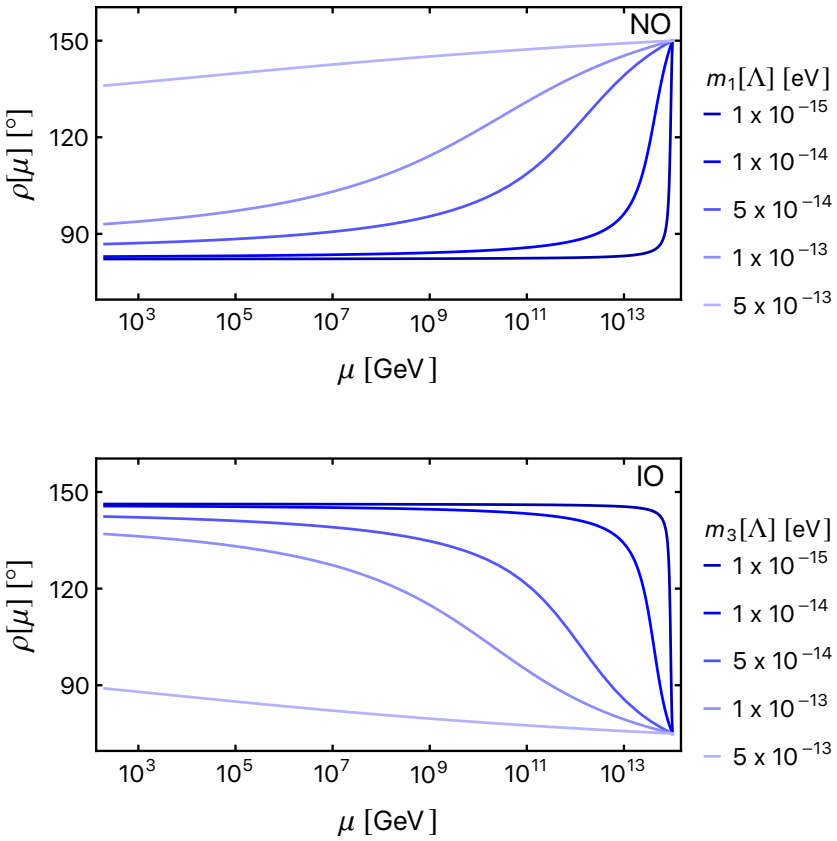

Figure 4.1.: Evolution of the Majorana phases connected to the light neutrino. Shown are the evolution with energy scale for the Majorana phase ρ for NO (top) and IO (bottom) with the initial conditions $(\rho, \sigma) = (5/6\pi, \pi/6)$ for NO and $(\rho, \sigma - \rho) = (5/12\pi, -1/3\pi)$ for IO. The RGE evolution is evaluated for different light neutrino masses. The smaller it is, the more rapid the initial change of the phase is.

NO. Similarly, the value of the Majorana phase fixpoint is governed by the initial values of σ and ρ, as demonstrated by fig. 4.3, which span the full parameter space. In the case of IO, an apparent discontinuity arises. It stems from the inherent constraint of ρ to the interval $[0, \pi]$. At the point of discontinuity, values exceeding π are identified with values within this interval, resulting in the non-continuous jump observed in the figure's central region.

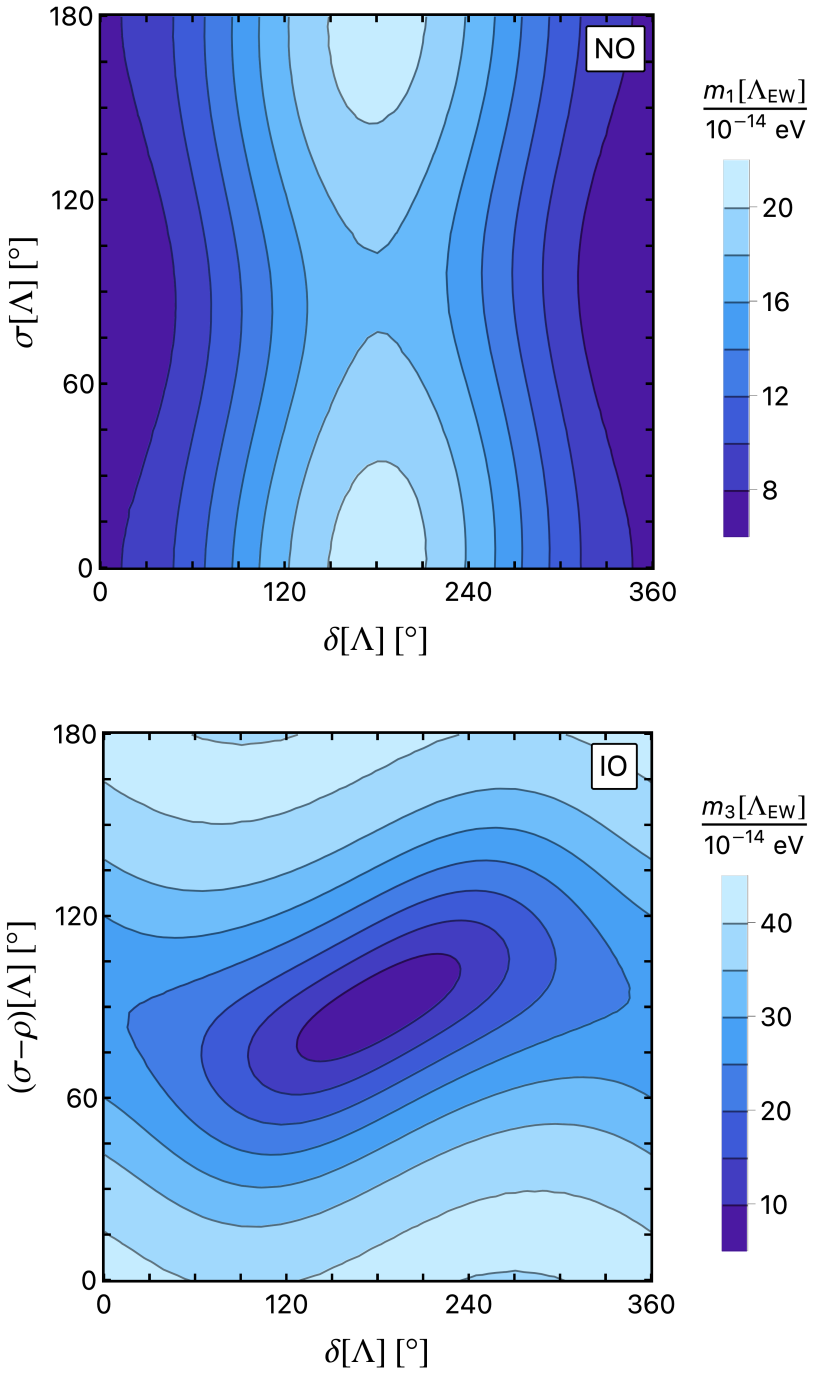

Figure 4.2.: Lightest neutrino for different initial conditions. Shown are the generated mass evaluated at the Electroweak (EW) scale for initially massless neutrino in the case of NO (top) and IO (bottom). Their dependence on initial conditions of the Dirac phase and one Majorana phase (while the other runs into a fixpoint) are displayed.

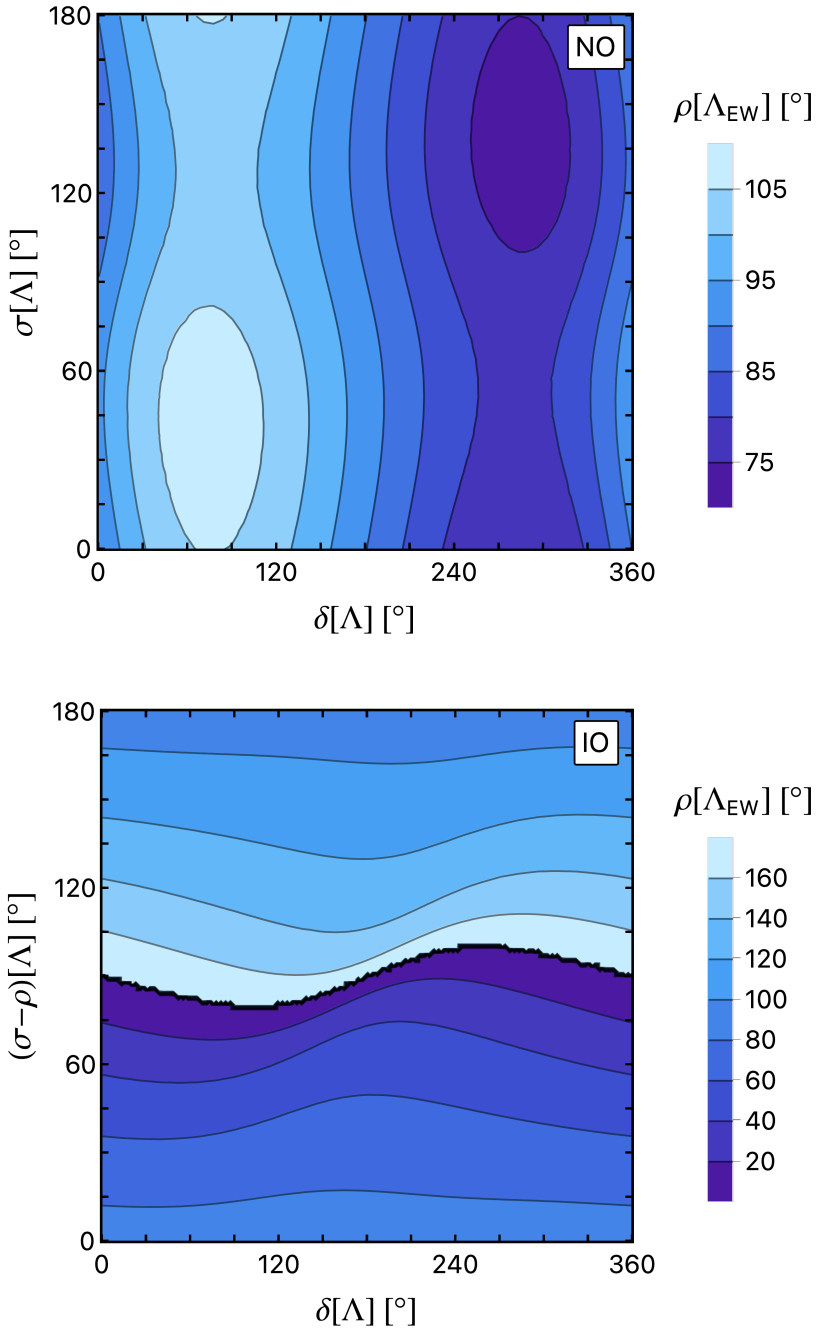

Figure 4.3.: Majorana phase for different initial conditions. Shown is the Majorana phase ρ evaluated at the electroweak scale connected to the initially massless neutrino in the case of NO (top) and IO (bottom). Its dependence on the initial conditions of the Dirac phase and the other Majorana phase (σ, $\sigma - \rho$ for NO and IO respectively) are displayed.

4.2.4. Neutrinoless Double Beta Decay

The parameter related to the neutrinoless double beta decay is

$$\left|m_{\beta\beta}\right| = \left|\sum_k m_k U_{ek}^2\right| = \begin{cases} \left|m_1 V_{e1}^2 \cdot e^{2\mathrm{i}\rho} + m_2 V_{e2}^2 \cdot e^{2\mathrm{i}\sigma} + m_3 V_{e3}^2\right| , & \text{(NO)}, \\ \left|m_1 V_{e1}^2 + m_2 V_{e2}^2 \cdot e^{2\mathrm{i}(\sigma-\rho)} + m_3 V_{e3}^2 \cdot e^{-2\mathrm{i}\rho}\right| , & \text{(IO)}. \end{cases} \tag{4.21}$$

Despite the potentially significant values of the Majorana phases, as illustrated in fig. 4.3, effects are greatly suppressed by the tiny neutrino mass. This can deduced from eq.4.13 by expressing U in terms of Majorana phases and CKM-type matrix elements:

$$\begin{aligned} m_1 &\sim \epsilon_\tau \left[m_2 e^{2\mathrm{i}\sigma} \left(V_{\tau 1}^* V_{\tau 2}\right)^2 + m_3 \left(V_{\tau 1}^* V_{\tau 3}\right)^2\right] \cdot e^{-2\mathrm{i}\rho} \qquad \text{(NO)}, \\ m_3 &\sim \epsilon_\tau \left[m_1 \left(V_{\tau 3}^* V_{\tau 1}\right)^2 + m_2 e^{2\mathrm{i}(\sigma-\rho)} \left(V_{\tau 3}^* V_{\tau 2}\right)^2\right] \cdot e^{2\mathrm{i}\rho} \qquad \text{(IO)}, \end{aligned} \tag{4.22}$$

with $\epsilon_\tau = 2y_\tau^2 \ln \frac{\Lambda}{\Lambda_{\mathrm{EW}}}/(16\pi^2)^2$. Putting these back into eq. 4.21 gives

$$\left|m_{\beta\beta}\right| \simeq \begin{cases} \left|m_2 e^{2\mathrm{i}\sigma} \left[V_{e2}^2 + \epsilon_\tau V_{e1}^2 \left(V_{\tau 1}^* V_{\tau 2}\right)^2\right] + m_3 \left[V_{e3}^2 + \epsilon_\tau V_{e1}^2 \left(V_{\tau 1}^* V_{\tau 3}\right)^2\right]\right| , \\ \left|m_1 \left[V_{e1}^2 + \epsilon_\tau V_{e3}^2 \left(V_{\tau 3}^* V_{\tau 1}\right)^2\right] + m_2 e^{2\mathrm{i}(\sigma-\rho)} \left[V_{e2}^2 + \epsilon_\tau V_{e3}^2 \left(V_{\tau 3}^* V_{\tau 2}\right)^2\right]\right| . \end{cases} \tag{4.23}$$

Consequently, it becomes evident that the corrections concerning the generated neutrino mass and its associated Majorana phase are negligible in magnitude (scaling proportionally to ϵ_τ). Hence, they do not contribute meaningfully to $m_{\beta\beta}$.

5. Right-Handed Neutrino Extensions

This chapter transitions from the effective Weinberg operator description of neutrino masses to explicit UV models. A natural addition to the SM, as detailed in section 2.2.1, involves introducing Right-Handed Neutrinos (RHNs). If these possess masses at the seesaw scale ($\sim 10^{14-15}$ GeV), they inherently generate the observed minute neutrino masses through the seesaw mechanism. Integrating them out effectively produces the Weinberg operator, suppressed by a high cut-off scale. Similar to the two-loop structures explored for light neutrinos (LHN) in the preceding chapters, analogous structures exist for RHNs as well (fig. 3.1 (a), fig. 5.1). These were first comprehensively investigated in [17–19]. However, it is crucial to recognize that corrections to the RHN masses occur above the cut-off scale and are consequently not encapsulated by the two-loop Weinberg operator RGEs. Despite this distinction, much of the analysis remains applicable, as the terms responsible for increasing the rank of the neutrino mass matrix share the same form. A critical difference lies in the potential magnitude of these contributions. Unlike LHN Yukawa couplings constrained by experimental data, RHN Yukawa couplings can be $\mathcal{O}(1)$, allowing for more significant quantum effects. The RGE for the RHN mass matrix M is provided by [18]:

$$\frac{\mathrm{d}M}{\mathrm{d}t} = MQ + Q^{\mathrm{T}}M + 4P^{T}MP, \tag{5.1}$$

where $P = \frac{1}{16\pi^2}Y^{\dagger}Y$ depends on the RHN Yukawa coupling Y. Q is a function of $P, g_1, g_2, Y_{\mathrm{u}}$. Solving the differential equation to second order gives [18]

$$M[t] \simeq M_0 + t\left(M_0P + P^{\mathrm{T}}M_0\right) - \frac{t}{4}(1-2t)\left(M_0P^2 + \left(P^{\mathrm{T}}\right)^2 M_0\right) + t(4+t)P^{\mathrm{T}}M_0P, \tag{5.2}$$

where M_0 denotes the initial value at a specific scale up to which the theory remains valid. As argued in [17], if this cut-off scale coincided with the Planck scale (Λ_{Pl}), and one neutrino remains massless at that scale while others have masses around Λ_{Pl}, the lightest

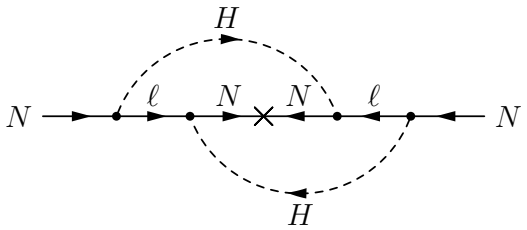

Figure 5.1.: Rank-increasing two-loop diagram for RHN. Massless RHN acquire masses proportional to the heavy RHN masses through this two-loop effect.

RHN would acquire a mass in the seesaw scale range. However, this scenario essentially replicates the inclusion of a single massive RHN at the seesaw scale, while the contribution of heavier two to the active neutrino masses is suppressed by $\mathcal{O}(P^2)$. Consequently, it cannot explain the observed neutrino mass hierarchy. An alternative approach involves introducing only one massive RHN at Λ_{Pl}. In this case, one massless neutrino gains a mass of the order $P^2 \cdot \Lambda_{\mathrm{Pl}}$(seesaw scale), while the other only becomes massive at the fourth order (P^4), rendering it too light for the seesaw mechanism. Ultimately, this necessitates the introduction of an additional scalar with the same quantum numbers as the Higgs fields (corresponding to the Two-Higgs Doublet Model (2HDM)). This additional source of flavor violation generates masses for both initially massless RHNs at P^2, making it a viable UV completion. Its advantage compared to the standard type-I seesaw lies in eliminating the need for another scale beyond the existing electroweak and Planck scales.

An open question, however, is the justification for having two massless neutrinos at the Planck scale. Usually, global symmetries are introduced to prohibit these mass terms. There is a commonly held belief, though, that gravity does not preserve global symmetries such that they will not survive at the Planck scale [68]. On the one hand, this further motivates the Planck scale cut-off as lepton number violation appears naturally. On the other hand, only gauge extension can explain the distinction between massless and massive RHNs. Furthermore, all emerging gauge anomalies must cancel.

5.1. Gauge Anomalies

Quantum effects can break symmetries which are present in the classic theory. This occurs because the path integral measure is not invariant under the symmetry. Chiral anomalies concern theories with massless chiral fermions, where vector and axial symmetry cannot be observed simultaneously. The breakdown of the axial current at one-loop is shown in fig. 5.2 [69] and evaluated to

$$D_\mu J^{A\mu} \propto \mathrm{Tr}\left[\gamma_5 T^A \left\{T^B, T^C\right\}\right], \tag{5.3}$$

where D_μ denotes the covariant derivative and $T^{A,B,C}$ the generators of the gauge group in their respective representations. The anomaly represents the incompatibility in

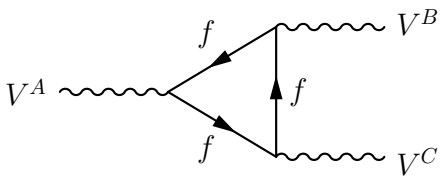

Figure 5.2.: Anomaly diagram. Shown is the one-loop triangle diagram, which leads to gauge anomalies. f denotes all chiral massless fermions that can run inside the loop, while $V^{A,B,C}$ denote gauge bosons (not necessarily of the same gauge group) with adjoint index A, B, C.

perturbative calculations between gauge invariance and chiral symmetry. In dimensional regularisation (which preserves gauge invariance), it is reflected in the form of γ_5, which cannot be trivially continued to d dimensions [70].

Breakdown of gauge symmetries would create inconsistencies with gauge boson masses and 3- and 4-point amplitudes, resulting in unphysical states [37]. Therefore, for the theory to be self-consistent and anomaly-free, triangle diagrams involving all gauge field combinations must cancel naturally. The Adler-Bardeen theorem affirms that if this condition is met at the one-loop level, the theory remains anomaly-free to all orders [71]. Conventionally, all fermions are defined to be left-handed, employing the charge conjugate as described in eq. 2.1.

5.2. General Considerations

5.2.1. Two Massive RHN in 2HDM

The scenario with two massive RHNs and only one scalar doublet proves insufficient to explain the observed active neutrino mass hierarchy, which, however, no longer remains true in the 2HDM. In the following, this scenario is investigated since it was not considered in [19]. As there are two scalar doublets H_1, H_2 and all Yukawa couplings in the type-I seesaw extension (eq. 2.21) should be replaced by $Y \to Y^{(a)}$

$$\mathcal{L} \subset \overline{N_{\alpha\mathrm{R}}} \mathrm{i}\partial\!\!\!/ N_{\alpha\mathrm{R}} - \left(Y^{(a)}_{\alpha\beta} \overline{\ell_{\alpha\mathrm{L}}} \widetilde{H}_a N_{\beta\mathrm{R}} + \frac{1}{2} M_{\alpha\beta} \overline{N^{\mathrm{c}}_{\alpha\mathrm{R}}} N_{\beta\mathrm{R}} + \mathrm{h.c.} \right) \tag{5.4}$$

and summed over $a = 1, 2$. The same applies to other Yukawa couplings but does not affect the discussion of RHN mass matrix. Furthermore, P from eq. 5.2 is replaced by $P^{ab} = \frac{1}{16\pi^2} {Y^{(a)}}^\dagger Y^{(b)}$ and the evolution of $M[t]$ after reorganizing some terms [18] reads:

$$\begin{aligned} M[t] \simeq & \left[1 + \sum_a \left(P^{(aa)} t + \frac{1}{2} {P^{(aa)}}^2 t^2 \right) \right]^{\mathrm{T}} M_0 \left[1 + \sum_a \left(P^{(aa)} t + \frac{1}{2} {P^{(aa)}}^2 t^2 \right) \right] \\ & + 4 \sum_{a,b} {P^{(ba)}}^{\mathrm{T}} M_0 P^{(ab)} t + \mathcal{O}({P^{(ab)}}^3). \end{aligned} \tag{5.5}$$

To isolate the rank-increase mechanism, all flavor diagonal contributions were disregarded. The critical term driving the rank-increase in the second line directly mirrors the corresponding term in beta function $\beta \subset 4 \sum_{a,b} {P^{(ab)}}^{\mathrm{T}} M_0 P^{(ab)}$ as demonstrated in eq. 5.1. Furthermore, it aligns with the discussion in 3.3.2 for the active neutrinos.

If two RHNs are massive, they should be integrated out successfully at their corresponding mass scale. Assuming $M_3 > M_2 > M_1 = 0$ and evolving the mass matric according to eq. 5.5 from the cut-off scale to M_3 yields at leading order:

$$M_1[M_3] = 4 \log \left(\frac{\Lambda_{\mathrm{Pl}}}{M_3} \right) \sum_{a,b} P^{(ab)}_{i1} P^{(ba)}_{i1} M_i, \quad M_2[M_3] = M_2, \quad M_3[M_3] = M_3, \tag{5.6}$$

which follows from evaluating the determinant of the leading order approximation of $M[M_3]$ (eq. 5.5). A summation over $i = 2, 3$ is implied. Without the rank-increasing

contribution, N_1 stays massless (after diagonalization). At the same time, the inclusion of this term gives $\det M[M3] = M_2 M_3 \times M_{11}[M_3]$ (from the correction to the $(1,1)$ matrix element) at the leading order. A field-redefinition $N \to UN$ to diagonalize the mass matrix only affects the Lagrangian at subleading order and can be ignored. Consequently, N_3 approximates the heaviest mass eigenstate and can be integrated out using the EOM (section 2.3.2) for N_3 Ao leading order ($\not{\partial} = 0$)

$$N_3 = -\frac{1}{M_3}\left(M_{3i} N_{i\mathrm{R}} - Y^{(a)}_{\alpha 3}\widetilde{H}^{\mathrm{T}}\ell^{\mathrm{c}}_{\alpha}\right) \tag{5.7}$$

for $i = 1, 2$. Reinserted into $\mathcal{L}$ yields

$$\mathcal{L}_{\text{eff}} \subset \frac{1}{2}\frac{Y^{(a)}_{\alpha 3} Y^{(b)}_{\beta 3}}{M_{33}}\left(\overline{\ell_{\alpha\mathrm{L}}}\widetilde{H}_a\right)\left(\widetilde{H}^T_b \ell^c_{\beta\mathrm{L}}\right) - \mathbb{Y}^{(a)}_{\alpha i}\overline{\ell_{\alpha\mathrm{L}}}\widetilde{H}_a N_{i\mathrm{R}} - \frac{1}{2}\mathbb{M}_{ij}\overline{N^{\mathrm{c}}_{i\mathrm{R}}}N_{j\mathrm{R}}. \tag{5.8}$$

Again $i, j = 1, 2$ and

$$\begin{aligned} \mathbb{Y}^{(a)}_{\alpha i} &\simeq \left(Y^{(a)}_{\alpha i} - \frac{M_{i3} Y^{(a)}_{\alpha 3}}{M_3}\right)\Bigg|_{\mu = M_3}, \\ \mathbb{M}_{ij} &\simeq \left(M_{ij} - \frac{M_{i3} M_{j3}}{M_3}\right)\Bigg|_{\mu = M_3}. \end{aligned} \tag{5.9}$$

This result alignes with one obtained for $M_3 \simeq \Lambda_{\mathrm{Pl}}, M_{1,2} = 0$ in [19]. In contrast to that scenario, the mass matrix is evolved down to $\mu = M_2$. Neglecting all $1/M_3$ corrections yields $\mathbb{M}[M_3] \simeq \mathrm{diag}(M_1[M_3], M_2)$ and $\mathbb{Y}^{(a)} = Y^{(a)}$, effectively reducing to a 3×2 matrix. When further evolved to M_2, this reduced setup yields a leading-order expression analogous to eq. 5.6.

$$M_1[M_2] = M_1[M_3] + 4\log\left(\frac{M_3}{M_2}\right)\sum_{a,b}\mathbb{P}^{(ab)^{\mathrm{T}}}\mathbb{M}[M_3]\mathbb{P}^{(ab)}, \quad M_2[M_2] = M_2, \tag{5.10}$$

with $\mathbb{P}^{(ab)} = \frac{1}{16\pi^2}\mathbb{Y}^{(a)^\dagger}\mathbb{Y}^{(b)}$. Inserting $M_1[M_3], \mathbb{M}[M_3]$ and ignoring all $1/M_3$ corrections gives

$$M_1[M_2] \simeq 4M_2 P^{(ab)}_{21} P^{(ba)}_{21}\log\left(\frac{\Lambda_{\mathrm{Pl}}}{M_2}\right) + 4M_3 P^{(ab)}_{31} P^{(ba)}_{31}\log\left(\frac{\Lambda_{\mathrm{Pl}}}{M_3}\right). \tag{5.11}$$

Overall minus signs in M_1 can be absorbed in a phase redefinition of N_1. Furthermore, $\mathbb{P}^{(ab)}_{12} \simeq P^{(ab)}_{12}$ and $\log(\Lambda_{\mathrm{Pl}}/M_3) + \log(M_3/M_2) = \log(\Lambda_{\mathrm{Pl}}/M_2)$ were used. Again, N_2 corresponds to the mass eigenstate to first order, and integrating it out yields

$$\mathcal{L}'_{\text{eff}} \subset \frac{1}{2}\frac{\mathbb{Y}^{(a)}_{\alpha 2}\mathbb{Y}^{(b)}_{\beta 2}}{M_2}\left(\overline{\ell_{\alpha\mathrm{L}}}\widetilde{H}_a\right)\left(\widetilde{H}^T_b \ell^c_{\beta\mathrm{L}}\right) - \mathbb{Y}'^{(a)}_{\alpha 1}\overline{\ell_{\alpha\mathrm{L}}}\widetilde{H}_a N_{1\mathrm{R}} - \frac{1}{2}\mathbb{M}'_{11}\overline{N^{\mathrm{c}}_{1\mathrm{R}}}N_{1\mathrm{R}}, \tag{5.12}$$

with

$$\begin{aligned} \mathbb{Y}'^{(a)}_{\alpha 1} &\simeq \left(\mathbb{Y}^{(a)}_{\alpha 1} - \frac{\mathbb{M}_{12}\mathbb{Y}^{(a)}_{\alpha 2}}{M_2}\right)\Bigg|_{\mu = M_2}, \\ \mathbb{M}'_{\alpha i} &\simeq \left(\mathbb{M}_{11} - \frac{\mathbb{M}_{12}\mathbb{M}_{12}}{M_2}\right)\Bigg|_{\mu = M_2}. \end{aligned} \tag{5.13}$$

Similar to $1/M_3$ corrections, those involving $1/M_2$ are negligible and can be safely disregarded. Effectively, the Lagrangian describes the SM extended by one RHN of mass $M_1 \simeq \mathcal{O}\left(P^{(ab)^2}\Lambda_{\mathrm{Pl}}\right) = 10^{14-15}\mathrm{GeV}$ for $Y^{(a)} \simeq \mathcal{O}(1)$. Between the scales M_2 and M_1 (eq. 5.11) corrections to $M_1[\mu]$ of the form $M_1 P^{(ab)} \log(M_2/M_1)$ can be safely dropped. Ultimately, N_1 can be integrated out as well, leading to 2HDM Lagrangian supplemented by four Weinberg operators

$$\mathcal{L}''_{\mathrm{eff}} = \mathcal{L}_{\mathrm{2HDM}} + \frac{1}{2}\frac{\mathbb{Y}^{(a)}_{\alpha 1}\mathbb{Y}^{(b)}_{\beta 1}}{M_2}\left(\overline{\ell_{\alpha \mathrm{L}}}\widetilde{H}_a\right)\left(\widetilde{H}_b^T \ell^c_{\beta \mathrm{L}}\right). \tag{5.14}$$

Moreover, the $1/M_1$ contribution justifies neglecting the subdominant $1/M_3, 1/M_2$. To leading order, the matching procedure yields

$$C^{(ab)}_{5\alpha\beta}\Big|_{\mu=M_1} \simeq \frac{Y^{(a)}_{\alpha 1}Y^{(b)}_{\beta 1}}{M_1}. \tag{5.15}$$

The expansion to four dimension-five operators directly mirrors the presence of two scalar doublets in the 2HDM framework. This has significant implications for active neutrino masses due to the mixing between the different operators. Without considering this mixing, only one active neutrino would acquire mass. This is because the three rows of the C_5 matrix become linearly dependent when $a = b = 1$. In other words, the rank-increasing mechanisms explored in chapter 4 fall short of explaining the observed mass differences among active neutrinos.

The mixing between the different Weinberg operators relates to the scalar potential, which includes [72]

$$V(H_a, H_b) \subset \sum_{a,b,c,d} \lambda_{abcd}\left(H_a^\dagger H_b\right)\left(H_c^\dagger H_d\right). \tag{5.16}$$

Upon choosing a basis such that $\langle H_1^0\rangle = v/\sqrt{2}$ and $\langle H_2^0\rangle = 0$, the active neutrino mass reads

$$m_\nu = \frac{v^2}{2} C_5^{(11)}\left[\Lambda_{\mathrm{EW}}\right], \tag{5.17}$$

however, operator mixing gives contributions stemming from $C_5^{(ab)}$. A connection can be established with the observed neutrino masses by evolving $C_5^{(11)}$ from its matching scale M_1 to the electroweak scale. In the process, corrections in the form

$$C_5^{(11)}[\Lambda_{\mathrm{EW}}] \simeq C_5^{(11)}[M_1] + \underbrace{B_{1a}C_5^{a1}[M_1] + C_5^{1a}[M_1]B_{1a}^{\mathrm{T}} + bC_5^{22}[M_1]}_{=\delta C_5^{(11)}} \tag{5.18}$$

arise [73]. For simplicity, the contributions depending on B are dropped, and only the ones related to b are analyzed. Nevertheless, the quantitive behavior remains the same. b relates to the term $\lambda_5\left(H_1^\dagger H_1\right)\left(H_2^\dagger H_2\right)$ in the scalar potential [73]

$$b = -2\frac{\lambda_5}{16\pi^2}\log\left(\frac{M_1}{\Lambda_{\mathrm{EW}}}\right). \tag{5.19}$$

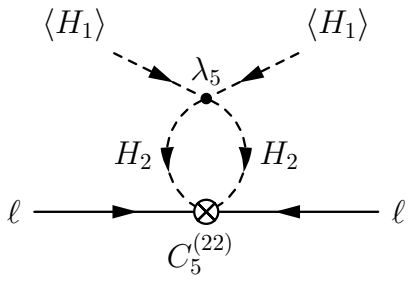

Figure 5.3.: One-loop operator mixing. In the case of an extended scalar sector, interaction terms between different scalars lead to mixing between the Wilson coefficients of the distinct Weinberg operators.

Fig. 5.3 displays the operator mixing diagrammatically. Defining $Y^{(a)}_{\alpha 1} \equiv y^{(a)} \cdot u^{(a)}_{\alpha}$ in terms of the unit vecor $\vec{u}^{(a)}$ and $y^{(a)} = \sqrt{Y^{(a)2}_{11} + Y^{(a)2}_{21} + Y^{(a)2}_{31}}$. The active neutrino mass matrix reads according to eq. 5.17

$$m_\nu = \frac{1}{2}\frac{v^2}{M_1}\left(\left(y^{(1)}\right)^2 \vec{u}^{(1)}\vec{u}^{(1)\mathrm{T}} + b\left(y^{(2)}\right)^2 \vec{u}^{(2)}\vec{u}^{(2)\mathrm{T}}\right), \tag{5.20}$$

with overall minus signs absorbed in phase redefinitions and $u^{(a)}u^{(a)\mathrm{T}}$ understood as a 3×3 matrix. At leading order, the eigenvalues b read:

$$m_1 = 0, \quad m_2 \simeq \frac{1}{8}\frac{v^2}{M_1} b\left(\left(y^{(2)}\right)^2 + 4\frac{\left|\vec{u}^{(1)} \times \vec{u}^{(2)}\right|}{\left(y^{(1)}\right)^2}\right), \quad m_3 = \frac{1}{2}\frac{v^2}{M_1}\left(y^{(1)}\right)^2, \tag{5.21}$$

which means that for $\lambda, y^{(a)} = \mathcal{O}(1)$, the mass hierarchy matches experimental data for NO:

$$m_3 \sim 0.1\,\mathrm{eV}, \quad m_2 \sim 0.1\,\mathrm{eV} b\mathcal{O}\left(\left(y^{(1,2)}\right)^2\right) \sim \mathcal{O}(0.01\,\mathrm{eV}). \tag{5.22}$$

Fig. 5.3 presents a qualitative analysis based on a parameter scan across randomized RHN Yukawa matrices entries, assuming $\lambda_5 = 1$. Additionally, a scan over absolute active neutrino masses with $m_1 = 0$ is included. Notably, the figure illustrates that the oscillation data and expected neutrino masses are roughly consistent with the predicted values. The initially massless neutrino acquires a mass term through the rank-increasing two-loop contributions detailed in section 3.1.

5.2.2. Additional Scalar

In all considerations, a mass matrix with rank < 3 is assumed. The existence of some gauge symmetry that justifies this form is indirectly implied, as it was argued that gravity breaks global symmetries. Consequently, the mass matrix arises from combining mass terms not forbidden by any symmetry and those generated by the VEVs of scalars after

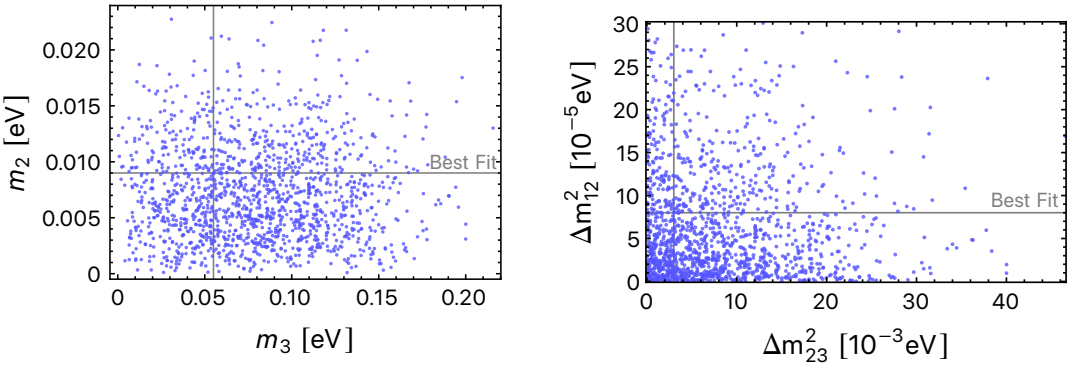

Figure 5.4.: Scatter plot for Neutrino mass parameters. A parameter scan for randomized RHN Yukawa matrices of $\mathcal{O}(1)$ is performed for $\lambda_5 = 1$ and $M_2 = 0.4 \cdot \Lambda_{\text{EW}}, M_3 = 0.6 \cdot \Lambda_{\text{EW}}$. The resulting active neutrino masses with $m_1 = 0$ are displaced on the left, and the corresponding squared mass differences on the right. The experimental best-fit values for $m_1 = 0$ are indicated in grey.

SSB. Before considering explicit models, the RGE effects on the scalar couplings are studied. For that, a simple Majoron-type model is assumed:

$$\mathcal{L}_\phi = \mathcal{L}_{\text{SM}} - \left(\alpha_{ij}\overline{N^c_{i\text{R}}}N_{j\text{R}}\phi + \text{h.c.}\right) - V(\phi). \tag{5.23}$$

N_i denote n_i additional chiral fermions and $\phi \xrightarrow{SSB} \langle\phi\rangle$ a scalar that aquires a VEV after SSB of some imposed extra symmetry. One such possibility for the given Lagrangian is a $U(1)$ with the charges $Q(N) = 1$, $Q(\phi) = -2$ and $V(\phi) = \delta\phi\phi^* + \lambda_2\left(\phi\phi^*\right)^2 + \lambda_3\phi\phi^* H^\dagger H$ and ignoring gauge anomlies for the time being. The two-loop RGEs for renormalizable theories can be calculated with SARAH and read:

$$\beta_\alpha = \kappa\alpha + \alpha F + F^*\alpha + \alpha Q + Q^{\text{T}}\alpha - G^* P^T\alpha - \alpha PG + 4P^T\alpha P + 28G^*\alpha G, \tag{5.24}$$

with

$$\begin{aligned}
\kappa &= 2\alpha\text{Tr}[\alpha\alpha^*] + \frac{1}{(16\pi^2)^2}\left(\lambda_2^2 + \frac{\lambda_3^2}{4} - 6\text{Tr}[\alpha {Y_\nu}^\dagger Y_\nu \alpha^*]\right) - 12\text{Tr}[F^2], \\
F &= \frac{1}{16\pi^2}2G + \frac{1}{16\pi^2}\left(8\lambda_2 + 6\text{Tr}[\alpha\alpha^*]\right)G, \\
Q &= P + \frac{1}{16\pi^2}\left(\frac{17}{8}{g_1}^2 + \frac{51}{8}{g_2}^2 - 2\lambda_3 - \frac{9}{2}\text{Tr}[Y_u {Y_u}^\dagger] - \frac{3}{2}\text{Tr}[YY^\dagger]\right)P - \frac{1}{4}P^2, \\
P &= \frac{1}{(16\pi^2)^2}Y^\dagger Y, \\
G &= \frac{1}{(16\pi^2)^2}\alpha^*\alpha.
\end{aligned} \tag{5.25}$$

Here, Y_e, Y_u contributions were neglected. The transformation behavior of β_α under chiral fermion redefinitions ($N \to UN$) must mirror that of α itself, thus $\alpha \to U^{\text{T}}\alpha U$. The

flavor structures involving G ($G \to U^\dagger G U$) exhibit the correct transformation property, justifying the general form of eq. 5.24. Compared to the result from eq. 5.1 and the explicit factors in [18], all terms not involving additional α contributions agree. For the model under consideration, the freedom to redefine N allows us to diagonalize α. After SSB, this translates to working in the mass basis. Consequently, all additional flavor structures involving G (particularly $G^*\alpha G$), which could potentially lead to effects similar to $P^{\mathrm{T}}\alpha P$, remain diagonal. Therefore, the discussions on two-loop mass generation presented at the beginning of this chapter are expected to hold for masses generated via SSB. Depending on the specific model and the scalar sector's form, extra terms of the form $G_i^*\alpha G_i$ might contribute to the rank increase if they cannot be simultaneously diagonalized.

5.3. Additional Gauge Symmetries

This section explores extensions of the SM incorporating gauge groups constructed from the simplest representations: trivial, fundamental, and triplet/adjoint. Drawing on their implications for tree-level neutrino mass matrices and potential rank-increasing contributions similar to the one depicted in fig. 5.1, the concluding section discusses the general features of these extensions.

5.3.1. U(1)

The simplest extension includes several chiral fermions and a scalar sector charged under gauged $\mathrm{U}(1)_{\mathrm{D}}$ ("dark") symmetry and uncharged under any SM gauge group. The only gauge anomalies involve $\mathrm{U}(1)_{\mathrm{D}}^3$ with three external dark bosons and $\mathrm{U}(1)_{\mathrm{D}} \times \mathrm{graviton}^2$. The latter involves one external dark gauge boson and two gravitons. Since only fermions are running inside the loop, no theory of quantum gravity is necessary. The resulting conditions on cancelation of both anomalies based on eq. 5.3 lead to

$$\sum_i Q_i^3 = 0 \quad , \qquad \sum_i Q_i = 0, \tag{5.26}$$

where i denotes all chiral fermions charged under $\mathrm{U}(1)_{\mathrm{D}}$ and Q_i their corresponding charges. The most straightforward solution amounts to extend the SM with three right handed fermions $(N_{1\mathrm{R}}, N_{2\mathrm{R}}, N_{3\mathrm{R}})$ with charges $+1, -1, 0$. Even without including a scalar sector that couples N, S to the active neutrinos, the following mass terms are allowed:

$$M_3 \overline{N_{3\mathrm{R}}^{\mathrm{c}}} N_{3\mathrm{R}}, \quad M_{12} \overline{N_{1\mathrm{R}}^{\mathrm{c}}} N_{2\mathrm{R}}, \quad M_{12} \overline{N_{2\mathrm{R}}^{\mathrm{c}}} N_{1\mathrm{R}}, \tag{5.27}$$

where the last two are related by hermitian conjugation. The resulting Majorana mass matrix for $\vec{N} = (N_1, N_2, N_3)$ reads

$$M = \begin{pmatrix} 0 & M_{12} & 0 \\ M_{12} & 0 & 0 \\ 0 & 0 & M_3 \end{pmatrix}, \tag{5.28}$$

which has full rank. The same argument also holds for more chiral fermions with charges $Q_i = \pm 1, \pm a, \ldots, 0$. Other non-trivial solutions that are non-symmetric might exist; however, it remains complicated to couple N_i to ℓ_α without introducing multiple scalars of various $\mathrm{U}(1)_\mathrm{D}$ charges. More desirable solutions, therefore, include non-abelian gauge groups.

5.3.2. SU(2) + SU(N)

Instead of $\mathrm{U}(1)_\mathrm{D}$, $\mathrm{SU}(2)_\mathrm{D}$ is introduced. The following fields with representation in regard to $\mathrm{SU}(3)_C \times \mathrm{SU}(2)_\mathrm{L} \times \mathrm{U}(1)_Y \times \mathrm{SU}(2)_\mathrm{D}$ extend the matter content: one chiral fermion doublet $N = (\mathbf{1}, \mathbf{1}, 0, \mathbf{2})$, one scalar singlet S, one scalar bi-doublet $\Phi = (\mathbf{1}, \mathbf{2}, 0, \overline{\mathbf{2}})$ and a one scalar doublet $\varphi = (\mathbf{1}, \mathbf{1}, 0, \mathbf{2})$. Since $\mathrm{SU}(2)_D$ is pseudo-real, all anomalies cancel automatically. The Lagrangian amounts to

$$\mathcal{L}_\mathrm{D} = -\left(Y_\alpha \overline{\ell_{\alpha\mathrm{L}}} \Phi N_\mathrm{R} + Y_S \overline{N_\mathrm{R}} \varphi S_\mathrm{R}^\mathrm{c} + \tilde{Y}_S \overline{N_\mathrm{R}} \widetilde{\varphi} S_\mathrm{R}^\mathrm{c} + M_S \overline{S_\mathrm{R}^c} S_\mathrm{R} + \mathrm{h.c.}\right) - V(H, \Phi, S). \quad (5.29)$$

For every term involving φ, an analogue one with the charge cojugated $\widetilde{\varphi} = \mathrm{i}\sigma_2 \varphi^*$ exists, because SU(2) is pseudo-real. Furthermore, it is assumed that $V(H, \Phi, S)$ develops minima such that $\langle \varphi \rangle \lesssim M_S \sim \Lambda_\mathrm{Pl}$, while $\langle H, \Phi \rangle \sim \Lambda_\mathrm{EW}$. The large separation in scales demands fine-tuning on potential parameters, which is a general concern in any scalar extension for which no distinct solution is yet known.

Upon integrating out S, the resulting dimension-five operators, which approximate the emerging masses after SSB, read:

$$\mathcal{L}^{d=5} = \frac{C_{11}}{\Lambda_\mathrm{Pl}} \left(\overline{N_\mathrm{R}} \varphi\right) \left(\varphi^\mathrm{T} N_\mathrm{R}^c\right) + \frac{C_{12}}{\Lambda_\mathrm{Pl}} \left(\overline{N_\mathrm{R}} \varphi\right) \left(\widetilde{\varphi}^\mathrm{T} N_\mathrm{R}^c\right) + \frac{C_{22}}{\Lambda_\mathrm{Pl}} \left(\overline{N_\mathrm{R}} \widetilde{\varphi}\right) \left(\widetilde{\varphi}^\mathrm{T} N_\mathrm{R}^c\right) + \mathrm{h.c.}, \quad (5.30)$$

with $\langle \varphi \rangle = (v_\varphi, 0)$. Choosing the VEV is convention. By performing a gauge transformation on φ, any other direction in the $\mathrm{SU}(2)_\mathrm{D}$ plane can be selected. The Wilson coefficients C_{ii} depend on Y_S, $\tilde{Y}_S$ and the resulting entries in the mass matrix M_N are

$$M_{ij} \sim \frac{v_\varphi^2}{\Lambda_\mathrm{Pl}}, \quad (5.31)$$

hence, all entries are non-zero, and both mass eigenstates are massive. Including multiple generations of N does not impact the mass generation scenario, as the underlying mechanism responsible for their masses remains identical. Without φ, however, N will not acquire Majorana masses.

To prevent the appearance of the charge conjugated scalar field, an additional $\mathrm{U}(1)_\mathrm{D}$ symmetry – similarly to the $\mathrm{SU}(2)_\mathrm{L} \times \mathrm{U}(1)_Y$ gauge symmetry – with $Q_\mathrm{D}^\varphi \neq 0$ can be included. This addition, then again, makes anomaly cancelation very difficult. $U(1)_\mathrm{D}^3$ and gravity related $U(1)_\mathrm{D}$ anomalies demand for multiple generations $N_{a,b}$ with opposing charges, like ± 1. The Lagrangian reads:

$$\begin{aligned} \mathcal{L}'_D = &-\left(Y_\alpha \overline{\ell_{\alpha\mathrm{L}}} \Phi N_\mathrm{R} + Y_S^{(a)} \overline{N_{a\mathrm{R}}} \varphi S_\mathrm{R}^\mathrm{c} + Y_S^{(b)} \overline{N_{b\mathrm{R}}} \widetilde{\varphi} S_\mathrm{R}^\mathrm{c} + M_S \overline{S_\mathrm{R}^c} S_\mathrm{R} + \mathrm{h.c.}\right) \\ &- \left(M_{ab} \overline{N_{a\mathrm{R}}^\mathrm{c}} \mathrm{i}\sigma_2 N_{b\mathrm{R}} + \mathrm{h.c.}\right) - V[H, \Phi, S]. \end{aligned} \quad (5.32)$$

Integrating out S as in eq. 5.30 but only with $C_{11}^{(a)}$ and $C_{22}^{(b)}$ then gives the mass matrix for $(N_{a1}, N_{a2}, N_{b1}, N_{a2})$

$$M_N = \begin{pmatrix} M_{11} & 0 & 0 & M_{12} \\ 0 & 0 & M_{12} & 0 \\ 0 & M_{12} & 0 & 0 \\ M_{12} & 0 & 0 & M_{22} \end{pmatrix}. \tag{5.33}$$

Here M_{12} contributions correspond to Dirac type mass terms when identifying $\mathrm{i}\sigma_2 N_{b\mathrm{R}}$ with N_L. The matrix's full rank excludes the model; however, a similar approach based on $\mathrm{SU}(2)_\mathrm{R} \times \mathrm{U}(1)_{\tilde{Y}}$ is used in LR models. Similarly, when considering $\mathrm{SU}(N)_\mathrm{D}$ instead of $\mathrm{SU}(2)_\mathrm{D} \times \mathrm{U}(1)_\mathrm{D}$, the $\mathrm{SU}(N)_\mathrm{D}^3$ anomaly demands for any chiral fermion in the fundamental representation, a corresponding one in the anti-fundamental representation, which effectively makes the theory vector-like. The resulting Dirac mass terms render all RHNs massive.

Another option to prevent the charge conjugation is by using scalar triplets $\Sigma = \Sigma^i \tau_\mathrm{D}^i$ (τ_D^i being the generators of $\mathrm{SU}(2)_\mathrm{D}$ – similar to the type II seesaw model). This representation is real; thus, charge conjugation becomes trivial. Incorporating these scalar triplets leads to the following Lagrangian:

$$\mathcal{L}_\mathrm{D} \subset -Y\overline{N_{\alpha\mathrm{R}}}\mathrm{i}\sigma_2 \Sigma N, \quad \text{with} \quad \Sigma = \begin{pmatrix} \Sigma^3 & \mathrm{X} \\ \mathrm{X}^\dagger & -\Sigma^3 \end{pmatrix} \tag{5.34}$$

and with $\mathrm{X} = \Sigma^1 - \mathrm{i}\Sigma^2$. Without loss of generality, the VEV is assumed to be in the Σ^3 direction. Consequently, both $N_{1,2}$ become massive. In contrast, if both Σ and $N = N^i \tau_\mathrm{D}^i$ transform in the triplet representation and a singlet fermion S is added, the Lagrangian amounts to:

$$\mathcal{L}_\mathrm{D} \subset -Y\overline{S_\mathrm{R}^\mathrm{c}}\mathrm{Tr}[N\Sigma] - M_S\overline{S_\mathrm{R}^\mathrm{c}}S_\mathrm{R} - \overline{\ell_{\alpha\mathrm{L}}}\eta N + \mathrm{h.c.}\,. \tag{5.35}$$

Here, $\eta = (\mathbf{2}, \overline{\mathbf{3}})$ under $(\mathrm{SU}(2)_\mathrm{L}, \mathrm{SU}(2)_\mathrm{D})$. Assuming again $\langle\Sigma\rangle = (0, 0, v_\Sigma)$, only N_3 becomes massive at the tree level:

$$\mathcal{L}^{d=5} = \frac{C}{\Lambda_\mathrm{Pl}} \left(\mathrm{Tr}[N\Sigma]\right)^\mathrm{c} \left(\mathrm{Tr}[N\Sigma]\right). \tag{5.36}$$

The problem amounts to η being diagonal in the RHN generation index – other than H – and hence will not increase the rank. This phenomenon is likely to be a general feature of any gauge theory. Additionally, the diagrams in fig. 5.5 featuring charged gauge bosons of the $\mathrm{SU}(2)_\mathrm{D}$ group will naturally contribute only diagonal terms in the gauge indices, as anticipated.

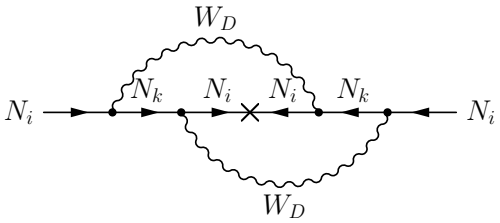

Figure 5.5.: Rank increase via charged bosons. Two-loop diagrams involving charged $\mathrm{SU}(2)_\mathrm{D}$ (W_D) increase the rank via flavor-changing charged currents.

5.3.3. Necessary conditions

A gauge extension that gives a Majorana mass matrix with rank < 3 at the cut-off scale must exhibit the following features:

1. All gauge anomalies must be canceled.

2. Source for lepton number violation in the form $\overline{\psi^\mathrm{c}_\mathrm{L/R}}\psi_\mathrm{L/R}$ that relates to at least one tree level Majorana mass must be present.

3. If one or more components inside a fermionic gauge multiplet stay massless at tree level, a remaining gauge symmetry protects the massless particle from acquiring quantum corrections as Yukawa couplings do not contribute (diagonal in gauge indices).

4. To allow for rank-increasing type diagrams displayed in fig. 5.1, RHNs must couple to LHNs via the same scalar. This demands multiple copies (generations) of the RHN in the same representation. Furthermore, at least one of these generations must be massless.

As shown in the next section, the last point can be fulfilled by considering the seesaw mechanism for the RHNs.

5.4. Left-Right Symmetric Models

Section 2.2.3 explored left-right extensions to the SM. These extensions represent another way to achieve an additional $\mathrm{SU}(2) \times \mathrm{U}(1)$ group (discussed in the previous section) but with RHNs forming part of the $\mathrm{SU}(2)_\mathrm{R}$ doublet. Consequently, right-handed neutrinos are massless at tree level (ignoring SSB). Importantly, all gauge anomalies vanish as L^c_R, L_L as well as Q^c_R, Q_L have opposite $\mathrm{U}(1)_{\tilde{Y}}$ charges. Hence $\mathrm{U}(1)^3_{\tilde{Y}}$ and all $\mathrm{U}(1)_{\tilde{Y}}$ related (graviton$^2 \times \mathrm{U}(1)_{\tilde{Y}}$ and $\mathrm{SU}(2)^2\mathrm{U}(1)_{\tilde{Y}}$) cancel. All remaining anomalies vanish similarly to the SM. Moreover, three generations exist as required for the rank increase. All conditions presented in the previous section are met upon the coupling to a singlet fermion.

The fermionic matter content of the LR symmetric models is extended by a chiral singlet S_{L} and a scalar $\Xi = (\mathbf{1}, \mathbf{1}, \mathbf{2}, -1)$ under $\mathrm{SU}(3) \times \mathrm{SU}(2)_{\mathrm{L}} \times \mathrm{SU}(2)_{\mathrm{R}} \times \mathrm{U}(1)_{\tilde{Y}}$. The extension to the LR Lagrangian reads

$$\mathcal{L}_{\mathrm{LR}}^{\mathrm{ext}} = -\left(Y_{S\alpha}\overline{L_{\alpha\mathrm{R}}}\Xi S_{\mathrm{L}} + M_S\overline{S_{\mathrm{L}}^{\mathrm{c}}}S_{\mathrm{L}} + \mathrm{h.c.}\right) - V(\Phi, \Xi). \tag{5.37}$$

The full scalar potential, including the bi-doublet Φ and the right doublet Ξ, can be found in appendix B. In order to break $\mathrm{SU}(2)_{\mathrm{L}} \times \mathrm{SU}(2)_{\mathrm{R}} \times \mathrm{U}(1)_{\tilde{Y}}$ down to $\mathrm{SU}(2)_{\mathrm{L}} \times \mathrm{U}(1)_Y$, the VEV of Ξ must be invariant under the later. For

$$\Xi = \begin{pmatrix} v_{\mathrm{R}} \\ 0 \end{pmatrix}, \tag{5.38}$$

the VEV remains invariant under $\tilde{Y} + 2T_{3\mathrm{R}}$. This, however, precisely corresponds to the weak hypercharge Y according to eq. 2.30. Furthermore, the right-handed lepton doublet $L_{\mathrm{R}} = (N_{\mathrm{R}}, E_{\mathrm{R}})$ contains the right-handed neutrino N_{R} in the upper component. After SSB of $\mathrm{SU}(2)_{\mathrm{R}} \times \mathrm{U}(1)_{\tilde{Y}}$, the following mass terms emerge

$$\mathcal{L}_{\mathrm{LR}}^{\mathrm{mass}} = -\left(v_{\mathrm{R}}Y_{S\alpha}\overline{N_{\alpha\mathrm{R}}}S_{\mathrm{L}} + M_S\overline{S_{\mathrm{L}}^{\mathrm{c}}}S_{\mathrm{L}} + \mathrm{h.c.}\right), \tag{5.39}$$

yielding the Majorana mass matrix for $(\vec{N}, S^{\mathrm{c}})$:

$$M = \begin{pmatrix} 0_{3\times3} & v_{\mathrm{R}}\vec{Y}_S \\ v_{\mathrm{R}}\vec{Y}_S^{\mathrm{T}} & M_S \end{pmatrix}. \tag{5.40}$$

Here, $\vec{Y}_S = (Y_{S1}, Y_{S2}, Y_{S3})$ and $M_S \in \mathbb{R}$ is used. The Majorana mass matrix for $(\vec{N}, S^{\mathrm{c}})$ precisely corresponds to the type-I seesaw mechanism with one additional singlet only for the RHNs. The argument regarding the number of massive particles presented in [26] remains directly applicable. In this scenario, only one RHN acquires mass, while introducing two Majorana particles S would result in two massive RHNs. Without loss of generality, one can redefine $N \to UN$ to set $\vec{Y}_S = (0, 0, y_S)$. It is expected, that M_S and v_{R} are similar in size ($\mathcal{O}(\Lambda_{\mathrm{Pl}})$). While integrating out S provides a general understanding of the involved masses, retaining S within the theoretical framework yields greater precision. The mass matrix can be expressed as: $M = \mathrm{diag}(0, 0, M_1, M_2)$, with $M_{1,2} = \frac{1}{2}\left(M_S \pm \sqrt{M_S^2 + 4y_s^2v_{\mathrm{R}}^2}\right)$. Furthermore, $N_{3\mathrm{R}}$ and S mix with mixing angle θ, resulting in the mass eigenstates $(N_3', S') = O(\theta)(N_3, S)$. Here, $O(\theta)$ denotes an orthogonal matrix.

5.4.1. Fermion and Boson Masses

Assuming that $\langle\Xi\rangle = \mathcal{O}(\Lambda_{\mathrm{Pl}})$ and

$$\langle\Phi\rangle = \begin{pmatrix} k & 0 \\ 0 & k'e^{\mathrm{i}\alpha} \end{pmatrix}, \quad \text{with} \quad k = \mathcal{O}(\Lambda_{\mathrm{EW}}), \tag{5.41}$$

the VEVs arise in electromagnetic neutral components. By convention, the relative phase between $\langle\Phi_{11}\rangle$ and $\langle\Phi_{22}\rangle$ is absorbed in the latter. The gauge boson masses are derived from $\left(D_\mu\phi\right)^\dagger\left(D_\mu\phi\right)$ for $\phi = \Phi, \Xi$. Both neutral and charged boson mass matrices contain L/R mixed terms. However, $W^3_{\mu\mathrm{R}}W^{\mu 3}_{\mathrm{R}}$ and $W^+_{\mu\mathrm{R}}W^{\mu-}_{\mathrm{R}}$ are proportional to v_{R} while all other entries are of order Λ_{EW}. Consequently, the heavy $\mathrm{SU}(2)_{\mathrm{R}}$ bosons decouple due to the suppressed mixing, and the lighter ones obtain masses of order $\mathcal{O}(\Lambda_{\mathrm{Pl}})$, corresponding to the observed $W^\pm$ and Z bosons. Fermion masses are obtained by replacing $\Phi \to \langle\Phi\rangle$ and

$$\langle\tilde{\Phi}\rangle = \begin{pmatrix} k'e^{-\mathrm{i}\alpha} & 0 \\ 0 & k \end{pmatrix} \tag{5.42}$$

in all Yukawa terms, which yields:

$$\begin{aligned} M_U &= kh + k'e^{-\mathrm{i}\alpha}\tilde{h}, \qquad & M_D &= k'e^{\mathrm{i}\alpha}h + k\tilde{h}, \\ M_\nu^{\mathrm{Dirac}} &= kg + k'e^{-\mathrm{i}\alpha}\tilde{g}, \qquad & M_\ell &= k'e^{\mathrm{i}\alpha}g + k\tilde{g}. \end{aligned} \tag{5.43}$$

$g, \tilde{g}, h, \tilde{h}$ are 3×3 matrices that describe the Yukawa couplings between left and right fermions (section 2.2.3). To provide the observed fermion mass and the mass gap between M_U and M_U, $k \sim v_{\mathrm{SM}}$, while $k' \lesssim 0.01k$ and $g = \mathcal{O}(1)$, $\tilde{h} = \mathcal{O}(0.01)$. Analogously, RHN Yukawa couplings can be of order one, as discussed before, yielding $h = \mathcal{O}(1)$, $\tilde{h} = \mathcal{O}(0.01)$. Theoretically, $\tilde{h}$ and $\tilde{g}$ could be larger and of order one if they cancel with the g, h precisely in case of charged lepton and down quark masses. This opens the doors for interesting effects, as explored in the next section.

5.4.2. Rank Increasing Contributions

After SSB of $\mathrm{SU}(2)_{\mathrm{R}}$, all $\mathrm{SU}(2)_{\mathrm{R}}$ indices can be expanded. Furthermore, $\mathrm{SU}(2)_{\mathrm{R}} \times \mathrm{U}(1)_Y$ can be treated as unbroken as energies are still far above the EW scale. Hence, the parts of the Lagrangian that involve N are:

$$\mathcal{L}_{\mathrm{LR}}^{\mathrm{SSB}} \subset -\frac{1}{2}M_{Nij}\overline{N^c_{i\mathrm{R}}}N_{j\mathrm{R}} - g_{\alpha i}\overline{\ell_{\alpha\mathrm{L}}}\Phi^{(1)}_{\mathrm{L}}N_{i\mathrm{R}} - \tilde{g}_{\alpha i}\overline{\ell_{\alpha\mathrm{L}}}\tilde{\Phi}^{(1)}_{\mathrm{L}}N_{i\mathrm{R}}, \tag{5.44}$$

with

$$\Phi = \begin{pmatrix} \Phi^{(1)}_{\mathrm{L}} & \Phi^{(2)}_{\mathrm{L}} \end{pmatrix}, \quad \tilde{\Phi} = \begin{pmatrix} \tilde{\Phi}^{(1)}_{\mathrm{L}} & \tilde{\Phi}^{(2)}_{\mathrm{L}} \end{pmatrix}. \tag{5.45}$$

Furthermore, the mass matrix in terms of (N_i, S) is given by

$$M = \begin{pmatrix} 0_{2\times 2} & \cdots & \\ \vdots & 0 & v_{\mathrm{R}}y_S \\ & v_{\mathrm{R}}y_S & M_S \end{pmatrix}. \tag{5.46}$$

The effects of the additional generation on mass matrix RGEs and the charge conjugated coupling $\tilde{g}$ from eq. 2.33 are discussed in the following. The rank-increasing contributions to the Majorana matrix M_N mirror the 2HDM scenario discussed in section 5.2.1

$$\beta_M \subset \frac{1}{(16\pi^2)}\left[4\left(g^\dagger g\right)^{\mathrm{T}} M \left(g^\dagger g\right)\right]. \tag{5.47}$$

Moreover, the same structure also exists with $g \to \tilde{g}$ and in mixed form as in the 2HDM case. The question arises if all RHN become massive at P^2 or if a second bi-doublet is needed (see the beginning of this chapter). The two effects decouple and can be analyzed individually.

In presence of S but ignoring $\tilde{g}$, the Yukawa sector in terms of $\hat{N} \equiv (N_1, N_2, N_3', S')$ becomes

$$\mathcal{L}_{\mathrm{LR}}^{\mathrm{Yuk}} \subset -\hat{g}_{\alpha\beta}\overline{L_{\alpha\mathrm{L}}}\Phi^{(1)}\hat{N}_{\beta\mathrm{R}} + \mathrm{h.c.}, \tag{5.48}$$

with $\Phi^{(1)}$ denoting the first row of Φ that couples to N. $\hat{g}$ describes the modified coupling to $\hat{N}$:

$$\hat{g} = \begin{pmatrix} \vec{g}_{1\alpha} & \vec{g}_{2\beta} & \cos\theta\vec{g}_{3\beta} & \sin\theta\vec{g}_{3\beta} \end{pmatrix}, \tag{5.49}$$

with $\vec{g}_{\alpha\beta} = (g_{\alpha 1}, g_{\alpha 2}, g_{\alpha 3})$ and the mixing angle chosen such that it diagonalizes M (see also section 5.4.1). Consequently, $P \to \hat{P} = \frac{1}{16\pi^2}\hat{g}^\dagger\hat{g}$ in the RGEs from eq. 5.1. The mass eigenvalues are reconstructed using the Fadeeve-LeVerrier algorithm [74] for the first 4 tensor invariants. Keeping only leading order terms gives:

$$\begin{aligned}
I_1 &= \mathrm{Tr}M \simeq M_3 + M_4, \\
I_2 &= \frac{1}{2}\left((\mathrm{Tr}M)^2 - \mathrm{M}^2\right) \simeq M_3 M_4, \\
I_3 &= \frac{1}{6}\left((\mathrm{Tr}M)^3 - 3\mathrm{Tr}M\mathrm{Tr}M^2 + 2\mathrm{Tr}M^3\right) \simeq (M_1 + M_2)\, M_3 M_4, \\
I_4 &= -\frac{1}{24}\left(6\mathrm{Tr}M^4 - 8\mathrm{Tr}M^3\mathrm{Tr}M + \mathrm{Tr}M^2(\mathrm{Tr}M)^2 - \left(\mathrm{Tr}M^2\right)^2 - (\mathrm{Tr}M)^4\right) \\
&= M_1 M_2 M_3 M_4.
\end{aligned} \tag{5.50}$$

Explicit evaluation of eq. 5.2 gives $I_4 = 0$ and hence $M_1 = 0$. With $I_3/I_2 = M_1 + M_2 = M_2$ one obtains

$$M_2 = 4t\left(P_{13}^2 + P_{23}^2\right)\left(M_3\cos^2\theta + M_4\sin^2\theta\right). \tag{5.51}$$

Thus, in perturbation theory, the mixing does not produce a full rank at a lower order.

The existence of a second Yukawa coupling $\tilde{g}$ presents a unique scenario, effectively mimicking a second Higgs doublet in [18]. Theoretically, $\tilde{g}$ can still be of similar size to g if both their contributions in the Yukawa sector cancel partially to yield lighter charged lepton masses. In this case, $\tilde{g}$ is sufficient to produce active neutrino masses in the ballpark of measurements. In the case of a single singlet S, the presence of $\tilde{g}$ leads to massive RHNs at second order in PT. If two singlet fermions, $S_{1,2}$, are introduced to produce two massive neutrinos at tree level, operator mixing occurs, as detailed in section 5.2.1.

However, without some 'magical' cancelation between g and $\tilde{g}$, a suppressed $\tilde{g}$ ($\sim\mathcal{O}(0.01)$) is favored. In that case, the scalar sector is incapable of generating a sufficiently massive second RHN for the seesaw mechanism, as the RHN mass scales quadratically with $\tilde{g}$. Furthermore, operator mixing between C_5^{12} or C_5^{11} (both containing at least one $\tilde{g}$ factor) is suppressed due to the smallness of $\tilde{g}$.

Ultimately, assuming a small $\tilde{g}$ necessitates a LR model with two bi-doublets Φ, X to recover the impact of a second sizeable Yukawa coupling, akin to $\tilde{g}$. This goes under the name Two-Higgs Bi-Doublet Model (2HBDM).

5.4.3. 2HBDM

With the introduction of a second bi-doublet, two potential mechanisms emerge to explain the observed hierarchical structure of active neutrino masses. In analogy to [19], the first involves a single singlet fermion, S. In this scenario, one RHN gains mass at the Planck scale, while the remaining two acquire masses through two-loop contributions. Ignoring $\tilde{g}$, the Yukawa Lagrangian from eq. 5.44 with a second bi-doublet after $\mathrm{SU}(2)_\mathrm{R}$ SSB becomes equvivalent to the 2HDM case and the results from [18] apply. The second involves two singlets S, according to the discussion from section 5.2.1, that gives two heavy and one light RHNs (the lighter at the seesaw scale). Operator mixing among the bi-doublets between the seesaw and electroweak scale then generates a neutrino mass scale that matches experimental observations.

In the following, the scalar potential, including two bi-doublets and one $\mathrm{SU}(2)_\mathrm{R}$ doublet, is analyzed. The discussion follows [75], which considers two bi-doublets and two triplet scalars. Appendix B contains the full scalar potential. The VEVs read:

$$\langle\Phi\rangle = \begin{pmatrix} k & 0 \\ 0 & k' e^{\mathrm{i}\alpha_2^p} \end{pmatrix}, \quad \langle\mathrm{X}\rangle = \begin{pmatrix} w e^{\mathrm{i}\alpha_1^c} & 0 \\ 0 & w' e^{\mathrm{i}\alpha_2^c} \end{pmatrix}, \quad \langle\Xi\rangle = \begin{pmatrix} 0 \\ v_\mathrm{R} \end{pmatrix}, \tag{5.52}$$

where the phases accompaning k and v_R were rotated away. The VEVs of the charge conjugated fields follow analog to 5.48. The minimalization conditions are:

$$0 = \frac{\partial V}{\partial k} = \frac{\partial V}{\partial k'} = \frac{\partial V}{\partial w} = \frac{\partial V}{\partial w'} = \frac{\partial V}{\partial v_\mathrm{R}} = \frac{\partial V}{\partial \alpha_2^p} = \frac{\partial V}{\partial \alpha_1^c} = \frac{\partial V}{\partial \alpha_2^c}. \tag{5.53}$$

There are 8 conditions and 7 bilinear terms $\mu^2\phi^\dagger\phi$ with $\phi = \Phi, \tilde{\Phi}, \mathrm{X}, \tilde{\mathrm{X}}, \Xi$. Eliminating all μ results in one equation that relates all quartic couplings α, γ (with two bi-doublets and two doublets), δ (four doublets) and λ (four bi-doublets)

$$\begin{aligned} &\left(\tilde{\gamma}_2^{cp} - \gamma_2^{cp}\right)\left[k'w' \sin\left(\alpha_2^c - \alpha_2^p\right) + kw \sin\left(\alpha_1^c\right)\right] \\ &- \left(\tilde{\gamma}_1^{cp} - \gamma_1^{cp}\right)\left[k'w \sin\left(\alpha_1^c + \alpha_2^p\right) + kw' \sin\left(\alpha_2^c\right)\right] \\ &- \left(\tilde{\gamma}_1^{c} - \gamma_1^{c}\right) ww' \sin\left(\alpha_1^c + \alpha_2^c\right) \\ &- \left(\tilde{\gamma}_1^{p} - \gamma_1^{p}\right) ww' \sin\left(\alpha_2^p\right) = \lambda_i \mathcal{O}\left(\frac{(k, k', w, w')^4}{v_\mathrm{R}^2}\right). \end{aligned} \tag{5.54}$$

This means the smaller k' and w' become compared to w and k, the smaller $(\tilde{\gamma}_2^{cp} - \gamma_2^{cp})$ or α_1^c have to become. However, at least two phases satisfy non-trivial conditions and can contribute to CP violation. Furthermore, it was checked in analogy to [75], that for $k', w', (\tilde{\gamma}_2^{cp} - \gamma_2^{cp}) \to 0$ and solving the minimalization conditions for μ, both $\Phi^{(2)}$ and $\mathrm{X}^{(2)}$ become very heavy (Planck scale). At the same time, $\Phi^{(1)}, \mathrm{X}^{(1)}$ have masses around the electroweak scale and effectively correspond to the two Higgs bosons from the 2HDM model.

6. Conclusion

This thesis is divided into two parts, both investigating the radiative two-loop generation of neutrino masses. First, the two-loop renormalization of the Weinberg operator is performed and related to active neutrino masses. Second, gauge extensions of the seesaw type-I model are investigated, which allow for similar quantum corrections for the RHN masses.

Before performing the complete two-loop renormalization of the Weinberg operator, the calculation of the individual rank-increasing diagrams was presented in this work. Although there are more diagrams than accounted for in [16], their contribution to the beta function cancels, and our result agrees with theirs. Nevertheless, we found that including the additional diagrams is mandatory to fulfill the recursion relations between the $1/\epsilon$ and $1/\epsilon^2$ poles. The background field method was used in this thesis for the complete two-loop renormalization in order to maintain explicit gauge invariance and simplify the gauge sector renormalization. The SM parameters and the Wilson coefficient of the Weinberg operator were renormalized at one-loop in this gauge to prepare for the two-loop calculations. Only single insertions of the Weinberg operator were considered, corresponding to cut-off suppression to first order. IR regular masses were introduced to prevent spurious IR divergences. We calculated the two-loop CT of dimension-five Wilson coefficient, which proved to be independent of the renormalization scale or regulator masses, as expected for local physical counterterms. Additionally, the second-order poles satisfy recursion relations that relate them to one-loop counterterms. Although this is not a direct proof of the two-loop beta function, both the cancelation of all logarithmic terms in our result and the consistency of the recursion relations make the obtained two-loop RGEs highly probable to be correct.

Phenomenological implications on neutrino mixing parameters and masses were derived here using the complete two-loop RGE of the Weinberg operator. The setup assumes one massless active neutrino at the cut-off scale, as oscillation experiments only require two massive neutrinos. Furthermore, a seesaw type-I extension with two RHNs realizes this situation and motivates a seesaw scale cut-off. Analytical relations of oscillation parameters were derived here, and numerical evolution of the running parameters was conducted. These results confirm a radiatively generated neutrino mass of approximately $10^{-14}\,\text{eV} - 10^{-13}\,\text{eV}$, which constitutes a lower limit on the lightest mass eigenstate (also discussed in [16]). In this work, the Majorana phase associated with the light neutrino was found to run into an infrared quasi-fixed point, which was explicitly confirmed by numerically evaluating its energy dependence. The calculation determined the dependence of the lightest neutrino mass and the Majorana phase fixed point on the remaining CP-violating phases. Although the fixed point takes non-trivial and sizeable values, its

association with the tiny light neutrino mass makes it nearly unobservable. Compared to the genuinely massless limit, only significantly suppressed corrections contribute to the neutrinoless double beta decay mass.

Similar diagrams that increased the rank of the active neutrino mass matrix exist for RHNs, too [17]. If the RHN mass eigenstates are highly hierarchical, the seesaw scale is generated via two-loop effects and does not need to be introduced separately. Gravity's violation of global symmetries further motivates the breaking of lepton number at the Planck scale. Justification for why some RHN become massive at the Planck scale while others remain massless at the cut-off should be provided through gauge extensions to the type-I seesaw model.

In this thesis, general considerations were made regarding the number of massive RHNs and the inclusion of mass terms via SSB. In the presence of a second Higgs doublet, both one [19] and two heavy RHNs – as was found here – predict mass hierarchies in accordance with oscillation experiments. Additionally, it was noted that Majorana masses via SSB do not affect the rank-increasing contributions. Based on the consideration of the most minimal gauge groups $\mathrm{U}(1), \mathrm{SU}(2), \mathrm{SU}(N)$, a set of minimal requirements was derived in this work. Any model must be anomaly-free and contain singlet fermions that break lepton number and couple the right-handed neutrinos via Yukawa interactions. Moreover, multiple generations of RHNs with the same quantum numbers must exist, allowing flavor-violating interactions and rank increase. These motivate a seesaw-type mechanism for the RHN masses. A natural implementation in the LR extension was found here that includes a SSB pattern different from the scalar triplet approach. The presented model provides sufficient sources of flavor violation to explain the observed active neutrino masses, provided there is slight fine-tuning and cancelation between the coupling to the bi-doublet and its charge conjugate. However, a second bi-doublet must be introduced if there is no accidental cancelation. This thesis demonstrated that, after SSB around the Planck scale, the resulting fermionic and Yukawa sectors correspond to the hierarchical RHN mass spectrum, which generates the seesaw scale radiatively and predicts active neutrino masses in the ballpark of experimental data.

Based on the effect of a second Higgs field on the RHN mass renormalization, future work could extend the two-loop beta functions of the Weinberg operator Wilson coefficient to 2HDM scenarios. These provide an additional source of flavor violation in the form of a second Yukawa coupling. Furthermore, there are three distinct Weinberg operators, and operator mixing occurs at the one-loop and two-loop levels. This opens the door to having larger lower bounds on the lightest neutrino mass, the possibility of only one massive active at the cut-off scale, and other interesting phenomenological implications.

A. Two-Loop Renormalization

A.1. Master Integrals

In this section, the master integrals introduced in qq. 3.67 are evaluated. These integrals represent two-loop vacuum polarization topologies involving either one or three massive propagators. The first integral, denoted for convenience as $\mathcal{J}_1$, represents the case with a single massive propagator:

$$\mathcal{J}_1 \equiv K^{(d)}_{\{1,M\},\{1,0\},\{1,0\}} = \tilde{\mu}^{4\varepsilon} \int \mathrm{d}\Pi_{k,l} \frac{1}{(l^2 - M^2)\, k^2\, (k-l)^2}. \tag{A.1}$$

Here, $\mathrm{d}\Pi_p$ denotes the d-dimensional invariant phase space volume element: $\int \frac{\mathrm{d}^d p}{(2\pi)^d}$, with $d = 4 - 2\varepsilon$. Including the renormalization scale $\tilde{\mu}$ serves two purposes: 1) maintaining dimensional scaling and 2) facilitating the cancelation of finite terms arising from dimensional regularization. Subsequently, the integral is decomposed into terms involving k and l and reformulated using Feynman parameterization.

$$\begin{aligned} \mathcal{J}_1 &= \tilde{\mu}^{4\varepsilon} \int \mathrm{d}\Pi_l \frac{1}{(l^2 - M^2)} \int \mathrm{d}\Pi_k \int_0^1 \mathrm{d}x \frac{1}{\left[xk^2 + \overline{x}(k-l)^2\right]^2} \\ &= \tilde{\mu}^{4\varepsilon} \int \mathrm{d}\Pi_l \frac{1}{(l^2 - M^2)} \frac{\mathrm{i}}{(4\pi)^{\frac{d}{2}}} \Gamma\left(2 - \frac{d}{2}\right) \int_0^1 \mathrm{d}x \left[-x\overline{x}l\right]^{-\varepsilon}. \end{aligned} \tag{A.2}$$

The k integration follows the usual steps: Wick rotation, momentum shift, and evaluating the phase space integral via Passariono-Veltman functions. With

$$\int_0^1 x^{\alpha-1} \overline{x}^{\beta-1} = \frac{\Gamma(\alpha)\Gamma(\beta)}{\Gamma(\alpha+\beta)} \tag{A.3}$$

$\mathcal{J}_1$ reduces to

$$\mathcal{J}_1 = \frac{\mathrm{i}(-1)^{-\varepsilon}}{(4\pi)^{\frac{d}{2}}} \frac{\Gamma\left(2 - \frac{d}{2}\right) \Gamma\left(\frac{d}{2} - 1\right)^2}{\Gamma(d-2)} \tilde{\mu}^{4\varepsilon} \int \mathrm{d}\Pi_l \frac{l^{-\varepsilon}}{(l^2 - M^2)}. \tag{A.4}$$

Abbreviating the constant prefactor with C for simplicity and applying Feynman parameterization once more yields:

$$\begin{aligned} \mathcal{J}_1 &= C \int \mathrm{d}\Pi_l \frac{\Gamma(1+\varepsilon)}{\Gamma(\varepsilon)} \int_0^1 \mathrm{d}x \underbrace{\frac{\overline{x}^{\varepsilon-1}}{\left[x\,(l^2 - M^2) + \overline{x} l^2\right]^{1+\varepsilon}}}_{= \frac{\overline{x}^{\varepsilon-1}}{[l^2 - xM^2]^{1+\varepsilon}}} \\ &= C\, \frac{\Gamma(1+\varepsilon)}{\Gamma(\varepsilon)} \int_0^1 \mathrm{d}x \frac{\mathrm{i}(-1)^{1+\varepsilon}}{(4\pi)^{\frac{d}{2}}} \overline{x}^{\varepsilon-1} \frac{\Gamma\left(1 + \varepsilon - \frac{d}{2}\right)}{\Gamma(1+\varepsilon)} \left(xM^2\right)^{d/2-1-\varepsilon}. \end{aligned} \tag{A.5}$$

Employing Wick rotation and using the Passarino-Veltman functions, the Feynman parameter integral is subsequently evaluated with the help of eq. A.3:

$$\begin{aligned}\mathcal{J}_1 &= \frac{\mathrm{i}C(-1)^{1+\varepsilon}}{(4\pi)^{\frac{d}{2}}}\frac{\Gamma\left(\frac{d}{2}-\varepsilon\right)}{\Gamma\left(\frac{d}{2}\right)}M^{2\,\frac{d}{2}-1-\varepsilon} \\ &= \frac{\mu^{4\varepsilon}e^{2\gamma\varepsilon}}{(4\pi)^4}\frac{\Gamma(\varepsilon)\,\Gamma(1-\varepsilon)^2\,\Gamma(2-2\varepsilon)\,\Gamma(-1+2\varepsilon)}{\Gamma(2-2\varepsilon)\,\Gamma(2-\varepsilon)}M^{2\,\frac{d}{2}-1-\varepsilon} \\ &= \frac{M^2}{(4\pi)^4}\left(\frac{\mu^2}{M^2}\right)^{2\varepsilon}\left(-\frac{1}{2\varepsilon^2}-\frac{3}{2\varepsilon}-\frac{1}{4}\left(14+\pi^2\right)\right),\end{aligned} \tag{A.6}$$

where the dimension regularization-specific terms $\log 4\pi - \gamma$ vanishes as espected in $\overline{\mathrm{MS}}$. Continuing with the second master integral, denoted as $\mathcal{J}_2$ for simplicity, which contains three massive propagators:

$$\mathcal{J}_2 \equiv K^{(d)}_{\{1,M\},\{1,M\},\{1,M\}} = \tilde{\mu}^{4\varepsilon}\int \mathrm{d}\Pi_{k,l}\frac{1}{(l^2-M^2)\,(k^2-M^2)\,((k-l)^2-M^2)}. \tag{A.7}$$

The $\int \frac{\mathrm{d}^8 p}{p^6}$ behavior leads to problematic divergences in the Feynman parameter integrals, which, however, can be cured by raising the overall degree of divergence (in analogy to [76]). For that, IBP relations are employed. Abbreviating $l^2 - M^2 = D_1$, $k^2 - M^2 = D_2$ and $(k-l)^2 - M^2 = D_3$ and inserting $1 = \frac{1}{2d}\left(\frac{\partial k^\mu}{\partial k^\mu} + \frac{\partial l^\mu}{\partial l^\mu}\right)$ into $\mathcal{J}_2$ yields:

$$\begin{aligned}\mathcal{J}_2 &= \frac{1}{2d}\tilde{\mu}^{4\varepsilon}\int \mathrm{d}\Pi_{k,l}\left(\frac{\partial k^\mu}{\partial k^\mu}+\frac{\partial l^\mu}{\partial l^\mu}\right)\frac{1}{D_1 D_2 D_3} \\ &\overset{\text{IBP}}{=} \frac{1}{2d}\tilde{\mu}^{4\varepsilon}\int \mathrm{d}\Pi_{k,l}\frac{2k^2}{D_1^2 D_2 D_3}+\frac{2l^2}{D_1 D_2^2 D_3}+\frac{2(k-l)^2}{D_1 D_2 D_3^2} \\ &= \frac{1}{d}\tilde{\mu}^{4\varepsilon}\int \mathrm{d}\Pi_{k,l}3\frac{1}{D_1 D_2 D_3}+3\frac{M^2}{D_1 D_2 D_3^2}, \\ \longrightarrow \mathcal{J}_2 &= \frac{3M^2}{d-3}\tilde{\mu}^{4\varepsilon}\int \mathrm{d}\Pi_{k,l}\frac{1}{D_1^2 D_2 D_3}.\end{aligned} \tag{A.8}$$

Here, surface terms from partially integrating were dropped (justified after going to Euclidean space), $\pm M^2$ was inserted in the third step, and k, l were shifted to unify terms as $\left(D_1^2 D_2 D_3\right)^{-1}$. To simplify the integral, $k, l \to M \cdot k, l$ to extract the overall scale:

$$\mathcal{J}_2 = -\tilde{\mu}^{4\varepsilon}\frac{3M^{2\,d-3}}{d-3}\int \mathrm{d}\Pi_{k,l}\frac{1}{(l^2-1)\,(k^2-1)\,((k-l)^2-1)^2}. \tag{A.9}$$

Decomposing in k, l and employing Feynman parameterization yields:

$$\begin{aligned}\mathcal{J}_2 &= \tilde{\mu}^{4\varepsilon}\frac{3M^{2\,d-3}}{d-3}\int \mathrm{d}\Pi_l\frac{1}{(l^2-1)^2}\int \mathrm{d}\Pi_k\int_0^1 \mathrm{d}x\,\frac{\underbrace{1}{\left[\overline{x}\,(k^2-1)+x\,((k-l)^2-1)\right]^2}}{\left[(k-xl)^2+x\overline{x}l^2-1\right]^{-2}} \\ &= \mathrm{i}\tilde{\mu}^{4\varepsilon}\frac{3M^{2\,d-3}}{d-3}\frac{\Gamma(\varepsilon)}{(4\pi)^{\frac{d}{2}}}\int \mathrm{d}\Pi_l\frac{1}{(l^2-1)^2}\int_0^1 \mathrm{d}x\left(1-x\overline{x}l^2\right)^{-\varepsilon}.\end{aligned} \tag{A.10}$$

Following momentum shift and Wick rotation, the scalar k integral was evaluated using Passarino-Veltman functions. Subsequently, factoring out $-x\overline{x}$ simplifies the introduction of another Feynman parameterization:

$$\begin{aligned}\mathcal{I}_2 &= \mathrm{i}\tilde{\mu}^{4\varepsilon}\frac{3M^{2\,d-3}}{d-3}\frac{\Gamma(\varepsilon)}{(4\pi)^{\frac{d}{2}}}\int \mathrm{d}\Pi_l \int_0^1 \mathrm{d}x \frac{(-x\overline{x})^{-\varepsilon}}{\left(l^2-1\right)^2\left(-\frac{1}{x\overline{x}}+l^2\right)^{\varepsilon}} \\ &= \mathrm{i}\tilde{\mu}^{4\varepsilon}\frac{3M^{2\,d-3}}{d-3}\frac{\Gamma(2+\varepsilon)}{(4\pi)^{\frac{d}{2}}}\int \mathrm{d}\Pi_l \int_0^1\int_0^1 \mathrm{d}x\mathrm{d}y \underbrace{\frac{\overline{y}y^{\varepsilon-1}(-1)^{\varepsilon}}{\left[\overline{y}\left(l^2-1\right)+y\left(l^2-\frac{1}{x\overline{x}}\right)\right]^{2+\varepsilon}}}_{\frac{\overline{y}y^{\varepsilon-1}(-1)^{\varepsilon}}{\left[l^2-1-\frac{y}{x\overline{x}}+y\right]^{2+\varepsilon}}}.\end{aligned} \tag{A.11}$$

After performing the second phase space integral, the remaining x, y integrals read:

$$\mathcal{I}_2 = -\tilde{\mu}^{4\varepsilon}\frac{3M^{2\,d-3}}{d-3}\frac{\Gamma(2+\varepsilon)}{(4\pi)^d}\frac{\Gamma(2\varepsilon)}{\Gamma(2+\varepsilon)}\int_0^1\int_0^1 \mathrm{d}x\mathrm{d}y\ \overline{y}y^{\varepsilon-1}(x\overline{x})^{-\varepsilon}\left(1+\frac{y}{x\overline{x}}-y\right)^{-2\varepsilon}. \tag{A.12}$$

While an analytical evaluation of the entire integral proves challenging, the first and second-order pole in ε can be systematically extracted. For that matter, rewriting

$$y^{\varepsilon-1} \quad \text{as} \quad \frac{1}{\varepsilon}\frac{\mathrm{d}y^{\varepsilon}}{\mathrm{d}y} \qquad \text{and} \qquad \Delta(x,y) \equiv 1+\frac{y}{x\overline{x}}-y \tag{A.13}$$

and partially integrating the expression in y yields:

$$\mathcal{I}_2 = \tilde{\mu}^{4\varepsilon}\frac{3M^{2\,d-3}}{d-3}\frac{\Gamma(2\varepsilon)}{(4\pi)^d}\frac{1}{\varepsilon}\int_0^1\int_0^1 \mathrm{d}x\mathrm{d}y\ (x\overline{x})^{-\varepsilon}y^{\varepsilon}\frac{\mathrm{d}}{\mathrm{d}y}\overline{y}\Delta(x,y)^{-2\varepsilon}. \tag{A.14}$$

In this form, $y^{\varepsilon} = 1+\varepsilon\log y$ can be expanded in ε. Hence, the y integral becomes

$$\begin{aligned}&\int_0^1 \mathrm{d}y\ (1+\varepsilon\log y)\frac{\mathrm{d}}{\mathrm{d}y}\overline{y}\Delta(x,y)^{-2\varepsilon} \\ &= \left[\overline{y}\Delta(x,y)^{-2\varepsilon}\right]_0^1 + \varepsilon\int_0^1 \mathrm{d}y\ \log y\frac{\mathrm{d}}{\mathrm{d}y}\overline{y}\Delta(x,y)^{-2\varepsilon} \\ &= -\Delta(x,0)^{-2\varepsilon} + \varepsilon\int_0^1 \mathrm{d}y\ \log y\frac{\mathrm{d}}{\mathrm{d}y}\overline{y}\left(1-2\varepsilon\log\Delta(x,y)\right)+\mathcal{O}\left(\varepsilon^3\right) \\ &= -1-\varepsilon\int_0^1 \mathrm{d}y\log y+\mathcal{O}\left(\varepsilon^2\right) = -1+\varepsilon+\mathcal{O}\left(\varepsilon^2\right).\end{aligned} \tag{A.15}$$

Since $\Delta(x,1)$ is non-singular in y, the upper boundary term vanished (line 2). Upon reinserting back into the $\mathcal{I}_2$:

$$\begin{aligned}\mathcal{I}_2 &= -\tilde{\mu}^{4\varepsilon}\frac{3M^{2\,d-3}}{d-3}\frac{\Gamma(2\varepsilon)}{(4\pi)^d}\frac{1}{\varepsilon}\int_0^1 \mathrm{d}x\ (x\overline{x})^{-\varepsilon}(1-\varepsilon)+\mathcal{O}\left(\varepsilon^2\right) \\ &= -\tilde{\mu}^{4\varepsilon}\frac{3M^{2\,d-3}}{d-3}\frac{\Gamma(2\varepsilon)}{(4\pi)^d}\frac{1}{\varepsilon}(1-\varepsilon)\frac{\Gamma(1-\varepsilon)^2}{\Gamma(2-2\varepsilon)}+\mathcal{O}\left(\varepsilon^0\right) \\ &= -\frac{3}{2}M^2\left(\frac{1}{\varepsilon^2}+\frac{1}{\varepsilon}\left(3-2\log\left(\frac{M^2}{\mu^2}\right)\right)+\mathcal{O}\left(\varepsilon^0\right)\right),\end{aligned} \tag{A.16}$$

where $\log 4\pi-\gamma$ vanished as expected.

A.2. One- and two-loop CTs

One-Loop CTs

The one-loop CTs determined with the BFM for all SM parameters, the Wilson coefficient of the Weinberg operator and the regulator masses read:

$$
\begin{aligned}
\delta Z_{\ell}^{(1)} &= -\frac{1}{16\pi^2\varepsilon\cdot 4}\left(g_1^2+3g_2^2+2Y_lY_l^\dagger\right)\,,\\
\delta Z_{e}^{(1)} &= -\frac{1}{16\pi^2\varepsilon}\left(g_1^2+Y_l^\dagger Y_l\right),\\
\delta Z_{q}^{(1)} &= -\frac{1}{16\pi^2\varepsilon\cdot 36}\left(g_1^2+27g_2^2+48g_3^2+18Y_{\mathrm{d}}Y_{\mathrm{d}}^\dagger+18Y_{\mathrm{u}}Y_{\mathrm{u}}^\dagger\right),\\
\delta Z_{u}^{(1)} &= -\frac{1}{16\pi^2\varepsilon\cdot 9}\left(4g_1^2+12g_3^2+9Y_{\mathrm{u}}^\dagger Y_{\mathrm{u}}\right),\\
\delta Z_{d}^{(1)} &= -\frac{1}{16\pi^2\varepsilon\cdot 9}\left(g_1^2+12g_3^2+9Y_{\mathrm{d}}^\dagger Y_{\mathrm{d}}\right),\\
\delta Z_{H}^{(1)} &= \frac{1}{16\pi^2\varepsilon\cdot 2}\left(g_1^2+3g_2^2-2T\right),\\
\delta Z_{M_H}^{(1)} &= \frac{1}{16\pi^2\varepsilon}\left(6\lambda+T\right),\\
\delta Z_{\lambda}^{(1)} &= \frac{1}{16\pi^2\varepsilon\cdot 16\lambda}\left[32\lambda T+3(g1^2+g2^2)^2+6g_2^4-24\lambda(g_1^2+3g_2^2)+192\lambda^2-16T'\right],\\
\delta Z_{Y_{\mathrm{u}}}^{(1)} &= \frac{1}{16\pi^2\varepsilon\cdot 24}Y_{\mathrm{u}}^{-1}\left[Y_{\mathrm{u}}\left(12T-17g_1^2-27g_2^2-96g_3^2\right)+18Y_{\mathrm{u}}Y_{\mathrm{u}}^\dagger Y_{\mathrm{u}}-18Y_{\mathrm{d}}Y_{\mathrm{d}}^\dagger Y_{\mathrm{u}}\right],\\
\delta Z_{Y_{\mathrm{d}}}^{(1)} &= \frac{1}{16\pi^2\varepsilon\cdot 24}Y_{\mathrm{d}}^{-1}\left[Y_{\mathrm{d}}\left(12T-5g_1^2-27g_2^2-96g_3^2\right)-18Y_{\mathrm{u}}Y_{\mathrm{u}}^\dagger Y_{\mathrm{d}}+18Y_{\mathrm{d}}Y_{\mathrm{d}}^\dagger Y_{\mathrm{d}}\right],\\
\delta Z_{Y_l}^{(1)} &= \frac{1}{16\pi^2\varepsilon\cdot 8}Y_l^{-1}\left(Y_l\left[4T-15g_1^2-9g_2^2\right)+6Y_lY_l^\dagger Y_l\right],\\
\delta C_5^{(1)} &= \frac{1}{16\pi^2\varepsilon\cdot 4}\left[2\left(4\lambda-3g_2^2+2T\right)C_5-3Y_lY_l^\dagger C_5-3C_5\left(Y_l^\dagger Y_l\right)^{\mathrm{T}}\right],\\
\delta Z_{M_{\hat{B}}}^{(1)} &= \frac{1}{16\pi^2\varepsilon}\frac{41}{6}g_1^2,\\
\delta Z_{M_{\hat{W}}}^{(1)} &= -\frac{1}{16\pi^2\varepsilon}\frac{7}{6}g_2^2.
\end{aligned}
$$

Two-loop CTs

The two-loop CTs determined with the BFM for Lepton and Higgs wavefunction as well as the Wilson coefficient of the Weinberg operator read:

$$
\begin{aligned}
\delta Z_\ell^{(2)} &= \frac{1}{(16\pi^2)^2\,\varepsilon^2\cdot 32}\Big[g_1^4+6g_1^2g_2^2+57g_2^4+2\left(17g_1^2+15g_2^2\right)Y_lY_l^\dagger \\
&\quad -8TY_lY_l^\dagger-8Y_lY_l^\dagger Y_lY_l^\dagger\Big] \\
&\quad +\frac{1}{(16\pi^2)^2\,\varepsilon\cdot 64}\Big[85g_1^4+18g_1^2g_2^2-231g_2^4-2\left(7g_1^2+33g_2^2\right)Y_lY_l^\dagger \\
&\quad +24TY_lY_l^\dagger+8Y_lY_l^\dagger Y_lY_l^\dagger\Big]\,,
\end{aligned}
$$

$$
\begin{aligned}
\delta Z_H^{(2)} &= \frac{1}{(16\pi^2)^2\,\varepsilon^2}\Big\{\frac{43}{16}g_1^4+\frac{3}{4}g_1^2g_2^2-\frac{15}{16}g_2^4+\frac{1}{8}g_1^2\mathrm{Tr}\left(11Y_lY_l^\dagger+5Y_{\mathrm{u}}Y_{\mathrm{u}}^\dagger-7Y_{\mathrm{d}}Y_{\mathrm{d}}^\dagger\right) \\
&\quad -\frac{3}{8}g_2^2T+12g_3^2\mathrm{Tr}\left(Y_{\mathrm{d}}Y_{\mathrm{d}}^\dagger+Y_{\mathrm{u}}Y_{\mathrm{u}}^\dagger\right)-\frac{3}{4}\mathrm{Tr}\left(Y_lY_l^\dagger Y_lY_l^\dagger+3Y_{\mathrm{u}}Y_{\mathrm{u}}^\dagger Y_{\mathrm{u}}Y_{\mathrm{u}}^\dagger\right. \\
&\quad \left.+\,3Y_{\mathrm{d}}Y_{\mathrm{d}}^\dagger Y_{\mathrm{d}}Y_{\mathrm{d}}^\dagger-6Y_{\mathrm{u}}Y_{\mathrm{u}}^\dagger Y_{\mathrm{d}}Y_{\mathrm{d}}^\dagger\right)\Big\} \\
&\quad +\frac{1}{(16\pi^2)^2\,\varepsilon}\Big\{-\frac{431}{192}g_1^4-\frac{9}{32}g_1^2g_2^2+\frac{163}{64}g_2^4-3\lambda^2 \\
&\quad -\frac{15}{16}g_2^2T+\frac{3}{8}\mathrm{Tr}\left(3Y_lY_l^\dagger Y_lY_l^\dagger+9Y_{\mathrm{u}}Y_{\mathrm{u}}^\dagger Y_{\mathrm{u}}Y_{\mathrm{u}}^\dagger+9Y_{\mathrm{d}}Y_{\mathrm{d}}^\dagger Y_{\mathrm{d}}Y_{\mathrm{d}}^\dagger-2Y_{\mathrm{u}}Y_{\mathrm{u}}^\dagger Y_{\mathrm{d}}Y_{\mathrm{d}}^\dagger\right) \\
&\quad -\frac{5}{48}g_1^2\mathrm{Tr}\left(15Y_lY_l^\dagger+17Y_{\mathrm{u}}Y_{\mathrm{u}}^\dagger+5Y_{\mathrm{d}}Y_{\mathrm{d}}^\dagger\right)-10g_3^2\mathrm{Tr}\left(Y_{\mathrm{d}}Y_{\mathrm{d}}^\dagger+Y_{\mathrm{u}}Y_{\mathrm{u}}^\dagger\right)\Big\}\,,
\end{aligned}
$$

$$
\begin{aligned}
\delta C_5^{(2)} &= \frac{1}{(16\pi^2)^2\,\varepsilon^2}\Big\{\Big[\frac{3}{16}g_1^4+\frac{3}{8}g_1^2g_2^2+\frac{65}{16}g_2^4-\lambda\left(\frac{3}{2}g_1^2+\frac{15}{2}g_2^2-14\lambda-4T\right) \\
&\quad -\frac{1}{8}g_1^2\mathrm{Tr}\left(15Y_lY_l^\dagger+17Y_{\mathrm{u}}Y_{\mathrm{u}}^\dagger+5Y_{\mathrm{d}}Y_{\mathrm{d}}^\dagger\right)-\frac{21}{8}g_2^2T-12g_3^2\mathrm{Tr}\left(Y_{\mathrm{u}}Y_{\mathrm{u}}^\dagger+Y_{\mathrm{d}}Y_{\mathrm{d}}^\dagger\right) \\
&\quad +T^2-\frac{1}{4}T'-\frac{9}{2}\mathrm{Tr}\left(Y_{\mathrm{u}}Y_{\mathrm{u}}^\dagger Y_{\mathrm{d}}Y_{\mathrm{d}}^\dagger\right)\Big]C_5+\left(\frac{45}{32}g_1^2+\frac{63}{32}g_2^2-\frac{3}{2}\lambda-\frac{9}{8}T\right) \\
&\quad \times\left[Y_lY_l^\dagger C_5+C_5\left(Y_lY_l^\dagger\right)^{\mathrm{T}}\right]-\frac{9}{32}\left[Y_lY_l^\dagger Y_lY_l^\dagger C_5+C_5\left(Y_lY_l^\dagger Y_lY_l^\dagger\right)^{\mathrm{T}}\right] \\
&\quad +\frac{9}{16}Y_lY_l^\dagger C_5\left(Y_lY_l^\dagger\right)^{\mathrm{T}}\Big\} \\
&\quad +\frac{1}{(16\pi^2)^2\,\varepsilon}\Big\{-\Big[\frac{129}{32}g_1^4+\frac{83}{16}g_1^2g_2^2+\frac{169}{96}g_2^4+\lambda\left(g_1^2+7\lambda+2T\right)-\frac{15}{16}g_2^2T \\
&\quad -\frac{5}{48}g_1^2\mathrm{Tr}\left(15Y_lY_l^\dagger+17Y_{\mathrm{u}}Y_{\mathrm{u}}^\dagger+5Y_{\mathrm{d}}Y_{\mathrm{d}}^\dagger\right)-10g_3^2\mathrm{Tr}\left(Y_{\mathrm{u}}Y_{\mathrm{u}}^\dagger+Y_{\mathrm{d}}Y_{\mathrm{d}}^\dagger\right) \\
&\quad +\frac{1}{8}T'-\frac{3}{4}\mathrm{Tr}\left(Y_{\mathrm{u}}Y_{\mathrm{u}}^\dagger Y_{\mathrm{d}}Y_{\mathrm{d}}^\dagger\right)\Big]C_5-\left(\frac{57}{64}g_1^2-\frac{33}{64}g_2^2-\frac{5}{16}T\right) \\
&\quad \times\left[Y_lY_l^\dagger C_5+C_5\left(Y_lY_l^\dagger\right)^{\mathrm{T}}\right]+\frac{19}{16}\left[Y_lY_l^\dagger Y_lY_l^\dagger C_5+C_5\left(Y_lY_l^\dagger Y_lY_l^\dagger\right)^{\mathrm{T}}\right] \\
&\quad +\frac{1}{2}Y_lY_l^\dagger C_5\left(Y_lY_l^\dagger\right)^{\mathrm{T}}\Big\}\,.
\end{aligned}
$$

A.3. Two-Loop SM RGEs

The two-loop RGE for the Weinberg operator Wilson coefficient is supplemented by the two-loop SM RGE. These were extracted from SARAH and RGBeta:

$$\mu\frac{\mathrm{d}g_1}{\mathrm{d}\mu} = \frac{1}{16\pi^2}g_1^3\left\{\frac{41}{6}+\frac{1}{16\pi^2}\left[\frac{199}{18}g_1^2+\frac{9}{2}g_2^2+\frac{44}{3}g_3^2-\frac{1}{6}\mathrm{Tr}\left(15Y_lY_l^\dagger+17Y_\mathrm{u}Y_\mathrm{u}^\dagger+5Y_\mathrm{d}Y_\mathrm{d}^\dagger\right)\right]\right\},$$

$$\mu\frac{\mathrm{d}g_2}{\mathrm{d}\mu} = -\frac{1}{16\pi^2}g_2^3\left\{\frac{19}{6}-\frac{1}{16\pi^2}\left(\frac{3}{2}g_1^2+\frac{35}{6}g_2^2+12g_3^2-\frac{1}{2}T\right)\right\},$$

$$\mu\frac{\mathrm{d}g_3}{\mathrm{d}\mu} = -\frac{1}{16\pi^2}g_3^3\left\{7-\frac{1}{16\pi^2}\left[\frac{11}{6}g_1^2+\frac{9}{2}g_2^2-26g_3^2-2\mathrm{Tr}\left(Y_\mathrm{u}Y_\mathrm{u}^\dagger+Y_\mathrm{d}Y_\mathrm{d}^\dagger\right)\right]\right\},$$

$$\begin{aligned}
\mu\frac{\mathrm{d}\lambda}{\mathrm{d}\mu} &= \frac{1}{16\pi^2}\left[\frac{3}{8}g_1^4+\frac{9}{8}g_2^4+\frac{3}{4}g_1^2g_2^2-2T'+\left(-3g_1^2-9g_2^2+24\lambda+4T\right)\lambda\right]\\
&+\frac{1}{(16\pi^2)^2}\left\{-\frac{379}{48}g_1^6+\frac{305}{16}g_2^6-\frac{289}{48}g_1^2g_2^4-\frac{559}{48}g_1^4g_2^2-\frac{3}{4}g_2^4T\right.\\
&-\frac{1}{4}g_1^4\mathrm{Tr}\left(25Y_lY_l^\dagger+19Y_\mathrm{u}Y_\mathrm{u}^\dagger-5Y_\mathrm{d}Y_\mathrm{d}^\dagger\right)+\frac{1}{2}g_1^2g_2^2\mathrm{Tr}\left(11Y_lY_l^\dagger+21Y_\mathrm{u}Y_\mathrm{u}^\dagger+9Y_\mathrm{d}Y_\mathrm{d}^\dagger\right)\\
&-\frac{4}{3}g_1^2\mathrm{Tr}\left(3Y_lY_l^\dagger Y_lY_l^\dagger+2Y_\mathrm{u}Y_\mathrm{u}^\dagger Y_\mathrm{u}Y_\mathrm{u}^\dagger-Y_\mathrm{d}Y_\mathrm{d}^\dagger Y_\mathrm{d}Y_\mathrm{d}^\dagger\right)\\
&-32g_3^2\mathrm{Tr}\left(Y_\mathrm{u}Y_\mathrm{u}^\dagger Y_\mathrm{u}Y_\mathrm{u}^\dagger+Y_\mathrm{d}Y_\mathrm{d}^\dagger Y_\mathrm{d}Y_\mathrm{d}^\dagger\right)+\lambda\left[\frac{629}{24}g_1^4-\frac{73}{8}g_2^4+\frac{39}{4}g_1^2g_2^2\right.\\
&+\frac{5}{6}g_1^2\mathrm{Tr}\left(15Y_lY_l^\dagger+17Y_\mathrm{u}Y_\mathrm{u}^\dagger+5Y_\mathrm{d}Y_\mathrm{d}^\dagger\right)+\frac{15}{2}g_2^2T+80g_3^2\mathrm{Tr}\left(Y_\mathrm{u}Y_\mathrm{u}^\dagger+Y_\mathrm{d}Y_\mathrm{d}^\dagger\right)-3T'\\
&\left.-42\mathrm{Tr}\left(Y_\mathrm{u}Y_\mathrm{u}^\dagger Y_\mathrm{d}Y_\mathrm{d}^\dagger\right)\right]+2\lambda^2\left(18g_1^2+54g_2^2-156\lambda^2-24T\right)+2\mathrm{Tr}\left(5Y_lY_l^\dagger Y_lY_l^\dagger Y_lY_l^\dagger\right.\\
&+15Y_\mathrm{u}Y_\mathrm{u}^\dagger Y_\mathrm{u}Y_\mathrm{u}^\dagger Y_\mathrm{u}Y_\mathrm{u}^\dagger+15Y_\mathrm{d}Y_\mathrm{d}^\dagger Y_\mathrm{d}Y_\mathrm{d}^\dagger Y_\mathrm{d}Y_\mathrm{d}^\dagger-3Y_\mathrm{d}Y_\mathrm{d}^\dagger Y_\mathrm{d}Y_\mathrm{d}^\dagger Y_\mathrm{u}Y_\mathrm{u}^\dagger\\
&\left.\left.-3\ Y_\mathrm{d}Y_\mathrm{d}^\dagger Y_\mathrm{u}Y_\mathrm{u}^\dagger Y_\mathrm{u}Y_\mathrm{u}^\dagger\right)\right\},
\end{aligned}$$

$$\begin{aligned}
\mu\frac{\mathrm{d}Y_l}{\mathrm{d}\mu} &= \frac{1}{16\pi^2}\left\{-\frac{15}{4}g_1^2-\frac{9}{4}g_2^2+T+\frac{3}{2}Y_lY_l^\dagger+\frac{1}{16\pi^2}\left[\frac{457}{24}g_1^4+\frac{9}{4}g_1^2g_2^2-\frac{23}{4}g_2^4+6\lambda^2\right.\right.\\
&+\frac{5}{24}g_1^2\mathrm{Tr}\left(15Y_lY_l^\dagger+17Y_\mathrm{u}Y_\mathrm{u}^\dagger+5Y_\mathrm{d}Y_\mathrm{d}^\dagger\right)+\frac{15}{8}g_2^2T-\frac{9}{4}T'+\frac{3}{2}\mathrm{Tr}\left(Y_\mathrm{u}Y_\mathrm{u}^\dagger Y_\mathrm{d}Y_\mathrm{d}^\dagger\right)\\
&\left.\left.+\left(\frac{129}{16}g_1^2+\frac{135}{16}g_2^2-12\lambda-\frac{9}{4}T\right)Y_lY_l^\dagger+\frac{3}{2}Y_lY_l^\dagger Y_lY_l^\dagger\right]\right\}Y_l\,,
\end{aligned}$$

$$
\begin{aligned}
\mu\frac{\mathrm{d}Y_\mathrm{u}}{\mathrm{d}\mu} = \frac{1}{16\pi^2}\Bigg\{ & -\frac{17}{12}g_1^2 - \frac{9}{4}g_2^2 - 8g_3^2 + T + \frac{3}{2}\left(Y_\mathrm{u}Y_\mathrm{u}^\dagger - Y_\mathrm{d}Y_\mathrm{d}^\dagger\right) \\
& + \frac{1}{16\pi^2}\Bigg[\frac{1187}{216}g_1^4 - \frac{23}{4}g_2^4 - 108g_3^4 - \frac{3}{4}g_1^2g_2^2 + \frac{19}{9}g_1^2g_3^2 + 9g_2^2g_3^2 + 6\lambda^2 \\
& + \frac{5}{24}g_1^2\mathrm{Tr}\left(15Y_lY_l^\dagger + 17Y_\mathrm{u}Y_\mathrm{u}^\dagger + 5Y_\mathrm{d}Y_\mathrm{d}^\dagger\right) + \frac{15}{8}g_2^2T + 20g_3^2\mathrm{Tr}\left(Y_\mathrm{u}Y_\mathrm{u}^\dagger + Y_\mathrm{d}Y_\mathrm{d}^\dagger\right) \\
& + \left(\frac{223}{48}g_1^2 + \frac{135}{16}g_2^2 + 16g_3^2 - 12\lambda - \frac{9}{4}T\right)Y_\mathrm{u}Y_\mathrm{u}^\dagger \\
& + \left(-\frac{43}{48}g_1^2 + \frac{9}{16}g_2^2 - 16g_3^2 + \frac{5}{4}T\right)Y_\mathrm{d}Y_\mathrm{d}^\dagger - \frac{9}{4}T' + \frac{3}{2}\mathrm{Tr}\left(Y_\mathrm{u}Y_\mathrm{u}^\dagger Y_\mathrm{d}Y_\mathrm{d}^\dagger\right) \\
& + \frac{3}{2}Y_\mathrm{u}Y_\mathrm{u}^\dagger Y_\mathrm{u}Y_\mathrm{u}^\dagger + \frac{11}{4}Y_\mathrm{d}Y_\mathrm{d}^\dagger Y_\mathrm{d}Y_\mathrm{d}^\dagger - Y_\mathrm{d}Y_\mathrm{d}^\dagger Y_\mathrm{u}Y_\mathrm{u}^\dagger - \frac{1}{4}Y_\mathrm{u}Y_\mathrm{u}^\dagger Y_\mathrm{d}Y_\mathrm{d}^\dagger\Bigg]\Bigg\}Y_\mathrm{u}\,,
\end{aligned}
$$

$$
\begin{aligned}
\mu\frac{\mathrm{d}Y_\mathrm{d}}{\mathrm{d}\mu} = \frac{1}{16\pi^2}\Bigg\{ & -\frac{5}{12}g_1^2 - \frac{9}{4}g_2^2 - 8g_3^2 + T - \frac{3}{2}\left(Y_\mathrm{u}Y_\mathrm{u}^\dagger - Y_\mathrm{d}Y_\mathrm{d}^\dagger\right) \\
& + \frac{1}{16\pi^2}\Bigg[-\frac{127}{216}g_1^4 - \frac{23}{4}g_2^4 - 108g_3^4 - \frac{9}{4}g_1^2g_2^2 + \frac{31}{9}g_1^2g_3^2 + 9g_2^2g_3^2 + 6\lambda^2 \\
& + \frac{5}{24}g_1^2\mathrm{Tr}\left(15Y_lY_l^\dagger + 17Y_\mathrm{u}Y_\mathrm{u}^\dagger + 5Y_\mathrm{d}Y_\mathrm{d}^\dagger\right) + \frac{15}{8}g_2^2T + 20g_3^2\mathrm{Tr}\left(Y_\mathrm{u}Y_\mathrm{u}^\dagger + Y_\mathrm{d}Y_\mathrm{d}^\dagger\right) \\
& + \left(\frac{187}{48}g_1^2 + \frac{135}{16}g_2^2 + 16g_3^2 - 12\lambda - \frac{9}{4}T\right)Y_\mathrm{d}Y_\mathrm{d}^\dagger \\
& + \left(-\frac{79}{48}g_1^2 + \frac{9}{16}g_2^2 - 16g_3^2 + \frac{5}{4}T\right)Y_\mathrm{u}Y_\mathrm{u}^\dagger - \frac{9}{4}T' + \frac{3}{2}\mathrm{Tr}\left(Y_\mathrm{u}Y_\mathrm{u}^\dagger Y_\mathrm{d}Y_\mathrm{d}^\dagger\right) \\
& + \frac{3}{2}Y_\mathrm{d}Y_\mathrm{d}^\dagger Y_\mathrm{d}Y_\mathrm{d}^\dagger + \frac{11}{4}Y_\mathrm{u}Y_\mathrm{u}^\dagger Y_\mathrm{u}Y_\mathrm{u}^\dagger - Y_\mathrm{u}Y_\mathrm{u}^\dagger Y_\mathrm{d}Y_\mathrm{d}^\dagger - \frac{1}{4}Y_\mathrm{d}Y_\mathrm{d}^\dagger Y_\mathrm{u}Y_\mathrm{u}^\dagger\Bigg]\Bigg\}Y_\mathrm{d}.
\end{aligned}
$$

Here, $T = \mathrm{Tr}\left[Y_lY_l^\dagger + 3Y_\mathrm{u}Y_\mathrm{u}^\dagger + 3Y_\mathrm{d}Y_\mathrm{d}^\dagger\right]$ and $T' = \mathrm{Tr}\left[\left(Y_lY_l^\dagger\right)^2 + 3\left(Y_\mathrm{u}Y_\mathrm{u}^\dagger\right)^2 + 3\left(Y_\mathrm{d}Y_\mathrm{d}^\dagger\right)^2\right]$.

B. Scalar Potential in LR Model

The full scalar potential introduced in section 5.2.1 is presented in this chapter. For simplicity, it is split into different types of couplings: dimensionful scales μ, quartic couplings α, γ (with two bi-doublets and two doublets), δ (four doublets), and λ (four bi-doublets) or schematically

$$V(\Phi, \mathrm{X}, \Xi) = V_\mu + V_\delta + V_\alpha + V_\gamma + V_\lambda. \tag{B.1}$$

In detail, these read:

$$\begin{aligned} V_\mu = &- \left(\mu_1^p\right)^2 \mathrm{Tr}\left[\Phi^\dagger \Phi\right] - \left(\mu_1^c\right)^2 \mathrm{Tr}\left[\mathrm{X}^\dagger \mathrm{X}\right] \\ &- \left(\mu_1^{pc}\right)^2 \mathrm{Tr}\left[\Phi^\dagger \mathrm{X} + \mathrm{X}^\dagger \Phi\right] \\ &- \left(\mu_2^p\right)^2 \mathrm{Tr}\left[\tilde{\Phi}\Phi^\dagger + \tilde{\Phi}^\dagger \Phi\right] - \left(\mu_2^p\right)^2 \mathrm{Tr}\left[\tilde{\mathrm{X}}\mathrm{X}^\dagger + \tilde{\mathrm{X}}^\dagger \mathrm{X}\right] \\ &- \left(\mu_2^{pc}\right)^2 \mathrm{Tr}\left[\tilde{\Phi}\mathrm{X}^\dagger + \tilde{\Phi}^\dagger \mathrm{X}\right] \\ &- \mu_\Xi^2 \Xi^\dagger \Xi, \end{aligned} \tag{B.2}$$

$$V_\rho = \delta \left(\Xi^\dagger \Xi\right)^2, \tag{B.3}$$

$$\begin{aligned} V_\alpha = &\, \alpha_1^p \mathrm{Tr}\left[\Phi^\dagger \Phi\right] \Xi^\dagger \Xi + \alpha_1^c \mathrm{Tr}\left[\mathrm{X}^\dagger \mathrm{X}\right] \Xi^\dagger \Xi \\ &+ \alpha_1^{pc} \mathrm{Tr}\left[\Phi^\dagger \mathrm{X} + \mathrm{X}^\dagger \Phi\right] \Xi^\dagger \Xi \\ &+ \alpha_2^p \mathrm{Tr}\left[\tilde{\Phi}\Phi^\dagger + \tilde{\Phi}^\dagger \Phi\right] \Xi^\dagger \Xi + \alpha_2^p \mathrm{Tr}\left[\tilde{\mathrm{X}}\mathrm{X}^\dagger + \tilde{\mathrm{X}}^\dagger \mathrm{X}\right] \Xi^\dagger \Xi \\ &+ \alpha_2^{pc} \mathrm{Tr}\left[\tilde{\Phi}\mathrm{X}^\dagger + \tilde{\Phi}^\dagger \mathrm{X}\right] \Xi^\dagger \Xi, \end{aligned} \tag{B.4}$$

$$\begin{aligned} V_\gamma = &\, \gamma_1^p \Xi^\dagger \Phi^\dagger \Phi \Xi + \gamma_1^c \Xi^\dagger \mathrm{X}^\dagger \mathrm{X} \Xi \\ &+ \tilde{\gamma}_1^p \Xi^\dagger \tilde{\Phi}^\dagger \tilde{\Phi} \Xi + \tilde{\gamma}_1^p \Xi^\dagger \tilde{\mathrm{X}}^\dagger \tilde{\mathrm{X}} \Xi \\ &+ \gamma_1^{pc} \Xi^\dagger \left(\Phi^\dagger \mathrm{X} + \mathrm{X}^\dagger \Phi\right) \Xi + \tilde{\gamma}_1^{pc} \Xi^\dagger \left(\tilde{\Phi}^\dagger \tilde{\mathrm{X}} + \tilde{\mathrm{X}}^\dagger \tilde{\Phi}\right) \Xi \\ &+ 2\gamma_2^p \Xi^\dagger \left(\Phi^\dagger \tilde{\Phi} + \tilde{\Phi}^\dagger \Phi\right) \Xi + 2\gamma_2^c \Xi^\dagger \left(\mathrm{X}^\dagger \tilde{\mathrm{X}} + \tilde{\mathrm{X}}^\dagger \mathrm{X}\right) \Xi \\ &+ \gamma_2^{pc} \Xi^\dagger \left(\mathrm{X}^\dagger \tilde{\Phi} + \tilde{\Phi}^\dagger \mathrm{X}\right) \Xi \\ &+ \tilde{\gamma}_2^{pc} \Xi^\dagger \left(\tilde{\mathrm{X}}^\dagger \Phi + \Phi^\dagger \tilde{\mathrm{X}}\right) \Xi. \end{aligned} \tag{B.5}$$

V_λ contains quartic couplings of Φ, X and their charge conjugated respectively. Since V_λ does not include the doublet Ξ that was newly introduced, its form remains the same (for details, see [75]). Moreover, its contribution is highly suppressed as only electroweak scales are involved, and the exact structures become less relevant.

List of Figures

List of Tables

Acronyms

1PI One-Particle-Irreducible

2HBDM Two-Higgs Bi-Doublet Model

2HDM Two-Higgs Doublet Model

BFM Background Field Method

CKM Cabibbo-Kobayashi-Maskawa

CP Charge-Parity

CT Counterterm

DOF Degree-of-Freedom

EFT Effective Field Theory

EOM Equations-of-Motion

EW Electroweak

GS Ground State

IBP Integration-by-Parts

IO Inverted Ordering

IR Infrared

LHN Left-Handed Neutrino

LR Left-Right

$\overline{\text{MS}}$ Modified-Minimal-Substration

NO Normal Ordering

σ^i Pauli matrices

PMNS Pontecorvo–Maki–Nakagawa–Sakata

PT Pertubation Theory

RGE Renormalization Group Equation

RHN Right-Handed Neutrino

SM Standard Model

SMEFT Standard Model Effective Field Theory

SSB Spontaneous Symmetry Breaking

SVD Singular Value Decomposition

UV Ultraviolet

VEV Vacuum Expectation Value

Bibliography

[1] M. Tanabashi *et al.*, "Review of particle physics", *Phys. Rev. D*, vol. 98, 3 2018.

[2] M. Aker *et al.*, "Direct neutrino-mass measurement with sub-electronvolt sensitivity", *Nature Phys.*, vol. 18, no. 2, 2022.

[3] E. Ma, "Verifiable radiative seesaw mechanism of neutrino mass and dark matter", *Physical Review D*, vol. 73, no. 7, 2006.

[4] S. Dodelson and L. M. Widrow, "Sterile neutrinos as dark matter", *Physical Review Letters*, vol. 72, no. 1, 1994.

[5] M. Fukugita and T. Yanagida, "Baryogenesis Without Grand Unification", *Phys. Lett. B*, vol. 174, 1986.

[6] H. Georgi and S. L. Glashow, "Unity of All Elementary Particle Forces", *Phys. Rev. Lett.*, vol. 32, 1974.

[7] P. Minkowski, "M→e at a rate of one out of 109 muon decays?", *Physics Letters B*, vol. 67, no. 4, 1977.

[8] T. Yanagida, "Horizontal gauge symmetry and masses of neutrinos", *Conf. Proc. C*, vol. 7902131, O. Sawada and A. Sugamoto, Eds., 1979.

[9] M. Gell-Mann, P. Ramond, and R. Slansky, "Complex Spinors and Unified Theories", *Conf. Proc. C*, vol. 790927, 1979.

[10] S. L. Glashow, "The Future of Elementary Particle Physics", *NATO Sci. Ser. B*, vol. 61, 1980.

[11] R. N. Mohapatra and G. Senjanovic, "Neutrino Mass and Spontaneous Parity Nonconservation", *Phys. Rev. Lett.*, vol. 44, 1980.

[12] S. Weinberg, "Baryon and Lepton Nonconserving Processes", *Phys. Rev. Lett.*, vol. 43, 1979.

[13] P. H. Chankowski and Z. Płuciennik, "Renormalization group equations for seesaw neutrino masses", *Physics Letters B*, vol. 316, no. 2–3, 1993.

[14] K. Babu, C. Leung, and J. Pantaleone, "Renormalization of the neutrino mass operator", *Physics Letters B*, vol. 319, no. 1–3, 1993.

[15] S. Antusch, M. Drees, J. Kersten, M. Lindner, and M. Ratz, "Neutrino mass operator renormalization revisited", *Physics Letters B*, vol. 519, no. 3–4, 2001.

[16] S. Davidson, G. Isidori, and A. Strumia, "The smallest neutrino mass", *Physics Letters B*, vol. 646, no. 2–3, 2007.

[17] A. Ibarra, P. Strobl, and T. Toma, "Neutrino masses from Planck-scale lepton number breaking", *Phys. Rev. Lett.*, vol. 122, no. 8, 2019.

[18] A. Ibarra, P. Strobl, and T. Toma, "Two-loop renormalization group equations for right-handed neutrino masses and phenomenological implications", *Phys. Rev. D*, vol. 102, no. 5, 2020.

[19] C. Bonilla, J. Herms, A. Ibarra, and P. Strobl, "Neutrino parameters in the Planck-scale lepton number breaking scenario with extended scalar sectors", *Phys. Rev. D*, vol. 103, no. 3, 2021.

[20] M. Kachelriess, *Quantum fields: from the Hubble to the Planck Scale*. 2017.

[21] M. Thomson, *Modern Particle Physics*. Cambridge University Press, 2013.

[22] F. Halzen and A. D. Martin, *Quarks And Leptons: An Introductory Course In Modern Particle Physics*. 1984.

[23] A. J. Larkoski, *Elementary Particle Physics: An Intuitive Introduction*. Cambridge University Press, 2019.

[24] M. Tanabashi *et al.*, "Review of Particle Physics", *Phys. Rev. D*, vol. 98, no. 3, 2018.

[25] I. Esteban, M. Gonzalez-Garcia, M. Maltoni, T. Schwetz, and A. Zhou, "The fate of hints: Updated global analysis of three-flavor neutrino oscillations", *Journal of High Energy Physics*, vol. 2020, no. 9, 2020.

[26] W. Grimus and H. Neufeld, "Radiative Neutrino Masses in an SU(2) X U(1) Model", *Nucl. Phys. B*, vol. 325, 1989.

[27] P.-H. Gu, H. Zhang, and S. Zhou, "Minimal type ii seesaw model", *Physical Review D*, vol. 74, no. 7, 2006.

[28] N. D. Barrie, C. Han, and H. Murayama, "Type II Seesaw leptogenesis", *JHEP*, vol. 05, 2022.

[29] S. Ashanujjaman and K. Ghosh, "Type-iii see-saw: Phenomenological implications of the information lost in decoupling from high-energy to low-energy", *Physics Letters B*, vol. 819, 2021.

[30] J. C. Pati and A. Salam, "Lepton number as the fourth "color"", *Phys. Rev. D*, vol. 10, 1 1974.

[31] R. N. Mohapatra and J. C. Pati, "Left-right gauge symmetry and an "isoconjugate" model of CP violation", *Phys. Rev. D*, vol. 11, 3 1975.

[32] G. Senjanovic and R. N. Mohapatra, "Exact left-right symmetry and spontaneous violation of parity", *Phys. Rev. D*, vol. 12, 5 1975.

[33] G. Senjanović, "Spontaneous breakdown of parity in a class of gauge theories", *Nuclear Physics B*, vol. 153, 1979.

[34] L. V. Silva, *Phenomenology of left-right models in the quark sector*, 2016.

[35] A. V. Manohar, *Introduction to effective field theories*, 2018.

[36] T. Cohen, *As scales become separated: Lectures on effective field theory*, 2020.

[37] M. E. Peskin and D. V. Schroeder, *An Introduction to quantum field theory*. Reading, USA: Addison-Wesley, 1995.

[38] Z. Zhang, "Covariant diagrams for one-loop matching", *Journal of High Energy Physics*, vol. 2017, no. 5, 2017.

[39] G. Hooft, "Dimensional regularization and the renormalization group", *Nucl. Phys., B, v. B61*, 1973.

[40] S. Antusch, "The running of neutrino masses, lepton mixings and cp phases", 2003.

[41] A. Denner, G. Weiglein, and S. Dittmaier, "Application of the background-field method to the electroweak standard model", *Nuclear Physics B*, vol. 440, no. 1–2, 1995.

[42] L. F. Abbott, "The Background Field Method Beyond One Loop", *Nucl. Phys. B*, vol. 185, 1981.

[43] L. F. Abbott, "Introduction to the Background Field Method", *Acta Phys. Polon. B*, vol. 13, 1982.

[44] L. Abbott, M. Grisaru, and R. Schaefer, "The background field method and the s-matrix", *Nuclear Physics B*, vol. 229, no. 2, 1983.

[45] Z.-z. Xing and D. Zhang, "On the two-loop radiative origin of the smallest neutrino mass and the associated majorana cp phase", *Physics Letters B*, vol. 807, 2020.

[46] R. Mertig, M. Bohm, and A. Denner, "FEYN CALC: Computer algebraic calculation of Feynman amplitudes", *Comput. Phys. Commun.*, vol. 64, 1991.

[47] V. Shtabovenko, R. Mertig, and F. Orellana, "New Developments in FeynCalc 9.0", *Comput. Phys. Commun.*, vol. 207, 2016.

[48] V. Shtabovenko, R. Mertig, and F. Orellana, "FeynCalc 9.3: New features and improvements", *Comput. Phys. Commun.*, vol. 256, 2020.

[49] R. Mertig and R. Scharf, "Tarcer — a mathematica program for the reduction of two-loop propagator integrals", *Computer Physics Communications*, vol. 111, no. 1–3, 1998.

[50] J. Kublbeck, M. Bohm, and A. Denner, "Feyn Arts: Computer Algebraic Generation of Feynman Graphs and Amplitudes", *Comput. Phys. Commun.*, vol. 60, 1990.

[51] T. Hahn, "Generating Feynman diagrams and amplitudes with FeynArts 3", *Comput. Phys. Commun.*, vol. 140, 2001.

[52] N. D. Christensen and C. Duhr, "FeynRules - Feynman rules made easy", *Comput. Phys. Commun.*, vol. 180, 2009.

[53] A. Alloul, N. D. Christensen, C. Degrande, C. Duhr, and B. Fuks, "FeynRules 2.0 - A complete toolbox for tree-level phenomenology", *Comput. Phys. Commun.*, vol. 185, 2014.

[54] G. 't Hooft and M. J. G. Veltman, "Scalar One Loop Integrals", *Nucl. Phys. B*, vol. 153, 1979.

[55] G. Passarino and M. J. G. Veltman, "One Loop Corrections for e+ e- Annihilation Into mu+ mu- in the Weinberg Model", *Nucl. Phys. B*, vol. 160, 1979.

[56] K. Chetyrkin, M. Misiak, and M. Münz, "Beta functions and anomalous dimensions up to three loops", *Nuclear Physics B*, vol. 518, no. 1–2, 1998.

[57] J. Brod and Z. Polonsky, "Two-loop beta function for complex scalar electroweak multiplets", *Journal of High Energy Physics*, vol. 2020, no. 9, 2020.

[58] A. Denner, H. Eck, O. Hahn, and J. Kublbeck, "Feynman rules for fermion number violating interactions", *Nucl. Phys. B*, vol. 387, 1992.

[59] Z. Alam and S. P. Martin, "Standard model at 200 gev", *Physical Review D*, vol. 107, no. 1, 2023.

[60] G.-y. Huang and S. Zhou, "Precise values of running quark and lepton masses in the standard model", *Physical Review D*, vol. 103, no. 1, 2021.

[61] F. Staub, "SARAH", 2008.

[62] F. Staub, "SARAH 4 : A tool for (not only SUSY) model builders", *Comput. Phys. Commun.*, vol. 185, 2014.

[63] A. E. Thomsen, "Introducing RGBeta: a Mathematica package for the evaluation of renormalization group β-functions", *Eur. Phys. J. C*, vol. 81, no. 5, 2021.

[64] M. E. Machacek and M. T. Vaughn, "Two Loop Renormalization Group Equations in a General Quantum Field Theory. 1. Wave Function Renormalization", *Nucl. Phys. B*, vol. 222, 1983.

[65] M. E. Machacek and M. T. Vaughn, "Two Loop Renormalization Group Equations in a General Quantum Field Theory. 2. Yukawa Couplings", *Nucl. Phys. B*, vol. 236, 1984.

[66] M. E. Machacek and M. T. Vaughn, "Two Loop Renormalization Group Equations in a General Quantum Field Theory. 3. Scalar Quartic Couplings", *Nucl. Phys. B*, vol. 249, 1985.

[67] Y. Wang, D. Zhang, and S. Zhou, "Complete one-loop renormalization-group equations in the seesaw effective field theories", *Journal of High Energy Physics*, vol. 2023, no. 5, 2023.

[68] R. Kallosh, A. Linde, D. Linde, and L. Susskind, "Gravity and global symmetries", *Physical Review D*, vol. 52, no. 2, 1995.

[69] S. L. Adler, "Axial-vector vertex in spinor electrodynamics", *Phys. Rev.*, vol. 177, 5 1969.

[70] G. 't Hooft and M. J. G. Veltman, "Regularization and Renormalization of Gauge Fields", *Nucl. Phys. B*, vol. 44, 1972.

[71] S. L. Adler and W. A. Bardeen, "Absence of higher order corrections in the anomalous axial vector divergence equation", *Phys. Rev.*, vol. 182, 1969.

[72] G. Branco, P. Ferreira, L. Lavoura, M. Rebelo, M. Sher, and J. P. Silva, "Theory and phenomenology of two-higgs-doublet models", *Physics Reports*, vol. 516, no. 1–2, 2012.

[73] A. Ibarra and C. Simonetto, "Understanding neutrino properties from decoupling right-handed neutrinos and extra higgs doublets", *Journal of High Energy Physics*, vol. 2011, no. 11, 2011.

[74] G. Helmberg, P. Wagner, and G. Veltkamp, "On faddeev-leverrier's method for the computation of the characteristic polynomial of a matrix and of eigenvectors", English, *Linear Algebra and Its Applications*, vol. 185, 1993.

[75] J.-Y. Liu, L.-M. Wang, Y.-L. Wu, and Y.-F. Zhou, "Two higgs bidoublet model with spontaneous p and cp violation and decoupling limit to the two higgs doublet model", *Physical Review D*, vol. 86, no. 1, 2012.

[76] H. Kleinert and V. Schulte-Frohlinde, "Critical properties of ϕ4-theories", 2001.